RÉPUBLIQUE ALGÉRIENNE DÉMOCRATIQUE ET POPULAIRE
Ministere de l'Enseignement Superieur et de la Recherche Scientifique

École Nationale Polytechnique

Département de Génie Mécanique

End-of-study project dissertation for obtaining the State Engineer's degree in Mechanical Engineering

---

SubmarineEye: Design of an Advanced ROV Prototype

Presented by:

MEHABA HANI
BOUARROU SAMY

Presented and defended publicly on 21 octobre 2023

Composition of the jury :

President:	**LARBI Salah**	PROF	ENP
Examiner:	**BENBRAIKA Mohamed**	MAA	ENP
Incubator representative:	**BELOUADAH Zouheyr**	MCA	ENP
Promoter:	**BENKOUSSAS Bouzid**	PROF	ENP
Promoter:	**SEDJAL Hamid**	MAA	ENP

ENP 2023

بسم الله الرحمن الرحيم

RÉPUBLIQUE ALGÉRIENNE DÉMOCRATIQUE ET POPULAIRE
Ministere de l'Enseignement Superieur et de la Recherche Scientifique

École Nationale Polytechnique

Département de Génie Mécanique

End-of-study project dissertation for obtaining the State Engineer's degree in Mechanical Engineering

---

SubmarineEye: Design of an Advanced ROV Prototype

Presented by:

MEHABA HANI
BOUARROU SAMY

Presented and defended publicly on 21 octobre 2023

Composition of the jury :

President:	**LARBI Salah**	PROF	ENP
Examiner:	**BENBRAIKA Mohamed**	MAA	ENP
Incubator representative:	**BELOUADAH Zouheyr**	MCA	ENP
Promoter:	**BENKOUSSAS Bouzid**	PROF	ENP
Promoter:	**SEDJAL Hamid**	MAA	ENP

ENP 2023

RÉPUBLIQUE ALGÉRIENNE DÉMOCRATIQUE ET POPULAIRE
Ministere de l'Enseignement Superieur et de la Recherche Scientifique

École Nationale Polytechnique

Département de Génie Mécanique

Mémoire de Projet de Fin d'Études
pour l'obtention du Diplôme d'Ingénieur d'État en Génie Mécanique

---

SubmarineEye: Conception d'un prototype de ROV avancé

Présenté par:

MEHABA HANI
BOUARROU SAMY

Soutenu le 21 octobre 2023 devant le jury composé de :

Président:	**LARBI Salah**	PROF	ENP
Examinateur:	**BENBRAIKA Mohamed**	MAA	ENP
Représentant de l'incubateur:	**BELOUADAH Zouheyr**	MCA	ENP
Encadrant:	**BENKOUSSAS Bouzid**	PROF	ENP
Encadrant:	**SEDJAL Hamid**	MAA	ENP

ENP 2023

ملخص:
هدف مشروعنا هو إنشاء مركبة تعمل عن بعد تحت الماء تجارية عالية الجودة تنتمي إلى فئة المراصد ومجهزة بكاميرا موثوقة. بدأنا بدراسة سوق شاملة لتحديد الفجوة الخاصة بنا في السوق المحلية. ثم قمنا بتطوير نموذج حركي للمركبة وأجرينا دراسات هيدروديناميكية لتحسين هندستها. تم التركيز على تصميم المروحيات مع إجراء محاكاة عددية دقيقة. قمنا بتصميم الحجرات المحكمة للمركبة ودمجنا جميع المكونات بدقة، وقمنا بمعايرة توزيع وزنها بعناية لضمان توازنها في الماء.

كلمات مفتاحية:
مركبة بالتحكم عن بُعد، الدفع، ديناميات المياه، مرصد، قابلية التحكم، كفاءة الطاقة.

Résumé:

Notre projet vise la conception d'un véhicule sous-marin télécommandé. Le véhicule est de qualité appartenant à la classe des observatoires. Nous avons débuté par une étude de marché approfondie pour cerner les besoins locaux. Ensuite, nous avons développé un modèle cinématique pour le ROV et effectué des études hydrodynamiques pour optimiser sa géométrie. La conception des propulseurs a été minutieuse, incluant des simulations numériques. Nous avons élaboré les compartiments scellés du ROV, intégré tous les composants avec précision, et calibré sa répartition de poids pour garantir son équilibre dans l'eau.

Mots-clés:

Véhicule Télécommandé, Propulsion, Hydrodynamique, Observatoire, Maniabilité, Efficacité Énergétique.

Summary:

Our project aimed to create a high-quality submarine commercial Remotely Operated Vehicle (ROV) in the observatory class. We began with a thorough market study to understand local needs. We developed a kinematic model for the ROV, conducted hydrodynamic studies to optimize its geometry, and meticulously designed its propellers using numerical simulations. The ROV's sealed compartments were carefully integrated, and its weight distribution was calibrated for optimal balance in water.

Keywords:

Remotely operated Vehicule, Propulsion, hydrodynamics, observatory, maneuverability, Energy Efficiency.

Acknowledgments

We would like to express our deepest gratitude to our esteemed advisors, SEDJAL Hamid and BENKOUSSAS Bouzid, for their unwavering guidance, invaluable insights, and constant encouragement throughout the course of this research. Their mentorship has been instrumental in shaping our work and academic journey.

We extend our sincere appreciation to our distinguished examiners, LARBI Salah and BENBRAIKA Mohamed, for their time, expertise, and thoughtful evaluation of our work. Their feedback and constructive criticism have enriched our project and academic growth.

Our heartfelt thanks go to the Department of Mechanical Engineering at Ecole Nationale Polytechnique for providing us with a stimulating academic environment, a wealth of resources, and a platform to explore our research interests. We are indebted to our dedicated professors and instructors who imparted their knowledge and inspired us on this academic voyage.

We are grateful to ENP's Incubator for their support and resources, which have enabled us to bridge the gap between theory and practical application. The guidance of Zouheyr BELOUADAH and the expertise of Karim LAHLAH were invaluable assets to our project.

Last but certainly not least, we wish to acknowledge our families and friends for their unwavering support, understanding, and encouragement during the highs and lows of our academic pursuits. Their belief in us has been a constant source of motivation.

This project would not have been possible without the collective support of these individuals and institutions. We are deeply thankful for their contributions to our academic and personal growth.

Contents

List of Figures

List of Tables

Nomenclature

η : the state vector .
$\mathbf{v}$: velocity vector.
J_1 : The rotation matrix.
J_2 : Passage matrix.
ρ : density mass.
M : Inertia matrix.
C : matrix of Coriolis and centripetal.
D : damping matrix.
g : vector of gravitational forces.
τ : vector of control inputs.
$C_{d_{fr}}$: Skin friction coefficient.
ρ_∞ : Density of the free stream.
V_∞ : Free stream speed.
τ_w : Skin shear stress.
F_{SFD} : skin friction drag force.
V : the velocity of the ROV relative to the fluid.
F_{form} : the drag force.
C_{d_form} : the form drag coefficient.
$C_{d_{th}}$: the drag coefficient of the tether.
F_{tether} : the tether drag force
F_{form} : the drag force.
F_i : the lift force.
T : the thrust force.
Q : the torque force.
Z : the number of blades.
R : the propeller radius.
r_h : the hub radius
β_i : the inflow angle
ρ : the fluid density
V^* : the inflow velocity
Γ : the circulation
e_r : the radial unit vector
e_α : the tangential unit vector.
V_s : the ship speed.
ω : the angular velocity.
e_r : the radial unit vector.
n : the propeller rotational speed.
D : the propeller diameter.
T : the thrust.
J : the advance ratio.
$M_0(\theta)$: The righting moment.
K_T : Thrust coefficient.
K_Q : Moment coefficient.

General introduction

Throughout much of human history, the vast and mysterious ocean has captivated the human imagination, filled with enigmatic phenomena and mysteries that were largely inaccessible to us, particularly in the deep sea. Despite this, the ocean has played a vital role in our civilization, providing us with sustenance, transportation, and awe-inspiring wonder. In the modern era, the ocean has become increasingly important in a variety of fields, including oil and gas industries, environmental agencies, and academic institutions. Recent strides in technology and the advent of new tools have facilitated the exploration of the underwater world, enabling humans to visit places that were previously out of reach. This has led to a surge of research and development in this area, as scientists, engineers, and explorers seek to understand the ocean's vast and complex ecosystem.

However, the exploration of the ocean still poses significant risks to human life and requires substantial financial resources. Many underwater exploration tasks are dangerous and require specialized training and equipment. To address these challenges, researchers have developed Remotely Operated Vehicles (ROVs), which enable exploration of the deep sea without putting human life at risk.

Our goal for this project is to create a high-quality and cost-effective Commercial ROV that belongs to the observatory class and is equipped with a reliable camera. To ensure user-friendliness and ease of control, we plan to develop a ROV with excellent maneuverability that can be controlled by users on the surface through a joystick or application. Additionally, we aim to equip the ROV with a wide range of sensors, including depth, orientation, battery life, temperature, and pressure, to provide the user with all the necessary information. Our main focus is to provide an optimal user experience with a stable and efficient ROV that can perform its tasks seamlessly. We strive to keep the ROV affordable to enable broader accessibility and user satisfaction.

To ensure the success of our project, we began by conducting a comprehensive market study. This enabled us to pinpoint a specific gap or demand within the local market. Once we had a clear grasp of the market needs, we carefully selected the specifications for our ROV, tailored to meet the requirements of the local market [7].

Following the completion of the market research, we delved into the "Geometric Modeling and Identification of Different Parameters" phase. Here, we initiated the process by developing a kinematic model for the ROV [8]. This allowed us to gain a deeper understanding of its movements and acquire all the necessary kinematic equations early on, essential for programming the ROV.Then, we proceeded with a hydrodynamic study. This exploration

helped us comprehend both the internal and external forces and other parameteres impacting our ROV . Armed with this knowledge, we were able to refine the geometry of our ROV to minimize these forces, thereby enhancing its efficiency.

We've then embarked on a comprehensive exploration of the propeller design process [2]. We've taken a close look at different types of propellers and identified the most suitable type for our application. Following that, we discussed various thruster configurations for ROVs and carefully selected the optimal one. We then delved into the design of the propellers, employing a parametric study approach to determine the most efficient configuration [3]. Subsequently, we conducted rigorous testing of these propellers through numerical simulations [9], culminating in the completion of the thruster design. Additionally, we illustrated the final result of the thruster assembly with the appropriate seal.

And then comes the fourth chapter, where we initially addressed the hardware system, detailing the various electrical components employed in the ROV. We elucidated the specific functions each component serves within our system and culminated in presenting the conclusive schematic for our ROV's hardware system. Transitioning to the second part of this chapter, we shifted focus towards the software system and its programming [4]. This encompassed tasks such as autopilot programming, system configuration, and thorough verification of sensor functions. The efforts invested in this chapter will stand as a solid foundation, guaranteeing the reliability and proficiency of our ROV.

In the fifth chapter, We first started by establishing a waterproofing system for the electrical components [5], followed by assembling the internal parts of the ROV, including vertical and horizontal thrusters, sealed box, and camera. Subsequently, we dedicated our efforts to crafting an exterior shell that not only optimized performance but also presented an aesthetically pleasing design. Next, we meticulously calibrated the weight distribution of the ROV, a pivotal measure to ensure its stability and balance when submerged. Finally, we concluded with the meticulous final assembly of the ROV, culminating in a meticulously designed and fully functional underwater vehicle.

CHAPTER 0 : Generalities about ROVs

0.1 Introduction

In recent years, underwater exploration and research has been greatly facilitated by the use of remotely operated vehicles (ROVs). ROVs are underwater robots that explore and perform tasks in deep or hazardous waters while being remotely controlled from a control room or ship's deck using a tether or wireless communication system. They come in various sizes, from small portable systems to large work-class vehicles equipped with sensors, cameras, manipulators, and other tools that allow them to observe and interact with the underwater environment. They are used in various applications, including offshore oil and gas exploration, oceanographic research, environmental monitoring, marine archaeology, and underwater inspection, maintenance, and repair. ROVs are particularly useful in situations where human divers cannot operate due to extreme depth, pressure or other hazards. They have revolutionized underwater exploration, allowing access and mapping of areas that were previously inaccessible and are becoming more sophisticated and versatile, opening new opportunities for scientific discovery, resource exploitation, and environmental protection[1].

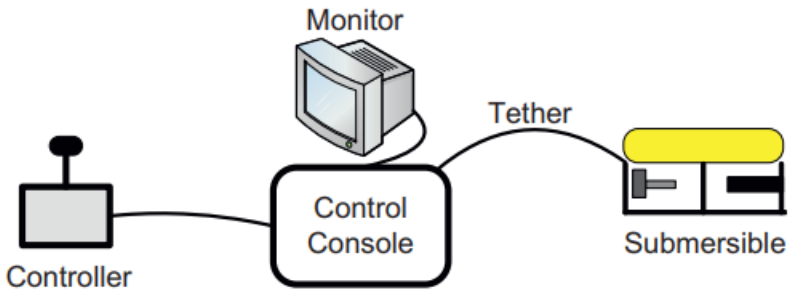

Figure 0.1: Basic ROV system components . From [1]

0.2 History of Submarines

The origins of ROVs can be traced back to the 1950s, when the United States Navy began experimenting with underwater vehicles that could be remotely controlled. These early vehicles were designed to perform various underwater tasks, such as mine clearance and reconnaissance, without risking the lives of human divers. One of the first successful ROVs was developed by the French inventor Dimitri Rebikoff in 1953 [1]. His vehicle was tethered to the surface and used to explore underwater caves and shipwrecks (figure 0.2).

Entrepreneurs such as Rebikoff were indeed making significant advancements in underwater technology, but it was ultimately the US Navy that took the first true steps towards a functional system. One particular issue that the Navy faced was the retrieval of lost torpedoes on the seafloor. In order to improve upon their existing grappling system, the Navy contracted VARE Industries in Roselle, New Jersey to develop a Mobile Underwater Vehicle

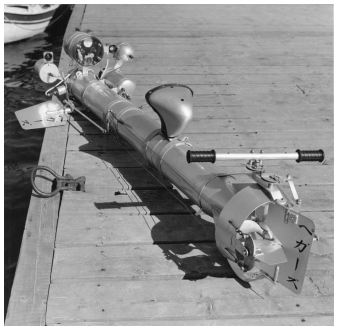

Figure 0.2: The first remotely operated vehicle (ROV). From [1]

System equipped with a maneuverable underwater camera. In 1961, the XN-3, the original VARE vehicle, was delivered to the Naval Ordnance Test Station (NOTS) in Pasadena, California. The design of the XN-3 eventually evolved into the Cable-Controlled Underwater Research Vehicle (CURV), which proved to be a significant development in the field of underwater exploration[1](figure 0.3).

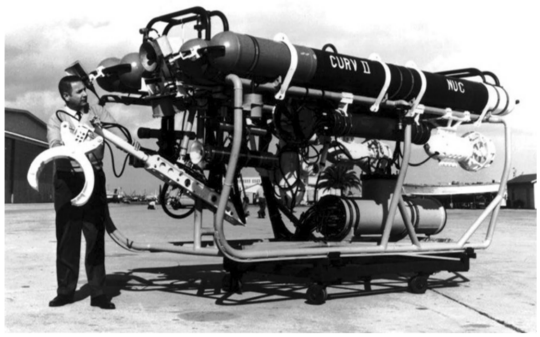

Figure 0.3: CURV II vehicle. From [1]

With such successes under its belt, the Navy expanded into more complex vehicles, such as the massive Pontoon Implacement Vehicle (PIV), which was developed to aid in the recovery of sunken submarines, shown with the integrated Work Systems Package (WSP) (Figure 0.4).

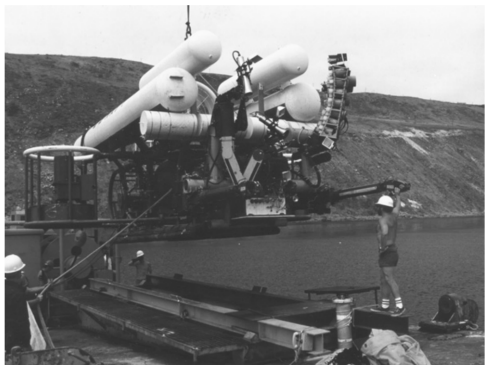

Figure 0.4: US Navy's WSP/PIV. From [1]

At the other end of the scale, the US Navy developed one of the very first small-size observation ROVs. The SNOOPY vehicle, which was hydraulically operated from the surface, was one of the first portable vehicles (Figure 0.5).This version was followed by the Electric SNOOPY, which extended the vehicle's reach by going with a fully electric vehicle. Eventually sonars and other sensors were added and the childhood of the small vehicles had begun[1].

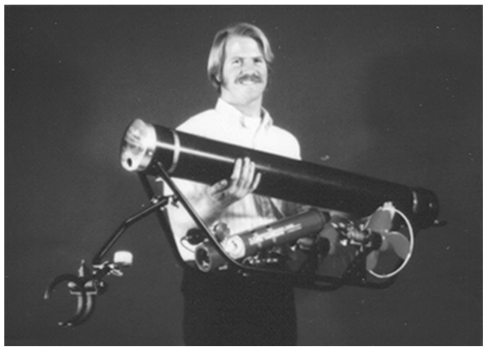

Figure 0.5: US Navy's hydraulic SNOOPY. From [1]

In the 1970s, the use of ROVs increased significantly, with the offshore oil and gas industry becoming one of the primary users of these vehicles. ROVs were used for a range of tasks, including pipeline inspection, installation, and maintenance, as well as platform maintenance and construction.

One of the most significant advancements in ROV technology during this time was the development of the Tether Management System (TMS), which allowed for the deployment and retrieval of ROVs from ships and other vessels. The TMS also allowed for longer dive times and greater maneuverability, as the ROV could be moved away from the ship without the risk of getting tangled in the tether.An example of an ROV that benefited from the TMS was the SCORPIO (Figure 0.6), built by Ametek. The SCORPIO had a depth capability of up to 1000 meters and featured a 5-function manipulator.

Figure 0.6: SCORPIO

In the 1980s, the scope of ROV applications broadened, extending beyond the oil and gas sector. Scientific research and military utilization saw a notable surge. Scientists turned to ROVs for probing the depths of the ocean and studying marine ecosystems, while global militaries adopted them for tasks like mine clearance and surveillance.

Since their inception in the 1950s, ROVs have undergone substantial evolution. They've become more compact, agile, and versatile in executing diverse functions across different environments. This transformation is owed to strides in electronics and computer technologies, enabling enhanced control and automation. The shift from hydraulic to electric thrusters has further amplified efficiency and reliability.

Modern ROVs are equipped with top-tier features like high-definition cameras and sophisticated sensors including sonars and magnetometers, enabling precise and comprehensive data acquisition. Innovations in battery technology have extended operational durations, and leaps in autonomy have ushered in smarter, self-reliant functioning. As a result, today's ROVs find application in a wide spectrum of endeavors, spanning underwater exploration, the oil and gas industry, scientific research, and military undertakings.

0.3 Classification of underwater vehicles.

At present, underwater vehicles are classified into two primary groups : those that are manned and those that are unmanned, also known as UUVs.

Manned underwater vehicles: are operated by human pilots who are inside the vehicle. These vehicles require a life support system to keep the pilot alive and often have limited range due to the need for human support. They are typically used for tasks that require human judgement or dexterity, such as complex maintenance or scientific research.

Unmanned underwater vehicles: are controlled remotely by operators from the surface. They are not limited by human endurance or life support systems, and can be designed to operate in harsh or dangerous environments. They are often used for tasks such as surveying, mapping, and inspection, and can be equipped with a variety of sensors and tools.

The focus of this project is on unmanned underwater vehicles, which are classified into two categories. The first type is the AUV,which functions independently without being tethered, operates autonomously and programmed to navigate using sensors and algorithms. The second type is the ROV, which can be controlled remotely by a user on the surface through a tether and control room, as mentioned in the introduction.

0.3.1 Classification of ROVs

ROVs have a wide range of applications including supporting divers and performing heavy marine subsea construction tasks. The ROV market can be divided into four main categories

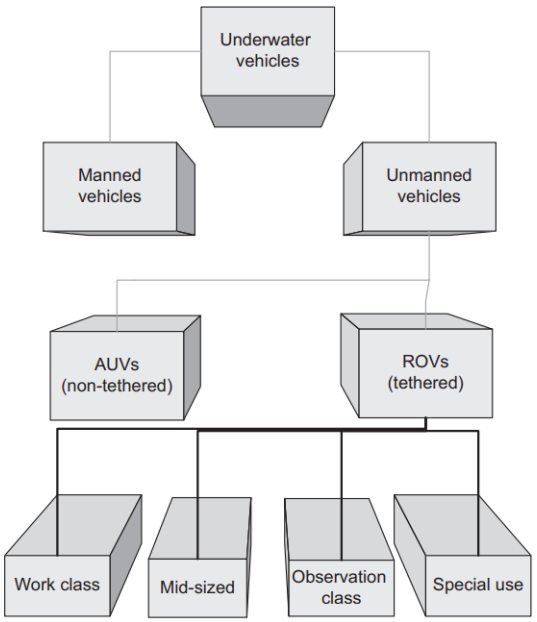

Figure 0.7: Underwater vehicles to ROVs.

based on the size and capabilities of the vehicle :

Observation class ROVs (OCROV): These vehicles go from the smallest micro-ROVs to a vehicle weight of 100kg.They are typically smaller, less expensive, DC-powered vehicles that serve as backup to divers or substitute for shallow water inspection tasks. Due to the weight of their power delivery components and pressure housings, they are generally limited to depths of less than 300 m and require neutral buoyancy for swimming. These vehicles are usually hand-launched and flown from the surface with tether hand tending.

Figure 0.8: Examples of OCROVs. From [1]

Mid-sized ROVs (MSROV): Weighing between 100 kg and 1000 kg, these vehicles are typically a deeper-rated version of OCROVs with AC power delivery components and pressure housings that enable them to reach greater depths with longer tether/umbilical

lengths. They are all-electric with some hydraulic power for manipulators and tooling, and their electrical power is stepped down for component operation, using either AC or DC power. These vehicles are sometimes referred to as "light work class" vehicles to distinguish them from OCROVs, and their weight necessitates the use of a launch and recovery system (LARS) and a tether management system (TMS).

Figure 0.9: Example of MSROV

Work class ROVs (WCROV): These vehicles are typically large and heavy electromechanical machines that run on high-voltage (over 3000 V) AC circuits from the surface to the vehicle. The power is then converted to mechanical (hydraulic) power at the vehicle for propulsion, as well as for all manipulation and tooling functions.

Figure 0.10: Example of WCROV

Special-use vehicles: Vehicles not falling under the main categories of ROVs due to their non-swimming nature such as crawling underwater vehicles, towed vehicles, or struc-

turally compliant vehicles. The special-use vehicle coverage is outside the purview of this text.

0.4 Deployment of underwater robotics

The applications of underwater vehicles are potentially very broad. They particularly affect two main sectors, which are:

1. The civil sector
2. The military sector

In the following sections, we will delve into the specific requirements and applications of ROVs in both the civil and military sectors.

0.4.1 The civil sector

We can distinguish three main applications for underwater robots: industry, environment, and scientific applications.

Industry: Oil, gas, and telecommunications companies have quickly been interested in the potential of underwater vehicles. Their needs are expressed in terms of mapping the seabed, assisting in the laying of pipelines or cables, and inspecting these structures.

Environment: The application of laws related to fishing restrictions and the protection of the maritime environment requires the detection, identification, pursuit, and prohibition of suspect boats. These robots could also help identify intentional pollutions (oil spills). Underwater vehicles equipped with biochemical sensors are capable of analyzing pollutants and can thus identify the responsible parties through chemical comparison of the tanks of ships docked at the port. The machine can also collect ice samples at different depths to study the history of the climate. This application requires the vehicle to have very precise relative positioning, as well as the ability to maintain a fixed position in the presence of strong disturbances.

Scientific applications: Archaeologists take advantage of the characteristics of underwater vehicles to explore wrecks and treasures hidden under the oceans. Where a diver's abilities are limited in terms of autonomy and immersion depth, underwater robots push the boundaries of human exploration to improve and expand research. Knowledge of the flow rate and salinity of underwater sources, and their variation over time, is important. This allows hydrologists to estimate the amount of water flowing into the sea and to assess its potential use.

0.4.2 The military sector

One of the most studied military applications concerns the detection and destruction of underwater mines. Destroying these objects is a dangerous and specific task, where robotic devices can locate and neutralize these bombs instead of humans. Another emerging activity is the surveillance of ports. To prevent the intrusion of enemy divers or underwater vehicles into ports, autonomous robots can perform a grid search in an area near the port entrance. In general, military applications are expressed in the following tasks:

1. Detailed mapping for espionage.
2. Detection and identification of underwater mines.
3. Detection and identification of ships, marine vessels, and submarines.
4. Protection of military ports and port environments.
5. Passive sonar listening (analysis of the noise emitted by each target).
6. Active sonar listening (analysis of the sound reflection coefficient of each target).

CHAPTER 1 : Market study

1.1 Overview of the market

The ROV and underwater drone market is a rapidly growing industry, with a global market size of $7.31 billion in 2021, and is expected to reach $14.84 billion by 2026, growing at a CAGR of 15.2% during the forecast period. This growth is mainly attributed to the increasing demand for underwater exploration, inspection, and maintenance activities in various end-use industries such as oil and gas, marine, and defense. The rise in offshore drilling and exploration activities, as well as the need for underwater inspection and maintenance of aging infrastructure, are also contributing to the growth of the ROV and underwater drone market. Moreover, technological advancements, such as the development of autonomous underwater vehicles (AUVs) and remotely operated underwater vehicles (ROVs), are further driving the growth of the market [7].

The market is segmented by product type, application, and geography. By product type, the market is further segmented into ROVs and underwater drones, with the former dominating the market in terms of revenue share. By application, the market is segmented into oil and gas exploration, marine research, defense, and others. Geographically, the market is segmented into North America, Europe, Asia Pacific, and Rest of the World, with North America and Europe dominating the market.

The key trends driving the market include the increasing adoption of ROVs and underwater drones in the oil and gas industry for exploration and inspection activities, rising demand for marine research, and increasing investments in defense applications. However, the market faces challenges such as high initial investment costs and strict regulatory requirements for operating ROVs and underwater drones.

Overall, the ROV and underwater drone market is poised for significant growth in the coming years, driven by increasing demand for underwater exploration and maintenance activities across various industries. Below is a summary table about the market segmentation:

Type	Work Class ROV Observatory Class ROV
Application	Oil and Gas Defense Other Applications
Activity	Survey Inspection, Repair, and Maintenance Burial and Trenching Other Activities
Geography	North America Europe Asia-Pacific South America Middle-East and Africa

1.2 Potentiel concurrents

During our market research, we analyzed successful ROVs available in the market. We studied their characteristics to understand our competitors and compared them to identify key differences.

There are a variety of ROVs with distinct features and capabilities. These ROVs have cameras that can capture high-quality video and images, with resolutions ranging from FHD to 4K and up to 12-megapixel resolution. The depth range of these ROVs varies from 15 meters to 100 meters, catering to various underwater applications.

The weight of these ROVs varies, with some weighing as little as 1.1 kg while others weigh up to 18 kg. They are powered by different battery capacities ranging from 4400mAh to 14400mAh, which offer varying battery life, with some ROVs able to operate up to 2.5 hours and others for up to 4 hours.

The temperature range of these ROVs varies as well, with some capable of operating in temperatures as low as $-10°C$ and as high as $60°C$. Some of these ROVs come with unique features such as underwater live streaming and the ability to use MIMO technology for multi-channel transmission, a fish detection sonar, and a lot of them which are work class ROVs have a gripper as a standard or optional feature.

In conclusion, there are various ROVs available with unique features and capabilities, catering to different underwater applications, and if we want to take a share of this market,

we have to find our specific niche, and apply a specialization based marketing strategy, since a cost based one already exists and is hard to beat.

1.3 Potential and target clients

In order to find our specific niche, we need to look more to our potential first clients and understand their needs, and these clients must be local ones who are based in Algeria since the policy of the Algerian government favors local companies and imposes restrictions on foreign products.

Additionally, in Algeria, there are no companies already making this type of drones, which is a key advantage to the success of our project. Therefore, our first product must satisfy the local needs.

When it comes to the underwater domain, Algeria has high potential with its 1200km of Mediterranean Sea. We find various types of fishing, including coral fishing, where the Coral Fishermen's Association has expressed their interest and need for our product. There are also fish farms located along the Mediterranean coast, which can benefit from our ROVs. Algerian aquaculture mostly focuses on freshwater fish such as trout and carp, as well as marine fish such as seabream, seabass, and tuna. The oil and gas industry in Algeria has significant reserves, and underwater drones can be used for exploration, pipeline inspection, and maintenance. Port authorities can also use underwater drones to assist in the maintenance of port infrastructure such as docks, piers, and navigational aids. The military and coast guard can benefit from underwater drones for intelligence gathering, surveillance, and search and rescue operations. Environmental agencies can use underwater drones to monitor and assess the health of marine ecosystems, detect pollution, and conduct research on marine species. Academic institutions such as universities and research institutes may use underwater drones for marine research and exploration.

All of these potential clients provide us with a strong foundation to develop a niche market in Algeria that satisfies local needs and benefits from the absence of local competition.

1.4 Definition of project objectives

Our primary goal is to develop a product that meets the specific needs of our local clients before expanding into international markets. To achieve this objective, we conducted extensive market research to identify the specifications required for our ROVs to satisfy most potential customers.

Our research revealed that an Observatory Class ROV is in high demand due to its versatility and affordability, making it an excellent option for several industries, including oil and gas, environmental agencies, and academic institutions. It also offers low production costs, making it the most feasible market entry option.

Also,the ROV's filming quality is a crucial factor for customers, and they prefer a high-resolution camera that can deliver excellent results in harsh conditions. Long battery life is

also a priority for customers, as it maximizes the ROV's operating time and reduces the need for frequent battery changes, enabling more efficient work time and larger operation areas. The ROV's speed is another critical factor that ensures timely data collection and maximum coverage during missions.

Moreover, the ROV's size and weight are significant considerations, as they affect its marketability, transportation, and deployment. As well lightweight and compact design enables the ROV to navigate in confined areas and ensure longer battery life, making it an ideal choice for most customers.

In conclusion, our market research has provided us with valuable insights into our customers' needs, preferences, and expectations. By developing an Observatory Class ROV with a high-resolution camera, long battery life, and excellent speed, we aim to provide our customers with a reliable, efficient, and cost-effective solution that can meet their diverse requirements.

We understand that the success of our product depends on our ability to listen to our customers, continuously improve our design and functionality, and provide exceptional customer service. We remain committed to delivering a product that exceeds our customers' expectations, builds trust and loyalty, and establishes us as a reputable player in the ROV industry.

Our focus on the local market first, followed by international expansion, reflects our strategic approach to building a sustainable and scalable business that can thrive in a highly competitive and dynamic environment. We are confident that our product's unique features, coupled with our customer-centric approach, will enable us to gain a competitive advantage and achieve long-term success in the global ROV market.

Specifications of our ROV

Our focus in this project is to develop a product that closely aligns with the needs and preferences of our customers. To achieve this, we have carefully chosen a set of specifications that are both feasible with our current resources and can be further refined after the release of the first prototype. so we decide to go for an Observatory Class ROV that meets these specifications, which include:

Table 1.1: Specifications of our Observatory Class ROV

Specifications	Details
Camera	1920x1080 pixels,30 fps,FOV=95°
Autonomy	Minimum of 2 hours
Maximum Depth	50 meters
Speed	1.2 m/s
Weight	2 to 3Kg
Data Collected	temperature, depth, pressure, fish (via sonar), and energy statistics.

To sum up, meeting the needs and preferences of customers is critical for a product's success. We are confident that the parameters we have chosen will provide our clients with a reliable, efficient, and cost-effective option that caters to their diverse needs. By prioritizing these specifications, our goal is to create a product that meets the demands of our customers while also ensuring that it is practical and can be improved upon in the future.

1.5 Risk Assessment and Potential Challenges

Designing and building an underwater remotely operated vehicle (ROV) requires careful consideration of a variety of technical challenges. One of the critical technical challenges is buoyancy control. The ROV must be designed and implemented with a system that can achieve and maintain neutral buoyancy in varying water depths and conditions. This requires an understanding of the physics of buoyancy and how to create a system that can adjust the ROV's buoyancy quickly and accurately. Failure to achieve neutral buoyancy can cause the ROV to drift or become unstable, making it difficult to maneuver and control.

Another important technical challenge is waterproofing. The ROV must be waterproofed to ensure that all electronic components and connections are fully sealed and protected from damage and short-circuits. This requires careful attention to detail during the design and construction of the ROV. Failure to achieve proper waterproofing can result in electrical failures and damage to critical components, rendering the ROV inoperable.

The power supply is also a critical technical challenge. The ROV must have enough power to operate all of its components and motors without adding too much weight or bulk. This requires an understanding of the power requirements of each component and how to optimize the power supply to provide maximum performance with minimal weight and bulk.

Another challenge is the propulsion system. The ROV must be designed with an efficient propulsion system that can maneuver the ROV in different directions and currents. This requires an understanding of hydrodynamics and how to optimize the design of the propulsion system for maximum efficiency and maneuverability.

Cable management is also a critical technical challenge. The ROV must have a system for managing and routing the cables that connect it to the surface without interfering with its movement or becoming tangled. This requires careful attention to the design and placement of the cables to ensure that they do not impede the ROV's movement or become tangled during operation.

Stability and control are also important technical challenges. The ROV must be designed with a system for stabilizing and controlling it in different water conditions and currents. This requires an understanding of the physics of underwater movement and how to optimize the design of the ROV for maximum stability and control.

Navigation is also a critical technical challenge. The ROV must have a reliable navigation system that can accurately guide it to specific locations and avoid obstacles. This requires an understanding of underwater navigation and how to integrate sensors and other technology

to create a reliable navigation system.

Sensing and imaging are also important technical challenges. The ROV must be designed with sensors and cameras that can capture high-quality images and data in different water conditions and depths. This requires an understanding of imaging and sensing technology and how to integrate it into the ROV design.

Maintenance and repair are also critical technical challenges. The ROV must be designed with a system for maintaining and repairing it, including access to all components and the ability to replace damaged parts. This requires careful attention to the design and construction of the ROV to ensure that it can be easily maintained and repaired.

Finally, durability and reliability are important technical challenges. The ROV must be designed to withstand the harsh underwater environment and operate reliably over a long period of time. This requires an understanding of materials science and how to select materials and components that can withstand the underwater environment and maintain their performance over time.

1.6 Conclusion

Initially, we conducted a market analysis to gain valuable insights into the current state of the market and its potential for growth. Our research of potential competitors revealed a variety of remotely operated vehicles (ROVs) with different features and capabilities that serve various underwater applications. Based on this, we concluded that we must identify a specific niche to capture a share of this market.

Our analysis of potential clients in Algeria uncovered a promising opportunity for success in this market. Firstly, the government's policies favor local companies, providing us with a competitive advantage. Secondly, we found that no other companies are currently operating in this field, creating significant market space for our product. Additionally, we discovered a high demand for our type of drone in several industries in Algeria, including academic institutions, the military, and port authorities. The need for our product in these industries further highlights the market potential in Algeria. Overall, our market study has revealed a clear path for success in Algeria, and we have identified a significant opportunity to capture market share and meet the needs of potential clients in various industries.

After gathering all this information, we gained a better understanding of the market's state and, more importantly, the needs of our local customers. Since our focus is on the local market first, we have established a set of feasible specifications that will meet the requirements of our potential clients.

CHAPTER 2 : Geometric Modeling and Identification of Differents Parameters

2.1 Introduction

In this chapter, we delve into two key challenges concerning the modeling and parametric identification of the ROV. Modeling necessitates a deep understanding of the system's parameters, employing a variety of variables to articulate the vehicle's position within the underwater realm. Essential concepts such as the local reference frame, global reference frame, center of mass, center of buoyancy, and more, are defined to facilitate the kinematic and hydrodynamic analyses of the submarine [8].

Furthermore, this chapter meticulously explores the diverse forces and moments impeding the ROV's movements, each originating from various sources. A detailed exploration of the dynamics of a non-deformable body, the intricacies of propulsion forces, the concept of neutral buoyancy, aspects of rolling stability, and hydrodynamic parameters are thoroughly elucidated.

2.2 Modeling of the ROV-Observer

2.2.1 Parametrization and Associated Frames

Modeling requires defining reference frames with respect to which the vehicle's motion will be described. To establish the equations describing the movement of an underwater robot in three-dimensional Euclidean space, two reference frames are used [31]. The first is the global inertial frame R0 = (O, X0, Y0, Z0) of reference, which is linked to the Earth and considered to be Galilean, with the following orientation : X0 is directed towards the North, Y0 is directed towards the East, and Z0 is directed downwards. Its origin O is chosen arbitrarily and could, for example, be the initial position of the ROV. Then, a local reference frame, having the center of buoyancy of the ROV 'C' as its origin, is defined as follows: The frame linked to the ROV, Rv = (C, Xv, Yv, Zv), also called the mobile frame , whose axes are chosen as follows: Xv is the longitudinal axis, Yv is the transverse axis, and Zv is the normal axis to the plane (Xv, Yv).

2.2.2 Kinematic Model

The movement of the ROV is described by the following parameters:
-We note $\eta = [x, y, z, \phi, \theta, \psi]^T$ the state vector representing the position and orientation of the vehicle in the terrestrial frame R_0.
-The coordinates x, y, and z, expressed in meters, represent the position of the origin of the frame R_v in the frame R_0. We note $\eta_1 = [x_0, y_0, z_0]^T$ the vector of the position of the center of gravity with respect to the reference frame R_v expressed in the reference frame R_0.

-The angles ϕ ,θ and ψ expressed in radians, are the angles that indicate the orientation of the frame R_v with respect to the reference frame R_0. Commonly referred to as Euler angles in the international literature, they represent the orientation of a vehicle with respect to a fixed reference frame R_0. These angles are respectively called roll, pitch, and yaw. We denote the vector altitude with respect to the fixed reference frame R_0 expressed in the reference frame R_0 by $\boldsymbol{\eta_2} = [\phi, \theta, \psi]^T$.

Let $\mathbf{v} = [u, v, w, p, q, r]^T$ be the vector that combines the linear and angular velocities in the body frame R_v of the vehicle. The linear velocities u, v, and w expressed in m/s correspond to the velocities along the x, y, and z axes of the vehicle, respectively, and are called longitudinal velocity (surge), lateral velocity (sway), and vertical velocity (heave), respectively. Let $\mathbf{v}_1 = [u, v, w]^T$ be the local translation velocity with respect to R_0 expressed in the local reference frame R_v.

The angular velocities p, q, and r expressed in rad/s correspond to the rates of rotation around the O_x, O_y, and O_z axes, respectively, i.e., the roll rate, pitch rate, and yaw rate of the vehicle, respectively. Let $\mathbf{v}_2 = [p, q, r]^T$ be the local rotational velocity with respect to R_0 expressed in the local reference frame R_v.

a) Definition of the transformation matrices

The configuration of the vehicle is described by means of three elementary rotations defined by three orientation angles, namely the yaw angle ψ, the pitch angle θ, and the roll angle ϕ:

$$\left(X_0,\ Y_0,\ Z_0\right) \rightarrow^{H_\psi} B\left(X_1,\ Y_1,\ Z_0\right) \rightarrow^{H_\theta} B\left(X_v,\ Y_1,\ Z_1\right) \rightarrow^{H_\phi} B\left(X_v,\ Y_v,\ Z_v\right) \quad (2.1)$$

where $B(X_0, Y_0, Z_0)$ is the base of the global frame R_0, $B(X_v, Y_v, Z_v)$ is the base of the local frame R_v, $B(X_1, Y_1, Z_0)$ and $B(X_v, Y_1, Z_1)$ are intermediate bases, and H_ψ, H_θ, and H_ϕ are orthogonal rotation matrices.

The first rotation of angle ψ is counted positively in the direct sense with respect to Z_0 (see Figure 2.1). It is represented by the transformation matrix H_ψ:

$$H_\psi = \begin{bmatrix} \cos\psi & -\sin\psi & 0 \\ \sin\psi & \cos\psi & 0 \\ 0 & 0 & 1 \end{bmatrix} \quad \text{in the } (X_1, Y_1, Z_0) \text{ frame}$$

The second rotation of angle θ describes the pitch around the Y_1 axis (see Figure 2.2) and gives the transformation matrix $\vec{H}_\theta$ between the frames $B(X_1, Z_1, Z_0)$ and $B(X_v, Y_1, Z_1)$:

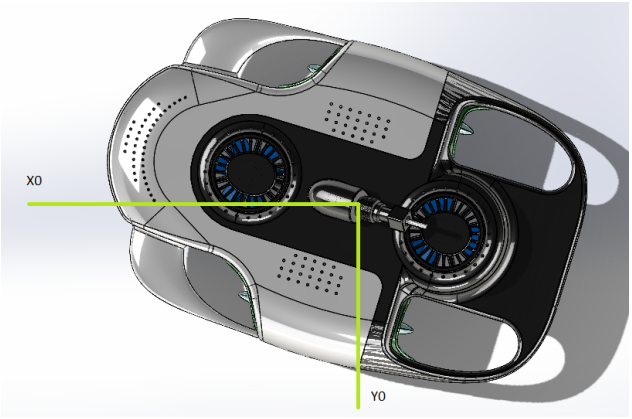

Figure 2.1: Yaw Movement

$$H_\theta = \begin{bmatrix} \cos\theta & 0 & \sin\theta \\ 0 & 1 & 0 \\ -\sin\theta & 0 & \cos\theta \end{bmatrix} \quad \text{in the } (X_v, Y_1, Z_1) \text{ frame}$$

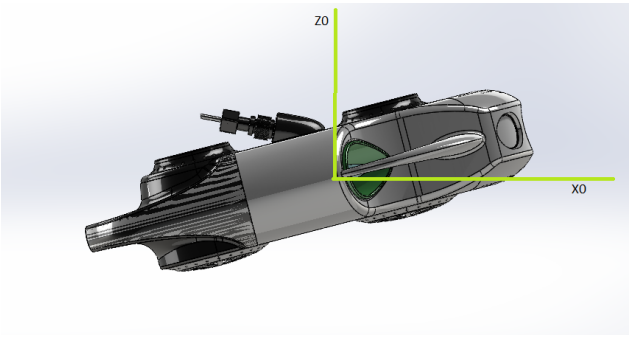

Figure 2.2: Pitch Movement

The third rotation of angle ϕ is performed around the X_v axis of the new frame (see Figure 2.3) given by:

$$H_\phi = \begin{bmatrix} 1 & 0 & 0 \\ 0 & \cos\phi & -\sin\phi \\ 0 & \sin\phi & \cos\phi \end{bmatrix} \quad \text{in the } (X_v, Y_1, Z_1) \text{ frame}$$

The rotation matrix that describes the transformation between the global frame R_0 and the local frame R_v is given by:

$$J_1 = J_1(\eta_2) = H_\psi H_\theta H_\phi$$

therefore

$$J_1 = \begin{pmatrix} \cos\psi\cos\theta & -\sin\psi\cos\phi + \sin\phi\cos\psi\sin\theta & \sin\phi\sin\psi + \sin\theta\cos\psi\cos\phi \\ \cos\theta\sin\psi & \cos\psi\cos\phi + \sin\theta\sin\psi\sin\phi & -\sin\phi\cos\psi + \cos\phi\sin\psi\sin\theta \\ -\sin\theta & \cos\theta\sin\phi & \cos\theta\cos\phi \end{pmatrix} \quad (2.2)$$

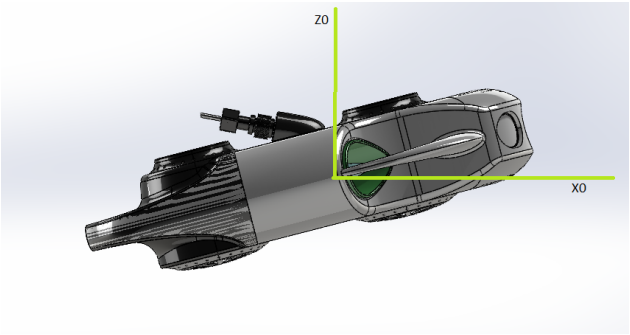

Figure 2.3: Roll Movement

Such as,

$$J_1^T J_1 = J_1 J_1^T = \mathrm{Id}_3$$

b)Transformation of Translation and Rotation Velocities

Using the change of basis matrix J_1, the transformation of the components of the translational velocity with respect to R_0 is given by:

$$\dot{\eta_1} = J_1(\eta_2)\mathbf{v}_1 \tag{2.3}$$

Based on the relation (2.1), the local rotational velocity can be expressed as:

$$\mathbf{v}_2 = \dot{\psi}Z_0 + \dot{\theta}Y_1 + \dot{\phi}X_v$$

$$\mathbf{v}_2 = \dot{\psi}Z_0 + \dot{\theta}H_\psi Y_0 + \dot{\phi}H_\psi H_\theta X_0$$

$$\mathbf{v}_2 = \dot{\psi}\begin{pmatrix}0\\0\\1\end{pmatrix} + \dot{\theta}\begin{bmatrix}\cos\psi & -\sin\psi & 0\\ \sin\psi & \cos\psi & 0\\ 0 & 0 & 1\end{bmatrix}\begin{pmatrix}0\\1\\0\end{pmatrix} + \dot{\phi}\begin{bmatrix}\cos\psi & -\sin\psi & 0\\ \sin\psi & \cos\psi & 0\\ 0 & 0 & 1\end{bmatrix}\begin{bmatrix}\cos\theta & 0 & \sin\theta\\ 0 & 1 & 0\\ -\sin\theta & 0 & \cos\theta\end{bmatrix}\begin{pmatrix}1\\0\\0\end{pmatrix}$$

$$\mathbf{v}_2 = \begin{pmatrix}0 & -\sin\psi & \cos\psi\cos\theta\\ 0 & \cos\psi & \sin\psi\cos\theta\\ 1 & 0 & -\sin\theta\end{pmatrix}\begin{pmatrix}\dot{\psi}\\ \dot{\theta}\\ \dot{\phi}\end{pmatrix} \tag{2.4}$$

We can then express the rotational velocity vector in the mobile frame $B(X_v, Y_v, Z_v)$ as:

$$\mathbf{v}_2 = \begin{pmatrix}p\\q\\r\end{pmatrix} = \begin{pmatrix}0 & -\sin\psi & \cos\psi\cos\theta\\ 0 & \cos\psi & \sin\psi\cos\theta\\ 1 & 0 & -\sin\theta\end{pmatrix}\begin{pmatrix}\dot{\psi}\\ \dot{\theta}\\ \dot{\phi}\end{pmatrix} \tag{2.5}$$

We can then define J_2 as the change of basis matrix that relates the components of the rotational velocity in the global frame to those in the local frame, given by:

$$J_2 = \begin{pmatrix}0 & -\sin\psi & \cos\psi\cos\theta\\ 0 & \cos\psi & \sin\psi\cos\theta\\ 1 & 0 & -\sin\theta\end{pmatrix}^{-1} = \begin{pmatrix}\dfrac{\cos(\psi)\sin(\theta)}{\cos(\theta)} & \dfrac{\sin(\psi)\sin(\theta)}{\cos(\theta)} & 1\\ -\sin(\psi) & \cos(\psi) & 0\\ \dfrac{\cos(\psi)}{\cos(\theta)} & \dfrac{\sin(\psi)}{\cos(\theta)} & 0\end{pmatrix} \tag{2.6}$$

Therefore, the second kinematic relation is given by:

$$\dot{\eta_2} = J_2(\eta_2)\mathbf{v}_2 \tag{2.7}$$

Remark 2.1 *It should be noted that the parameterization in pitch angle introduces a singularity at $\theta = \frac{\pi}{2} + k\pi$. This parameterization is inaccessible because in order for the ROV to be stable in water we will design it in a way where the hydrostatic, hydrodynamic, and propulsion phenomena, will make it impossible to reach a pitch angle of 90°.*

c) Kinematic equation Using equations (2.3) and (2.7), the kinematics of the ROV can be expressed as follows:

$$\begin{pmatrix} \dot{\eta_1} \\ \dot{\eta_2} \end{pmatrix} = \begin{pmatrix} J_1(\eta_2) & 0_{3\times3} \\ 0_{3\times3} & J_2(\eta_2) \end{pmatrix} \begin{pmatrix} \mathbf{v_1} \\ \mathbf{v_2} \end{pmatrix} \tag{2.8}$$

2.3 Hydrodynamics Study

2.3.1 Introduction

The hydrodynamic study holds immense significance in the design of our ROV project, as it directly influences its performance and efficiency. By delving into the intricacies of hydrodynamics, we can greatly enhance the maneuverability and overall efficiency of the ROV. Through a comprehensive understanding of factors such as drag, we can minimize resistance in the water, leading to reduced power requirements and enhanced energy efficiency. Moreover, by focusing on hydrodynamics, we can ensure improved stability and control, allowing the ROV to maintain its position and navigate effectively across various operating conditions. Furthermore, the hydrodynamic study enables us to determine the ROV's depth and speed capabilities accurately. This knowledge is crucial in tailoring the design to operate at specific depths and achieve optimal propulsion speeds. Lastly, by incorporating hydrodynamic considerations into our design, we can create a structure and shape that mitigates vibrations and turbulence caused by water flow, effectively safeguarding the integrity of sensitive payloads. Overall, the hydrodynamic study plays a pivotal role in optimizing our ROV's design, elevating its performance, and ensuring the successful accomplishment of its intended tasks.

2.3.2 Buoyancy

When an object is immersed in a fluid, either fully or partially, it experiences an upward force known as the 'Buoyant Force.' This force is a result of the net vertical component of the hydrostatic pressure exerted on the object. This phenomenon is referred to as 'Buoyancy.'

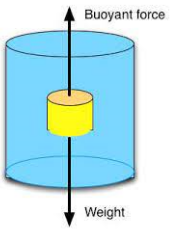

Figure 2.4: Buoyancy

it is given by the following Formula :

$$F_B = \iiint \rho \cdot g \cdot (dV) \tag{2.9}$$

Centre of buoyancy :

It is the point where the force of buoyancy is applied, it can calculated by the given formula:

$$X_B = \frac{1}{V} \cdot \iiint x \cdot dV \tag{2.10}$$

$$Y_B = \frac{1}{V} \cdot \iiint y \cdot dV \tag{2.11}$$

$$Z_B = \frac{1}{V} \cdot \iiint z \cdot dV \tag{2.12}$$

Buoyancy and Stability :

To ensure optimal stability of a remotely operated vehicle (ROV), achieving neutral buoyancy is essential. Neutral buoyancy occurs when the weight force of the ROV is precisely balanced by the buoyant force exerted on it. This equilibrium state is crucial for maintaining the desired depth and maneuverability.

To achieve neutral buoyancy, careful selection of materials during the fabrication of the ROV is vital. The choice of materials should take into account their specific gravity relative to the surrounding water conditions. Buoyancy materials play a crucial role in achieving neutral buoyancy by offsetting the excess weight of the ROV. These materials are selected based on their ability to be lighter than water, enabling them to provide additional upward buoyant force.

By utilizing buoyancy materials with lower specific gravity, the ROV's overall density is effectively reduced. This reduction in density allows the ROV to float or remain suspended at the desired depth without sinking or rising uncontrollably. The correct selection and incorporation of buoyancy materials contribute to the ROV's stability, enabling precise control and maneuvering underwater.

Transverse Stability :

Our objective is to design an ROV that maximizes stability, particularly in the pitch and roll axes, to provide the user with an optimal experience. Positive stability is essential for

achieving this goal. Positive stability is attained by ensuring that the center of gravity (CG) of the ROV is positioned below the center of buoyancy (CB) and both centers are aligned along the same vertical axis. The greater the separation between these two centers, the greater the stability of the ROV.

When the CG is positioned below the CB, the ROV naturally attempts to vertically align the two centers, leading to self-calibration. This alignment process is performed by considering the inclination of the vehicle's hull through various angles and calculating the resulting moments exerted by the opposing forces of gravity and buoyancy. As the vehicle inclines, the CB and CG undergo horizontal displacements relative to each other, creating a separation distance "d" that is dependent on the inclination θ. Although the magnitude of both forces remains constant and equal to the vehicle's weight (W), the moment (W $\times$ d) generated by these forces varies with θ. This alignment process generates a moment called the righting moment, which acts in the opposite direction of the inclination to rotate the vehicle around its CG. The righting moment plays a crucial role in restoring the ROV to a stable position and maintaining its equilibrium, thereby enhancing its stability.

To illustrate this concept, please refer to Figure 2.5, which provides a visual representation of the righting moment.

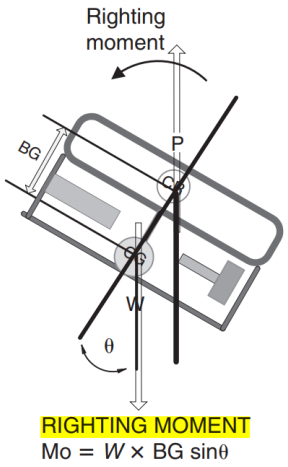

Figure 2.5: Righting Moment

2.3.3 Hydrodynamic model

The equations of motion describe the dynamics of a system in the Body-fixed frame. In this frame, the equations are given by [10]:

$$M\nu + C(\nu)\nu + D(\nu)\nu + g(\eta) = \tau \tag{2.13}$$

$$\dot{\eta} = J(\eta)\nu \tag{2.14}$$

In these equations, ν represents the velocity vector in $\mathbb{R}^n$, and η represents the position vector in $\mathbb{R}^n$. The following matrices and vectors are involved:

$M \in \mathbb{R}^{n\times n}$ (inertia matrix with added mass)

$C \in \mathbb{R}^{n\times n}$ (matrix of Coriolis and centripetal terms with added mass)

$D \in \mathbb{R}^{n\times n}$ (damping matrix)

$g \in \mathbb{R}^n$ (vector of gravitational forces)

$\tau \in \mathbb{R}^n$ (vector of control inputs)

To transform the equations of motion to the Earth-fixed frame(see , we apply the following kinematic transformations:

$$\dot{\eta} = J(\eta)\nu \quad \Rightarrow \quad \nu = J^{-1}(\eta)\dot{\eta} \tag{2.15}$$

$$\ddot{\eta} = J(\eta)\dot{\nu} + \dot{J}(\eta)\nu \quad \Rightarrow \quad \dot{\nu} = J^{-1}(\eta)(\ddot{\eta} - \dot{J}(\eta)\nu) \tag{2.16}$$

Here, $J(\eta)$ is a non-singular matrix that represents the transformation from the Earth-fixed frame to the Body-fixed frame. By substituting (2.15) and (2.16) into (2.13), we obtain

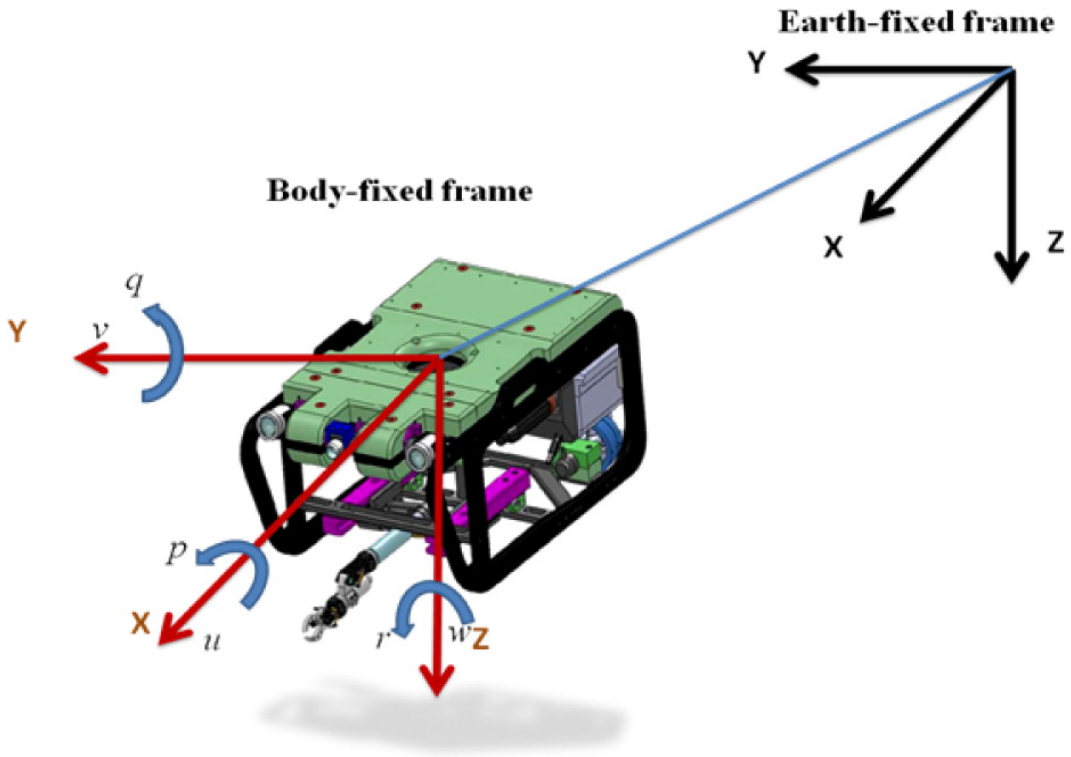

Figure 2.6: Frame coordinates of the ROV

the equations of motion in the Earth-fixed frame:

$$M\eta(\eta)\ddot{\eta} + C\eta(\nu,\eta)\dot{\eta} + D\eta(\nu,\eta)\eta + g\eta(\eta) = \tau \tag{2.17}$$

$$\tag{2.18}$$

In the Earth-fixed frame, the matrices and vectors are defined as follows:

$$\begin{aligned} M\eta(\eta) &= J^{-T}(\eta)MJ^{-1}(\eta) \\ C\eta(\nu,\eta) &= J^{-T}(\eta)[C(\nu) - MJ^{-1}(\eta)\dot{J}(\eta)]J^{-1}(\eta) \\ D\eta(\nu,\eta) &= J^{-T}(\eta)D(\nu)J^{-1}(\eta) \\ g\eta(\eta) &= J^{-T}(\eta)g(\eta) \\ \tau\eta(\eta) &= J^{-T}(\eta)\tau \end{aligned}$$

In summary, the equations of motion (2.13) and kinematic equations (2.14) in the Body-fixed frame can be transformed to the Earth-fixed frame using the kinematic transformations (2.15) and (2.16). The resulting equations of motion in the Earth-fixed frame are given by (2.17), with the corresponding matrices and vectors defined as above.

2.3.4 Drag forces

Drag forces play a crucial role in the hydrodynamics study of ROVs as they have a significant impact on the performance and power consumption of these vehicles. When operating in

underwater environments, two fundamental types of drag forces come into play: form drag and friction drag. However, for ROVs, there is an additional force , known as tether drag. Therefore, a total of three drag forces affect ROVs.
In this section, we will delve into a comprehensive discussion of these three types of drag forces and thoroughly examine their effects on our robot. By the conclusion of this section, we will have acquired a thorough understanding of how to design our ROV in a manner that minimizes drag forces, ultimately enhancing the performance of our vehicle.

Skin friction Drag :

Skin friction drag is a significant component of the drag forces experienced by an ROV. It occurs due to the interaction between water particles and the surface of the ROV's body. When water flows past the ROV, a thin layer of water molecules sticks to the surface, creating what is known as the boundary layer (see figure 2.7).

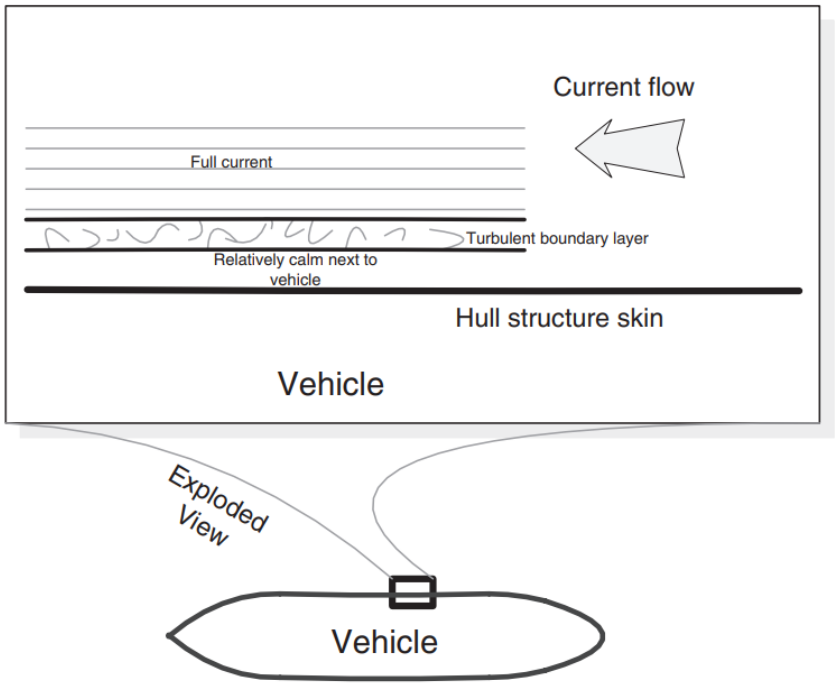

Figure 2.7: Ideal form with skin surface detail

At the surface of the ROV, the water velocity within the boundary layer is essentially zero, as it is in direct contact with the stationary surface. As we move away from the surface and towards the outer region of the boundary layer, the water velocity gradually increases and eventually matches the flow velocity of the surrounding water.

This velocity gradient within the boundary layer leads to the development of shearing stresses between the layers of water. In the beginning, the flow within the boundary layer is predominantly laminar, with smooth and orderly movement of water particles. However, as the velocity gradient increases, the flow transitions from laminar to turbulent.

As the flow transitions from laminar to turbulent in the transition region, the boundary

layer thickness increases. This thickening of the boundary layer leads to an increase in drag forces acting on the ROV.

The skin friction drag force produced by the ROV can be determined using the following formula:

$$\tau_w = \frac{1}{2} \cdot C_{d_{fr}} \cdot \rho_\infty \cdot V_\infty^2 \tag{2.19}$$

where:

$C_{d_{fr}}$: Skin friction coefficient.

ρ_∞ : Density of the free stream (far from the body's surface).

V_∞ : Free stream speed, which is the velocity magnitude of the fluid in the free stream.

τ_w : Skin shear stress on the surface.

Now we can proceed to the calculation of skin friction drag force by using the following empiric equation:

$$F_{SFD} = \int_{\text{Surface}} \tau_w \, dA = \int_{\text{Surface}} \frac{1}{2} \cdot C_{d_{fr}} \cdot \rho_\infty \cdot V_\infty^2 \, dA \tag{2.20}$$

To minimize skin friction drag, the design of the ROV's body shape can be optimized by reducing surface roughness and streamlining its form. These measures can delay the transition to turbulent flow and mitigate the effects of skin friction drag.

Form Drag :

Form drag occurs when an ROV is in motion through water. As the vehicle displaces water to accommodate its presence, it causes a deformation in the flow around its body. This deformation leads to a pressure disparity between the front and back regions of the ROV, as well as turbulence within the flow. Consequently, a force known as form drag force is generated, opposing the direction of the ROV's movement[1].
Form drag primarily depends on the cross-sectional area of the ROV's front section(see figure 2.8). It can be reduced by using streamlined shapes and minimizing abrupt changes in the cross-sectional area of the vehicle.

The drag force produced by form drag(vehicle drag)can be determined using the following formula[1]:

$$F_{form} = \frac{1}{2}.\rho.A_{tr}.V^2.C_{d_{form}} \tag{2.21}$$

Where :

- F_{form} is the drag force.
- ρ is the density of the water.

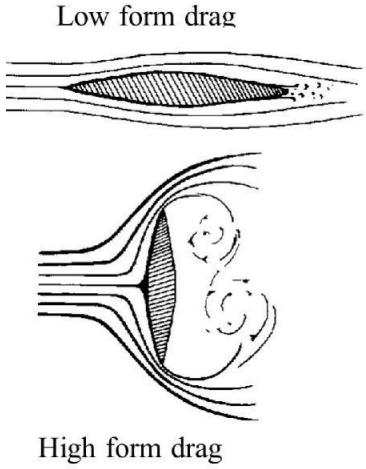

Figure 2.8: Effect of Cross-Sectional Shape on Form Drag

- A is the frontal cross-sectional area of the ROV.
- V is the velocity of the ROV relative to the fluid.
- C_{d_form} is the form drag coefficient, which depends on the shape and surface characteristics of the ROV, it is usually between 0.8 and 1.

Tether Drag :

Tether drag is an additional form of drag that ROVs encounter. It arises due to the friction between the tether, which is the cable connecting the ROV to its control system, and the surrounding water. This interaction between the tether and the water leads to the generation of significant drag forces[1].

The length of the tether plays a crucial role in the magnitude of the drag. The longer the tether, the more significant the drag becomes. This is because the extended length of the tether increases the surface area in contact with the water, leading to higher skin friction and subsequently increased drag forces.

The drag force exerted by the tether can be calculated using the following formula[1]:

$$F_{tether} = \frac{1}{2}.\rho.A_{th}.V^2.C_{d_{th}} \tag{2.22}$$

Where :

- F_{tether} is the tether drag force.
- ρ is the density of the water.
- A is the cable diameter times the length perpendicular to the flow.
- V is the velocity of the ROV relative to the fluid.

- $C_{d_{th}}$ is the drag coefficient of the tether

Total Drag :

It's the sum of all the drag forces applied to the system .

$$F_{t_{\text{drag}}} = F_{tether} + F_{form} + F_{SFD} \tag{2.23}$$

We will now determine the total drag force exerted on the ROV by utilizing the previously mentioned dimensions (300 mm x 210 mm x 100 mm) and the desired speed of 1.94384 knots (1.2 m/s). For the drag coefficients,$C_{d_{form}}$,$C_{d_{fr}}$ and $C_{d_{th}}$, we will assume a value of 1.

Given:

- ROV dimensions: 300 mm x 250 mm x 80 mm
- Desired speed: 1.2 m/s (equivalent to 1.94384 knots)
- Drag coefficients : $C_{d_{form}} = C_{d_{th}} = 1, C_{d_{fr}} = 1$

We can calculate the total drag force ($F_{t_{\text{drag}}}$) using the formula:

$$F_{t_{\text{drag}}} = \left(0.5 \cdot \rho \cdot A_{tr} \cdot V^2\right)_{\text{form}} + \left(0.5 \cdot \rho \cdot A_{\text{th}} \cdot V^2\right)_{\text{tether}} + \left(\int_{\text{Surface}} \frac{1}{2} \cdot C_{d_{fr}} \cdot \rho_\infty \cdot V_\infty^2 \, dA\right)_{\text{skin friction}} \tag{2.24}$$

Substituting the given values into the equation, we have:

$$F_{t_{\text{drag}}} = \left(0.5 \cdot 1.029 \cdot (0.25 \cdot 0.08) \cdot 1.2^2\right) + \left(0.5 \cdot 1.029 \cdot (0,004 \cdot 50) \cdot 1.2^2\right) + \left(0.5 \cdot 1.029 \cdot (0.1) \cdot 1.2^2\right)$$

Finally, we can compute the total drag force:

$$F_{t_{\text{drag}}} = 0.0148176 + 0.18522 + 0.074088$$

$$F_{t_{\text{drag}}} = 0.274 \ N$$

Therefore, the total drag force applied to the ROV is approximately 0.274 N.

2.4 Conclusion

In conclusion, this chapter focused on the geometric modeling and identification of different parameters for the ROV. It began by discussing the importance of modeling and the use of reference frames to describe the vehicle's motion in underwater space. The Newtonian and Lagrangian approaches were introduced, highlighting their respective advantages in analyzing forces and energies.

The chapter then delved into the parametrization and associated frames for modeling the ROV. The global inertial frame and the local frame linked to the ROV were defined,

along with the state vector representing the position and orientation of the vehicle. The transformation matrices for the different rotations were presented, allowing the conversion between global and local reference frames.

Next, the kinematic model of the ROV was explored, including the parameters for position, orientation, linear velocities, and angular velocities. The transformation of translation and rotation velocities using the change of basis matrices was explained. The kinematic equations relating the state vector and velocity vectors were derived.

The second part of the chapter focused on the hydrodynamics study of the ROV. The concept of buoyancy and its calculation, along with the center of buoyancy, were discussed. The importance of achieving neutral buoyancy for stability was emphasized. Transverse stability, which depends on the relative positions of the center of gravity and center of buoyancy, was also explained.

The chapter further explored drag forces and their impact on the performance of the ROV. Skin friction drag, form drag, and tether drag were discussed in detail. The formulas for calculating these drag forces were provided, and the importance of reducing drag through proper design and streamlining was emphasized.

In conclusion, this chapter laid the foundation for understanding the geometric modeling, kinematics, hydrodynamics, and drag forces related to the ROV. This knowledge is crucial for the subsequent design and control of the ROV, enabling optimal performance, stability, and efficiency in underwater operations.

CHAPTER 3 : ROV's Propulsion

3.1 Introduction

Propulsion is a critical component of any underwater remotely operated vehicle (ROV), enabling it to move and maneuver in water. There are various types of propulsion systems available, each with its own set of advantages and disadvantages. In this chapter, we will explore different propulsion systems, discuss their differences, and examine the criteria used to select the appropriate propulsion system for ROVs. We will also explain the specific configuration of two horizontal and one vertical thrusters chosen for our ROV, along with the rationale behind this selection. Furthermore, we will assess which propulsion system best suits our ROV's requirements, and finally proceed with the design and development of our thrusters. By the end of this chapter, we will have successfully determined and implemented the propulsion system for our ROV.

3.2 Overview of Propulsion Systems

In this section, we will examine various propulsion systems commonly found in the marine industry, with a specific focus on those used in underwater ROVs. Through examples and analysis, we will discuss the strengths and weaknesses of each propulsion system.

3.2.1 Different propulsion systems

Propulsion refers to the system or device used to move a vehicle through a fluid, such as water. In the context of underwater remotely operated vehicles (ROVs), propulsion systems are essential for enabling the vehicle to move and maneuver through the water.

Underwater ROVs are often used in applications such as marine exploration, underwater inspection and maintenance, and search and rescue missions. In these applications, it is important that the ROV can move precisely and efficiently to reach its target destination, navigate around obstacles, and conduct detailed inspections or sample collections. Propulsion systems play a critical role in achieving these objectives, allowing the ROV to move in any direction with speed and precision.

The choice of propulsion system for an underwater ROV will depend on a number of factors, including the intended use of the vehicle, the required level of maneuverability, and the size and weight of the ROV. It is important to select a propulsion system that is efficient, reliable, and suited to the specific needs of the ROV project.

There are several different types of propulsion systems available, some of them are adabtable for underwater ROVs and others are not, each with its own advantages and disadvantages. We will try to go through most of them and explain their advantages and

disadvantages, and then select the best propulsion system for our ROV [2].

Figure 3.1: Fixed Pitch Propeller, from [2]

Fixed Pitch Propellers The fixed pitch propeller has formed the basis of propeller production over the years in either its monoblock or built-up forms. So then what is the difference between a monoblock and a built-up propeller? What advantages and disadvantages do they have? What materials are used in the manufacture of propellers and for what sizes? What are the major factors that determine the choice of blade number for a propeller? What are some design considerations for propellers beyond optimizing efficiency?

A monoblock propeller is a propeller whose blades and boss are made from a single piece of material, while a built-up propeller has blades that are cast separately from the boss and then bolted or fixed to it after machining. The built-up propeller is now rarely used except in a few niche markets because the monoblock propeller has become more common. In the early years of the last century, built-up propellers were very common due to the inability to achieve good quality large castings at that time and difficulties in defining the correct propeller blade pitch. The bolting arrangements in the blade palms gave some latitude to correct pitch errors relatively easily.

Built-up propellers have the advantage of being able to correct pitch errors more easily due to the bolting arrangements in the blade palms. However, they generally have a larger diameter boss than their fixed pitch counterparts, which may cause difficulty with cavitation problems in the blade root regions as well as adversely affecting propeller efficiency to a limited extent.

The choice of materials used in the manufacture of propellers varies considerably depending on the design type and size. For larger propellers over 300mm in diameter, nonferrous materials such as high-tensile brass, manganese and nickel-aluminum bronzes are the most favored types of materials, with nickel-aluminum bronzes predominating. Stainless steel has also gained limited use in niche markets. Cast iron, once a common material to produce spare propellers, has now virtually disappeared from use. For smaller propellers, materials such as

polymers, aluminum, nylon, and more recently carbon fiber composites are frequently used.

The major factors that determine the choice of blade number for a propeller are the achievement of a mismatch with the range of hull, superstructure, and machinery vibration frequencies, which are considered likely to give rise unwelcome vibration characteristics in the ship, and the control of unwelcome cavitation characteristics generated on the blade surfaces during each revolution of the propeller. For most merchant vessels, four, five, and six blades are the generally used number, although many tugs and fishing vessels commonly use three-bladed designs. In the case of small work or pleasure power boats, two- and three-bladed propellers tend to predominate.

Design considerations for propellers beyond optimizing efficiency include the reduction of vibration excitation and radiated noise from the propeller. These considerations have been brought about by the increases in power transmitted per shaft and the use of after deck. Other constraints on design have emerged in response to calls for energy conservation and atmospheric emissions reduction, as witnessed by the introduction of the EEDI requirements and MARPOL Annex VI.

Ducted Propellers Ducted propellers consist of two primary components, an annular duct with an aerofoil cross-section and a propeller that has been modified to account for the presence of the duct. The duct can have certain asymmetric features to optimize performance, but symmetric ducts are more prevalent due to manufacturing costs. These propellers can be either fixed or controllable pitch and are sometimes used as a contrarotating pair in special applications. Ducted propellers are suitable for high thrust at low or zero ship speed, such as in towing and trawling situations. The contribution of the duct to the propulsor's total thrust at zero ship speed is about 50%. There are two nominal types of duct form, accelerating and decelerating duct. The choice of the duct form for a particular application must be balanced against practical manufacturing problems. Many standard and proprietary duct forms are available, but those most commonly selected are shown in 3.2.

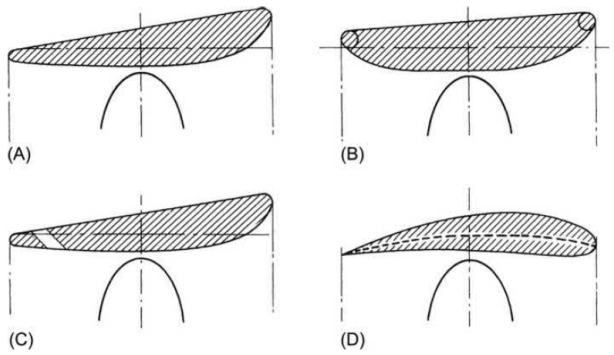

Figure 3.2: Ducted Propellers, from [2]

Ducted propellers are commonly used in remotely operated underwater vehicles (ROVs)

due to their numerous advantages. The duct surrounding the propeller increases the efficiency of the system by improving the thrust generated and reducing the losses from turbulence and flow separation. This leads to improved maneuverability, faster acceleration, and greater operational depths. In addition, the ducted design also protects the propeller from damage, which is particularly important in harsh underwater environments where rocks, debris, and other obstacles can cause serious damage to exposed propellers. Overall, ducted propellers have become a popular choice in ROVs due to their superior performance, reliability, and protection.

Podded and Azimuthing Propulsors Podded and azimuthing propulsors are a commonly used propulsion systems in marine applications. Azimuthing thrusters can be configured as nonducted or ducted propellers and classified as pusher or tractor units. Azimuthing propulsors have the engine or motor located in the ship's hull, connected to the propeller shaft through a mechanical drive system. On the other hand, podded propulsors have an electric motor directly coupled to the propeller shaft and supported by rolling element bearing systems. Podded propulsors typically utilize fixed pitch propellers and have found extensive use in cruise ships and ice breakers due to their maneuvering capabilities. Tractor arrangements of podded and azimuthing propulsors in a twin screw configuration offer improved inflow velocity field compared to conventional shafting arrangements, leading to reduced cavitation activity. However, these propulsors may exhibit broadband excitation characteristics that should be minimized during the design process. When multiple podded or azimuthing propulsors are used together, care should be taken to avoid mutual interference, as it can induce fluctuating forces, moments, and vibrations on the shaft system.

In the realm of Remotely Operated Vehicles (ROVs), podded propulsors are commonly employed for several reasons. Firstly, ROVs are often used for underwater operations that require precise maneuverability and control. Podded propulsors offer exceptional maneuvering capabilities, allowing ROVs to navigate through complex underwater environments with ease. The direct coupling of an electric motor to the propeller shaft in podded propulsors provides quick and accurate response to control inputs, enabling ROV operators to perform intricate tasks effectively.

Secondly, podded propulsors are known for their compact design and streamlined shape. ROVs are typically compact vehicles that need to operate in confined spaces and navigate through narrow passages. The compact size of podded propulsors allows for better integration within the ROV structure, minimizing the overall hydrodynamic drag and maximizing the vehicle's agility.

Moreover, podded propulsors offer a high degree of hydrodynamic efficiency. ROVs often operate in challenging and dynamic underwater conditions, where energy efficiency is crucial. Podded propulsors, with their streamlined design and optimized propulsion system, provide improved hydrodynamic performance, reducing energy consumption and extending

the operating range and endurance of the ROV.

Additionally, the use of podded propulsors in ROVs allows for easier maintenance and replacement. Since the electric motor and propeller are housed within a self-contained unit, they can be readily accessed and replaced if necessary. This modular design simplifies maintenance procedures and reduces downtime, ensuring that ROVs can quickly resume their missions.

Overall, the selection of podded propulsors in ROVs is driven by their maneuverability, compactness, hydrodynamic efficiency, and ease of maintenance. These factors contribute to the successful operation of ROVs in diverse underwater environments, enabling them to perform a wide range of tasks, including underwater inspections, research, exploration, and even subsea intervention activities.

Contrarotating Propellers Contrarotating propulsion systems offer hydrodynamic advantages by recovering rotational energy from the slipstream, which would otherwise be lost in conventional single-screw systems. In marine applications, the aft propeller is typically smaller in diameter than the forward propeller to account for slipstream contraction. The blade numbers also differ, with four blades for the forward propeller and five blades for the aft propeller. Additionally, contrarotating propellers provide torque balancing capabilities, which is crucial for control stability in torpedo and similar propulsion systems.

Contrarotating propulsion systems are not commonly used in small observatory underwater ROVs. This is primarily due to their complex design and higher cost compared to other propulsion systems. Small ROVs used for observational purposes typically prioritize maneuverability, compact size, and cost-effectiveness. While contrarotating propellers offer advantages in torque balancing and efficiency, their implementation in small ROVs may not justify the added complexity and cost, as other propulsion systems can adequately meet the requirements of these specific applications.

Controllable Pitch Propeller The controllable pitch propeller (CPP) has gained popularity in various propeller types and arrangements, except for podded propulsors, contrarotating propellers, and tandem propellers. It offers advantages such as fine thrust control, maneuverability, and the ability to adjust operational conditions without altering propulsion machinery speed. The CPP's ability to feather the propeller blades is beneficial for double-ended ferries, small warships, and vessels with hybrid propulsion systems. These propellers have different pitch actuating mechanisms, categorized as inboard and outboard hydraulic actuation. The hub of a CPP needs to be robust to withstand propulsive forces and often has a larger diameter than fixed pitch propellers. While certain specialized CPP designs exist, such as self-pitching and Pinnate propellers, their usage has been limited to smaller craft.

In small observatory underwater remotely operated vehicles (ROVs), the utilization of controllable pitch propellers (CPP) is generally limited. This is mainly due to the specific operational requirements and constraints of ROVs in scientific research and exploration mis-

sions. In fact, as mentioned below, small observatory ROVs typically prioritize precise maneuverability, stability, and low acoustic signature, which are achieved through other propulsion systems such as electric thrusters or ducted propellers. These alternative propulsion systems offer advantages such as compact size, enhanced maneuvering in confined spaces, reduced noise levels, and improved hydrodynamic performance for close-up inspections and delicate sampling tasks. Therefore, while CPPs are widely employed in various marine applications, their adoption in small observatory ROVs is relatively uncommon due to the specialized nature of ROV operations.

Thruster Systems Thrusters are typically used in underwater ROVs that require high maneuverability and precise control. They work by generating thrust through the rotation of a set of blades. There are several types of thrusters available, including tunnel thrusters, azimuth thrusters, and vectored thrusters. Tunnel thrusters are mounted in a tunnel on the side of the ROV and can be rotated to generate thrust in any direction. Azimuth thrusters are similar to tunnel thrusters but are mounted on a swivel that allows for even greater maneuverability. Vectored thrusters use a set of rotating blades to generate thrust in any direction, making them highly maneuverable but less efficient than other types of thrusters.

Other Propulsion Systems Other propulsion systems that are less commonly used in underwater ROVs include pump-jets and impellers. Pump-jets work by drawing water into a chamber and then expelling it through a nozzle to generate thrust. Impellers use a set of rotating blades to move water and generate thrust. These systems can offer advantages in specific applications but are less versatile than other types of propulsion systems.

In addition to the type of propulsion system used, other factors that can affect performance include the size and shape of the vehicle, the weight of the payload, and the depth of operation. Ultimately, the choice of propulsion system for an underwater ROV will depend on the specific needs of the project, including the required level of maneuverability, efficiency, and noise level.

3.2.2 Observatory ROV Propulsion Systems

In observatory ROVs, the propulsion system is typically selected based on the specific requirements of the mission. For example, if the ROV is required to perform close-up inspections of underwater structures, a thruster system may be used to provide precise maneuverability and control. If the ROV is required to perform long-range surveys, a propeller system may be used to provide greater efficiency and range. Additionally, the type of propulsion system used will depend on factors such as the size and shape of the vehicle, the weight of the payload, and the depth of operation. Although our ROV's recording tasks are relatively general, we have defined some target specifications. Therefore, we will examine similar ROVs that meet these specifications and evaluate their propulsion systems.

In general, observatory ROVs are equipped with vectorized thrusters, which can vary in terms of number, size, degrees of freedom, and specific thruster positioning.

3 Thrusters Configuration The three-thruster configuration is widely utilized and cost-effective for underwater remotely operated vehicles (ROVs). This configuration consists of two horizontal thrusters and one vertical thruster. The primary function of the horizontal thrusters is to control the ROV's surge (forward and backward movement) and yaw (rotation around the vertical axis). On the other hand, the vertical thruster is employed either for controlling the ROV's heave (vertical movement) directly or for managing the pitch (rotation around the transverse axis). By adjusting the pitch, the ROV's depth can be controlled by utilizing the surge motion. This configuration provides effective maneuverability and control over the ROV's movements in various underwater operations. The example depicted in Figure 3.3 illustrates a ROV equipped with a tri-thruster configuration.

Figure 3.3: 3 Thrusters Configuration

4 Thrusters Configuration (Heave and Pitch Control) In this configuration, the observatory ROV is equipped with two horizontal thrusters for surge and yaw control. Additionally, it features two vertical thrusters positioned on the same longitudinal axis. The purpose of this configuration is to provide control over heave (vertical movement) and pitch (rotation around the transverse axis). By adjusting the thrust produced by each vertical thruster, the ROV can control its vertical position in the water column and change its pitch angle. This configuration enables precise maneuverability and stability in tasks that require controlling vertical movement and pitch orientation, such as close-up inspections, data collection, or manipulating objects in underwater environments.
The image in Figure 3.4 illustrates a ROV with this configuration.

Figure 3.4: 4 Thrusters Configuration (Heave and Pitch Control)

4 Thrusters Configuration (Heave and Roll Control) In this configuration, the observatory ROV also has two horizontal thrusters for surge and yaw control. However, the two vertical thrusters are positioned on the transverse axis. This configuration allows the ROV to control heave (vertical movement) and roll (rotation around the longitudinal axis). By adjusting the thrust output of each vertical thruster, the ROV can control its vertical position and adjust its roll orientation. This configuration is useful in applications where precise control over heave and roll movements is required, such as underwater mapping, 3D modeling, or conducting research in marine ecosystems. Figure 3.5 showcases a ROV's layout featuring this 4 Thrusters Configuration.

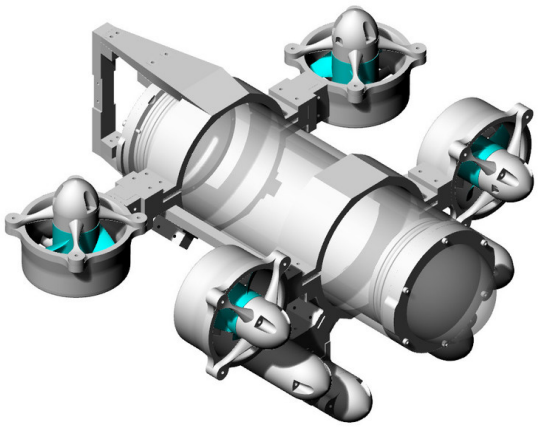

Figure 3.5: 4 Thrusters Configuration (Heave and Roll Control)

4-Horizontal Thrusters Configuration The 4-horizontal thrusters configuration is a highly versatile setup for underwater ROVs. It consists of four vectored horizontal thrusters that provide control over the three primary degrees of freedom: surge (forward and backward movement), sway (sideways movement), and yaw (rotation around the vertical axis). These four thrusters working together allow for precise maneuverability and agile navigation in various underwater environments.

In addition to the four horizontal thrusters, this configuration can include one or two vertical thrusters. The vertical thruster(s) serve to control the heave (vertical movement) of the ROV. If there is a single vertical thruster, it primarily focuses on controlling the heave alone, while the four horizontal thrusters handle the other movements. On the other hand, if there are two vertical thrusters, one of them can be dedicated to heave control while the other is utilized for controlling either roll (rotation around the longitudinal axis) or pitch (rotation around the transverse axis) in combination with heave.

The inclusion of one or two vertical thrusters in the 4-horizontal thrusters configuration adds an additional level of control and enables the ROV to perform complex maneuvers and maintain stability in varying underwater conditions. The specific placement and orientation of the vertical thruster(s) can be adjusted based on the desired control capabilities and operational requirements of the ROV.

Overall, the 4-horizontal thrusters configuration with one or two vertical thrusters offers enhanced maneuverability, precise control over multiple degrees of freedom, and the ability to adapt to different underwater tasks and environments. It is a popular choice for ROVs engaged in diverse underwater missions, including observation, inspection, research, and intervention. The image presented in Figure 3.6 serves as an illustration of a remotely operated vehicle (ROV) employing a 4-horizontal thrusters.

Vectored 6 Thrusters Configuration The vectored 6 thrusters configuration is a highly advanced setup that allows for precise control over all six degrees of freedom of an underwater ROV. This configuration consists of two horizontal thrusters oriented along the longitudinal axis, which control yaw and surge movements. Additionally, there are four thrusters, each providing components of thrust along the y and z axes, allowing for control over sway, pitch, roll, and heave.

The two horizontal thrusters, positioned along the longitudinal axis of the ROV, are responsible for controlling its yaw and surge movements. By independently adjusting the thrust of these thrusters, the operator can achieve precise rotation and forward/backward motion.

The remaining four thrusters are positioned in such a way that they provide thrust components along the y (sideways) and z (vertical) axes. By varying the thrust of these thrusters, different combinations of forces can be applied, resulting in control over sway (sideways movement), pitch (rotation around the transverse axis), roll (rotation around the longitudinal

Figure 3.6: 4-Horizontal Thrusters Configuration

axis), and heave (vertical movement).

The vectored 6 thrusters configuration enables the ROV to move in any direction within the water and maintain stability during complex maneuvers. By carefully adjusting the thrust output of each thruster, the operator can achieve precise control over the ROV's position, orientation, and movement.

This configuration is commonly used in advanced ROV systems, such as the FIFISH V6 ROV, to ensure exceptional maneuverability, versatility, and control. It is particularly beneficial for tasks requiring intricate navigation, precise inspections, and efficient data collection in challenging underwater environments.

In summary, the vectored 6 thrusters configuration includes two horizontal thrusters for yaw and surge control, along with four thrusters providing thrust components along the y and z axes for sway, pitch, roll, and heave control. This configuration offers precise maneuverability and control over all six degrees of freedom, allowing the ROV to perform complex tasks with ease and accuracy.

The configuration of a ROV utilizing six thrusters is exemplified in Figure 3.7.

8 Thrusters configuration This configuration which we can find in the Chasing M2 ROV exemplifies an advanced approach to control all six degrees of freedom with exceptional precision. It features eight thrusters arranged in a rectangular parallelepiped layout, where each thruster is strategically oriented with x, y, and z components. By synergistically combining the forces generated by these eight thrusters, the ROV achieves remarkable maneuverability and control over its surge, sway, heave, roll, pitch, and yaw. However, it is important to note that such enhanced control capabilities often come with a trade-off in terms of increased

Figure 3.7: Vectored 6 Thrusters Configuration

energy consumption. Nonetheless, the Chasing M2 serves as an excellent example of how this particular thruster configuration can be successfully employed to optimize maneuvering performance in underwater operations. The image shown in Figure 3.8 depicts a ROV with this configuration.

Figure 3.8: Vectored 8 Thrusters configuration

In summary, the choice of propulsion configuration for underwater remotely operated vehicles (ROVs) involves a careful consideration of several variables. We have explored various configurations, including the 3-thruster configuration, 4 vertical thrusters, vectored 6 thrusters, and the 8 thrusters configuration. Each configuration offers unique advantages and trade-offs in terms of maneuverability, control, energy consumption, and precision.

The number and orientation of thrusters directly impact the ROV's ability to control its six degrees of freedom, including surge, sway, heave, roll, pitch, and yaw. Configurations with two horizontal thrusters primarily control surge and yaw, while the addition of vertical thrusters enables control over heave, roll, or pitch. The arrangement of thrusters along different axes and their vectorial disposition further influences the ROV's capabilities.

It is important to note that the complexity of configurations increases with the inclusion of more thrusters, leading to enhanced control precision but also higher energy consumption. While we have covered several configurations in this discussion, it is worth mentioning that there are even more complex configurations employed in specialized ROVs.

Ultimately, the selection of the propulsion configuration depends on the specific requirements of the mission, including the desired maneuverability, control, energy efficiency, and operational constraints. Understanding the variables and their interplay allows ROV operators and designers to make informed decisions and optimize performance in various underwater operations.

3.3 Selection of Thruster Configuration

In the design of our propulsion system, we have been carefully evaluating two primary configurations: the 3 thruster configuration and the 4 thruster configuration. Initially, we chose the 3 thruster configuration based on its cost-effectiveness and energy efficiency, which align with our goal of providing an affordable solution with extended sailing time. However, during our evaluation process, we identified a potential weakness in this configuration related to the stability of the ROV in the rolling movement.

To address this concern and further enhance the performance of our ROV, we have been conducting a thorough assessment of the 4 thruster configuration. This configuration incorporates four thrusters, including two horizontal thrusters and two vertical thrusters, offering improved stability and control over the ROV's rolling movement. By strategically allocating counterbalancing forces, we aim to ensure a balanced and stable performance in all operational scenarios.

Alternatively, another solution to address the rolling problem would be to retain the 3 thruster configuration while introducing a rolling degree of freedom to the camera. By implementing counter-rolling mechanisms, we can maintain a horizontal stable image for the user, compensating for any rolling motion of the ROV.

Recognizing the significance of filming stability in underwater operations, we are dedicated to delivering a robust and reliable ROV to our customers. As we continue to evaluate and refine our propulsion system, the choice between the 3 thruster configuration and the 4 thruster configuration remains a focal point. We are rigorously assessing the technical feasibility, cost implications, and performance benefits of both options to make an informed decision that best aligns with our goals and customer requirements.

3.3.1 Energy Comparison

To assess the energy requirements for stabilizing the ROV, let's begin by estimating the energy consumption for each solution.

For the first solution, stabilizing the camera's rolling motion would involve employing a

servomotor, assuming our gyroscope functions correctly and provides real-time ROV orientation. The servomotor consumes 0.5A at 6V, resulting in a power consumption of **3W**.

In the case of the second solution, maintaining stability would necessitate the continuous operation of the two vertical propellers to counterbalance water disturbances. This would require the use of two DC motors, consuming approximately $\mathbf{2} \times \mathbf{5W}$.

While these estimations provide a general understanding, it is evident that the second solution would require significantly more energy compared to the first. Extracting 10W from our battery during a two-hour expedition would amount to approximately 40% of our total energy consumption if we're using a 3 Cells 4200mAh lipo battery.

It is important to note that these figures are estimates and may vary based on specific operating conditions. Nevertheless, they highlight the potential energy implications associated with each solution, aiding us in making informed decisions regarding our propulsion system design.

3.3.2 Cost Comparison

When comparing the costs of the two solutions, it becomes evident that the first solution is significantly more cost-effective than the second. The primary factors contributing to this cost advantage are the relatively lower prices of the actuators involved and the absence of motor sealing requirements, which are necessary in the second solution.

3.3.3 Other concideration

Furthermore, considering the observatory nature of our ROV and the filming requirements, the additional degree of freedom provided by the second configuration may not be necessary. By incorporating a rolling degree of freedom to the camera within the first configuration, we can effectively address the stability concerns without incurring the additional costs associated with the second configuration.

3.3.4 Conclusion

In conclusion, after carefully evaluating the two thruster configurations and considering our specific requirements for the ROV observatory mission, we have determined that the first configuration is the most suitable choice. This configuration offers several advantages, including cost-effectiveness, lower energy consumption, and sufficient capabilities to fulfill our objectives.

Furthermore, we have identified the opportunity to incorporate an additional degree of freedom, the pitch movement of the camera, within the chosen configuration. Even with this enhancement, the first configuration remains more efficient in terms of both energy usage and cost compared to the second configuration.

By selecting the first configuration, we can deliver a high-performance ROV that meets the stability and control requirements while maintaining affordability for our customers. This

strategic decision aligns with our goal of providing a reliable and cost-effective solution for underwater observations and reinforces our commitment to delivering a superior product in the market.

3.4 Sizing of the Rear Thrusters using OpenProp software

In order to correctly size the rear propellers, we will use the open source MIT code "OpenProp", which will enable us to design, simulate, and conduct a parametric study on different propellers to identify the one that best meets our specific requirements, and works best with the available motors in the market, while putting the cost and efficiency of the system as primary criteria.

But first, let's start by fixing all the design contraints and requirements.

3.4.1 Constraints and Requirements

To effectively size our propellers, we need to consider several important points. Firstly, the size of our propellers must fit within our dimensional limitations. To achieve this, we will fix their external diameter at 45 mm.

In addition to the dimensional constraints, our rear propellers must generate enough thrust to propel the ROV at a speed of 1.2 m/s. Therefore, they need to overcome the hydrodynamic forces calculated in the previous chapter. Each thruster should be capable of producing at least 0.15 N of nominal thrust.

Furthermore, it is crucial to ensure that the second thruster is the mirror-image of the first. Failure to do so could result in torque steering, which would cause the ROV to roll.

Finally, Our thrusters must operate at optimal efficiency and produce the required thrust at the motor's optimal rotation speed.

By considering these constraints and requirements, we can ensure that the selected rear propellers are appropriately sized, capable of providing the necessary thrust, and operate efficiently to meet the performance objectives of our ROV.

3.4.2 Introduction to OpenProp

OpenProp is a comprehensive software suite that facilitates the design, analysis, and fabrication of optimized propellers and horizontal-axis turbines. It employs a numerical model based on propeller lifting line theory, a widely utilized approach in parametric design codes employed by numerous commercial designers. The software is implemented using MATLAB M-code, providing a versatile platform for propeller and turbine design.

Furthermore, being open-source software, OpenProp offers the advantage of code modification to accommodate specific user requirements. This flexibility allows users to tailor the software to their specific needs, making it a valuable tool for propeller design and analysis. In our case, we made several modifications to address plotting errors, incorporate additional

features required for our design software compatibility, and meet our unique design requirements.

3.4.3 Background and Theory

In the document [3] published by MIT, the authors explain the theory behind the software and the equations used to calculate the propeller's performance. They first introduce the propeller lifting-line formulation. They enumerate the velocities involved in the propeller's motion and the forces acting on it, as shown in Figure 3.9.

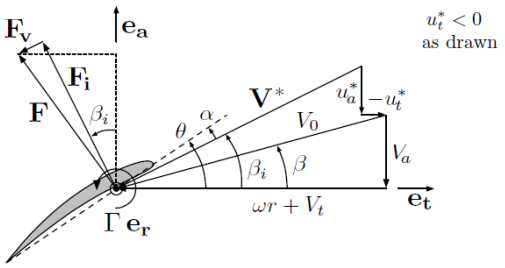

Figure 3.9: Propeller velocity/force diagram, as viewed from the tip towards the root of the blade. All velocities are relative to a stationary blade section at radius r. From [3]

Then, they use the Kutta-Joukowski lift force equation to calculate the lift force acting on the propeller blade and the momentum theory to calculate the thrust and torque forces. The equations are shown below:

$$F_i = \rho V^* \times (\Gamma e_r) \tag{3.1}$$

$$T = Z \int_{r_h}^{R} [F_i \cos(\beta_i) + F_v \sin(\beta_i)]\, dr\, (e_\alpha) \tag{3.2}$$

$$Q = Z \int_{r_h}^{R} [F_i \sin(\beta_i) + F_v \cos(\beta_i)]\, r\, dr\, (-e_\alpha) \tag{3.3}$$

Where F_i is the lift force, $F_v = \frac{1}{2}\rho(V^*)^2 C_D c$ is the viscous drag force, T is the thrust force, Q is the torque force, Z is the number of blades, R is the propeller radius, r_h is the hub radius, β_i is the inflow angle, ρ is the fluid density, V^* is the inflow velocity, Γ is the circulation, e_r is the radial unit vector, and e_α is the tangential unit vector.

OpenProp utilizes the standard propeller vortex lattice model to calculate the axial and tangential induced velocities. The software includes a propeller design optimization feature that allows users to optimize flow parameters and optionally optimize the chord distribution. Once the design operating state of the propeller/turbine is determined, the geometry can be established to achieve the desired performance. The 3D geometry is constructed by scaling and rotating given 2D section profiles based on the design lift coefficient, chord length, and inflow angle. The performance of the propeller can then be evaluated.

An important parameter that reflects the propeller's performance is its efficiency, which is defined as the useful power produced by the propeller divided by the power consumed by the propeller. The efficiency (η) can be calculated using the following equation:

$$\eta = \frac{TV_s}{Q\omega} \tag{3.4}$$

Where T represents the thrust, V_s is the ship speed, Q is the torque, and ω is the angular velocity."

It is not necessary to delve deeper into how the software works. What is important is to understand the limitations of the model.

In fact, the lifting line theory relies on the following assumptions:

1. The wing is infinitely long and straight.
2. The wing is thin.
3. The flow is two-dimensional and incompressible.
4. The flow is steady.
5. The wing is operating at a small angle of attack.
6. The wing is operating at a constant freestream velocity.
7. The wing is operating in a uniform freestream.
8. The wing is operating at a constant density.
9. The wing is operating at a constant temperature.
10. The wing is operating at a constant viscosity.
11. The wing is operating at a constant pressure.

These assumptions are discussed further in the introduction of the article [11]. Understanding these limitations is essential to appropriately use the OpenProp software for propeller design and analysis.

3.4.4 software interface

In the single design mode of OpenProp 3.3.4, users are provided with a user-friendly interface that allows them to input the necessary parameters for designing a propeller. The main menu offers options to specify the operating conditions such as the fluid density, rotational speed, and advance coefficient. Users can also define the desired propeller geometry by inputting parameters such as the number of blades, diameter, and blade section profiles. Additionally, users can set constraints and objectives for the design, including maximum efficiency or thrust requirements. By providing these inputs, users can initiate the design process and generate optimized propeller designs based on the given parameters and constraints. We can see the user interface in the Single Design mode in Figure 3.10.

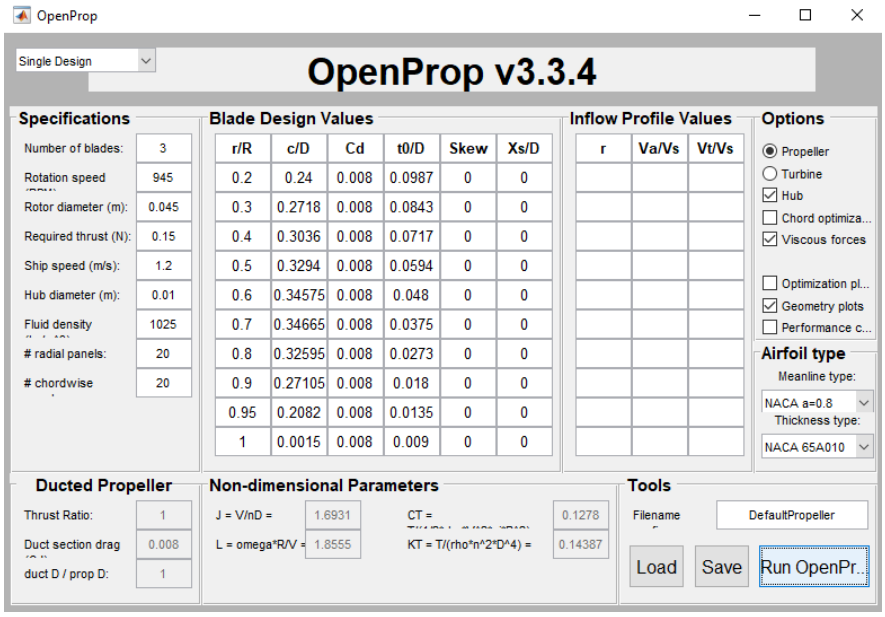

Figure 3.10: OpenProp V3.3.4 single design mode user interface

In the parametric study mode of OpenProp 3.3.4, users can explore the performance characteristics of propellers by varying multiple input parameters simultaneously. The interface allows users to specify ranges and step sizes for various design parameters such as diameter, pitch, and blade area ratio. Users can also define the ranges for operating conditions such as rotational speed and advance coefficient. By setting up these parameter ranges, users can initiate the parametric study and generate a series of propeller designs, each corresponding to a unique combination of the specified parameters. The software then evaluates the performance of each design and provides comprehensive results, allowing users to analyze the effects of different parameters on propeller performance and make informed design decisions. We can see the user interface in the Parametric Study mode in Figure 3.11.

3.4.5 Workflow and optimization methodology

- Input parameters :
  Our input parameters for the rear propellers as mensioned in the Constraints and Requirements section are as follows:

Table 3.1: Input parameters for the rear propellers

Parameter	**Value**
Rotor diameter (m)	0.045
Hub diameter (m)	0.01
Required thrust (N)	0.15
Ship speed (m/s)	1.2
Fluid density (kg/m^3)	1025

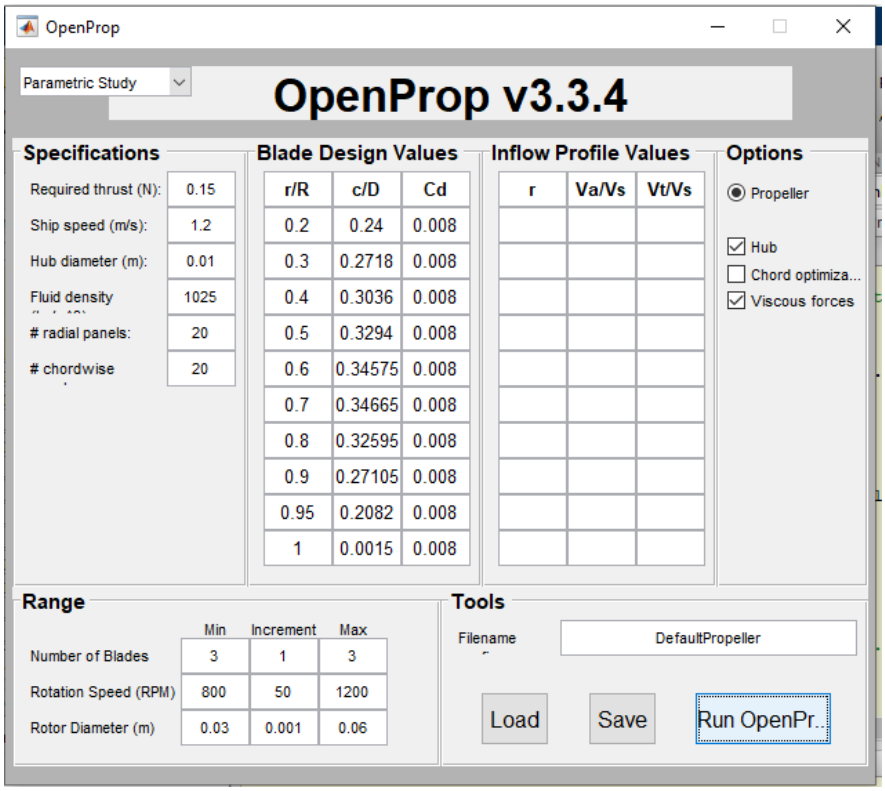

Figure 3.11: OpenProp V3.3.4 parametric study mode user interface

- Geometric optimization:
  OpenProp 3.3.4 offers a Chord Optimization feature that adjusts the chord length of each section of the propeller to maximize its efficiency. Initially, we experimented with this feature by conducting single design tests with and without chord optimization. While varying the rotation speed, we observed that the maximum efficiency achieved was 0.85 with chord optimization at a relatively high RPM of around 2000 RPM, compared to 0.81 without chord optimization at 945 RPM.

  However, we encountered a problem when enabling chord optimization. At high RPM where the maximum efficiency was achieved, the optimizer reduced the chord length to maintain the same thrust. This led to excessively thin blades that could not withstand the mechanical stresses in real working conditions. The resulting geometry is depicted in Figure 3.12.

  So we decided not to use the chord optimization feature in our design. Instead, we will keep the default chord and thickness distributions and multiply them by factors to improve the mechanical strength of the propeller. This decision is based on the fact that the default values are intended for relatively larger metallic boat propellers, which have lower relative thickness compared to ROV plastic propellers.

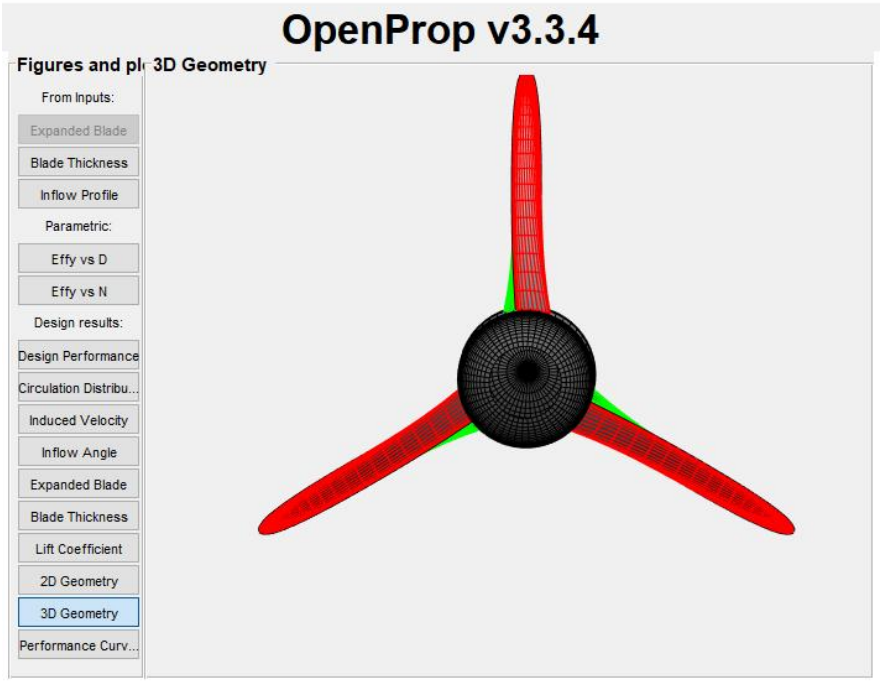

Figure 3.12: Resulted geometry with Chord optimization at maximum efficiency

- Parametric study:
  Here we are varying the blade number , rpm and propeller diameter, and plot the resulted efficiency to see what parameters best works for our diameter of 45mm.
  The results are plotted in the figure 3.13. As we can see, for the range of rpm we choose, in the 3 and 4 blades propellers we find the value of 45 mm diameter in the center of the max efficiency points, and the 3 blades propellers have a relatively higher efficiency than the 4 blade propellers, for the 2 blade propellers the interval is a little bit to the right, the center of our values interval is around 50mm diameter.
  So as a result the 3 blade propeller seems to be the best option for our case.
  After choosing the 3 blade propeller we determined the best rpm for the 45mm diameter with our inputs and it was 950 rpm with an efficiency of 80.4% as we can see in subfigure 3.13d.

  The resulted geometry is shown in the figure 3.14, and it's performance calculated by OpenProp is shown in 3.15

- Choosing the motor :
  The motor that we choose for our rear thruster must produce the required torque to move the propeller plus overcome the mechanical garniture resisting torque (around 10mN.m), it's rated speed must be around 950 rpm. There are many Brushed Planetary Gear Motor that have these specefications.

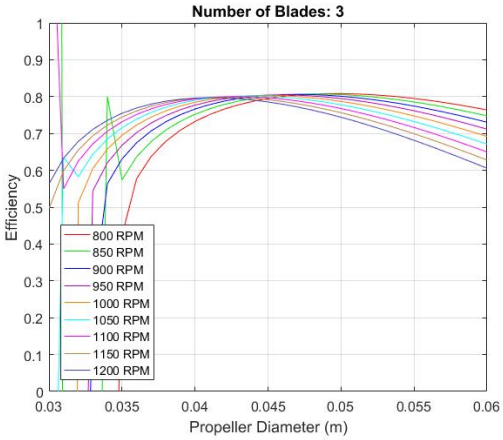

(a) Parametric study for 3 blades propeller

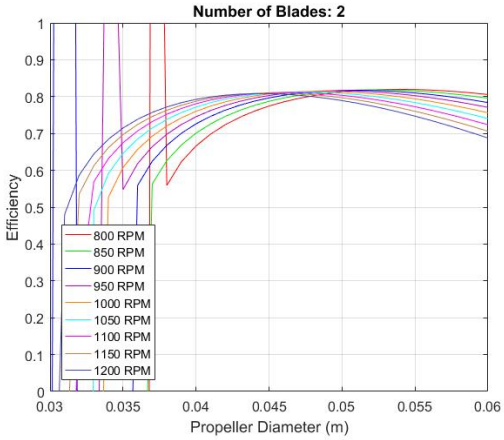

(b) Parametric study for 2 blades propeller

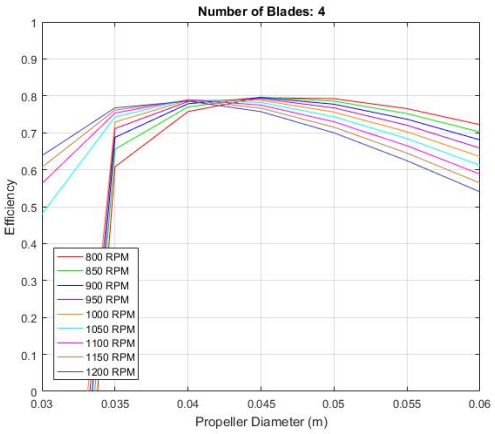

(c) Parametric study for 4 blades propeller

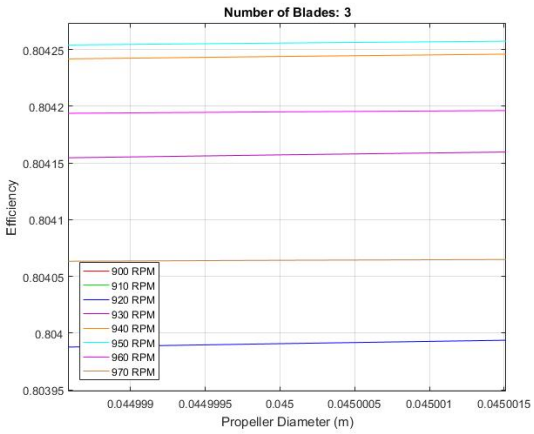

(d) RPM Optimisation

Figure 3.13: OpenProp V3.3.4 parametric studies for different blade configurations

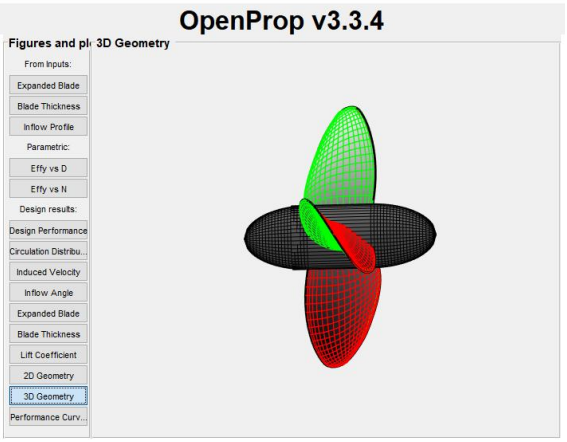

(a) 3D geometry

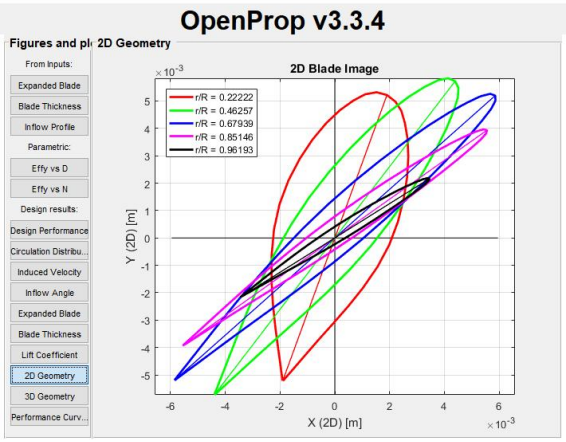

(b) 2D geometry

Figure 3.14: Final propeller geometry

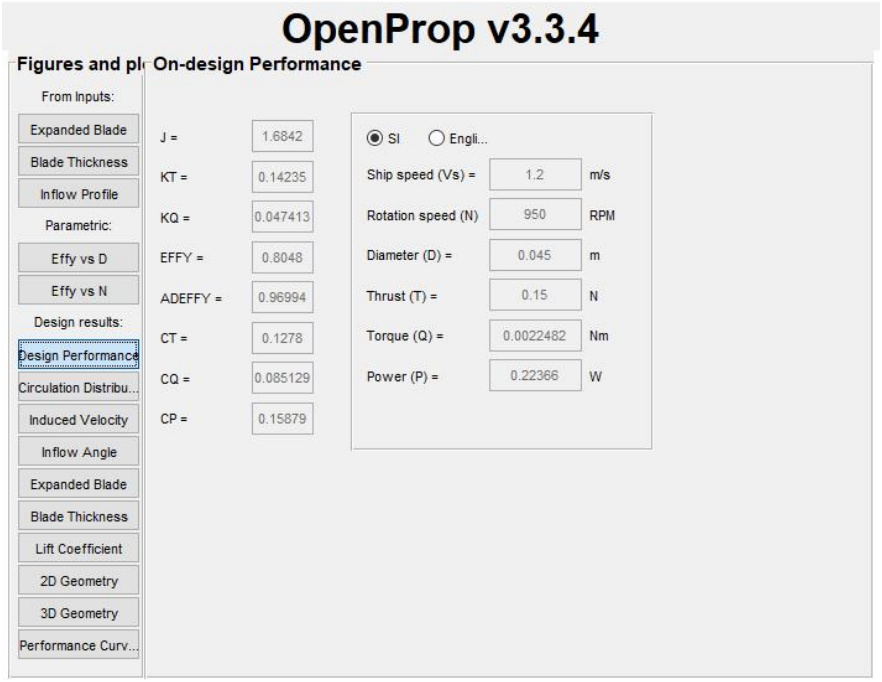

Figure 3.15: Design performance

3.5 CAD model of the propeller

OpenProp generates text files containing the coordinates of the generated propeller sections. These text files provide the necessary data for further propeller design and manufacturing processes. By utilizing these files, we can proceed with the conception and construction of our propeller, using the generated section points as a reference.

To illustrate this process, Figure 3.16 showcases a matrix of 8 pictures, each representing a different step of the conception.

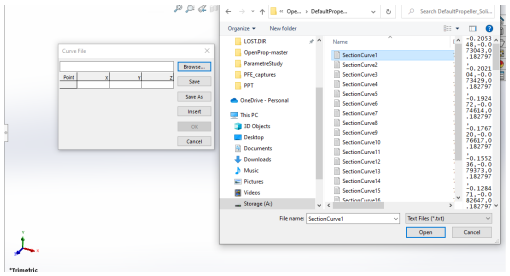

(a) Creating a curve with x,y,z coordinates

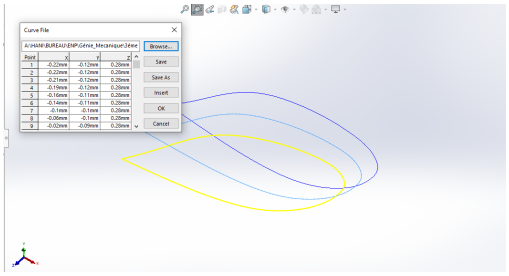

(b) Importing the text file and validate

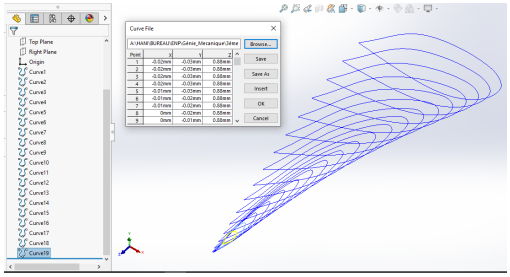

(c) Repeat the operation for the 20 sections

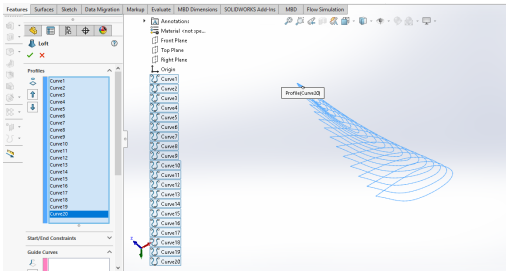

(d) Select all the curves

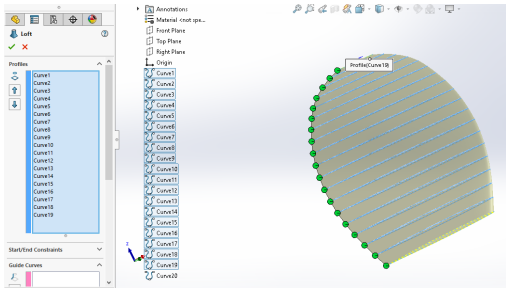

(e) Create a Loft volume using all the curves

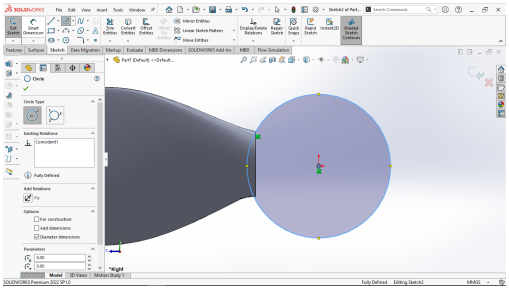

(f) Extruding a hub to the propeller

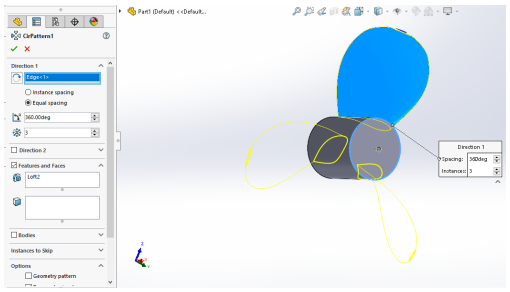

(g) Using a circular pattern to create the two other blades

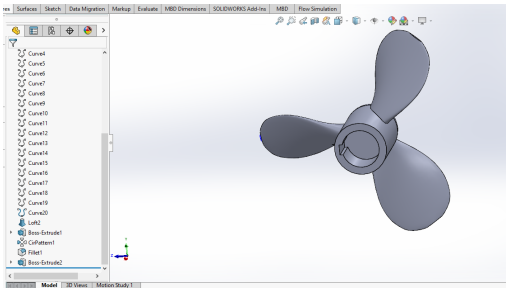

(h) Cuting the shaft mount in the hub

Figure 3.16: Propeller conception

3.6 Simulation and Validation of Propeller Performance using FLUENT

3.6.1 Background and Introduction

After designing the propeller, it becomes imperative to evaluate its performance. However, traditional experimental testing is often costly and time-consuming. To address this challenge, computational fluid dynamics (CFD) simulations are widely employed by researchers and engineers to model propeller performance.

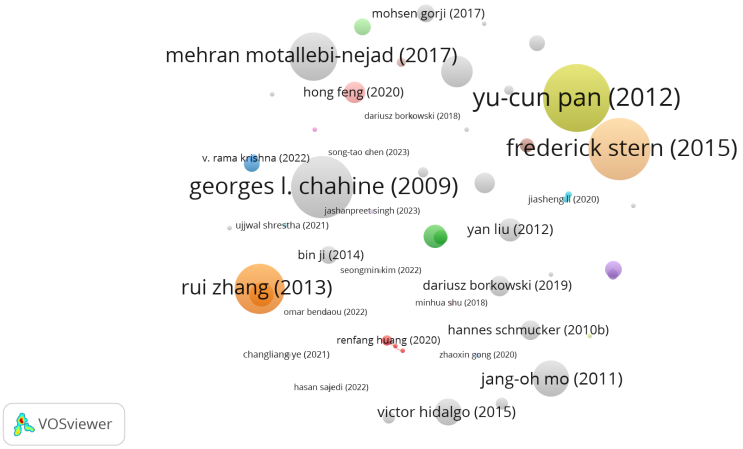

Figure 3.17: A Map of the scholarly work around hydro numerical analysis of propellers. Drawed with VOSViewer, with data from lens.org

We conducted an extensive bibliometric analysis of scholarly works related to hydro numerical analysis of propellers. Among the notable findings, Ansys Fluent emerged as the most frequently used software for such simulations. Figure 3.17 depicts a citation analysis map of the previously mentioned scholarly works, wherein each circle corresponds to a work, and its diameter is proportional to the number of citations received. Some highly cited documents include [12], who performed Reynolds-Averaged Navier-Stokes (RANS) simulations on the SUBOFF submarine model; [13], who employed the ANSYS-CFX solver to predict hydrodynamic forces on a pumpjet propulsion system; [14], presenting a study of a new RANS turbulence model for drag-reducing flows; [15], which investigated cavitating flow within a slanted axial-flow pump; and finally, [16], which offers an overview of recent CFD progress in naval architecture and ocean engineering.

Noteworthy works with substantial similarities to our study include Krishna et al., 2022 [17], Schmucker et al., 2010 [18], Yan et al.,2012 [19], Sahili et al., 2018 [20], J. Zhang et al., 2020 [21], and Bennaya et al., 2013 [22], all contributing to the field of numerical analysis of propellers.

These findings underscore the relevance and significance of our work within the broader context of hydro numerical analysis of propellers. In the subsequent sections, we detail our approach to simulating and validating the performance of the designed propeller using Ansys Fluent.

3.6.2 Ansys Fluent

Fluent is a powerfull CFD software package written in the C language. It is used to solve a wide variety of problems in fluid dynamics and heat transfer. The package is based on the finite volume method, which is a numerical method for solving the differential equations that describe fluid flow [9].

3.6.3 Hydrodynamic performance of propeller

Thrust and moment values are directly computed from fluid flow analysis. Thrust coefficient, moment coefficient, and efficiency are then calculated using Eqs. 3.5, 3.6, and 3.7 respectively for various operating conditions in this study.

$$K_T = \frac{T}{\rho n^2 D^4} \tag{3.5}$$

$$K_Q = \frac{Q}{\rho n^2 D^5} \tag{3.6}$$

$$\eta = \frac{J}{2\pi} \cdot \frac{K_T}{K_Q} \tag{3.7}$$

$$J = \frac{V}{nD} \tag{3.8}$$

Where ρ is the fluid density, n is the propeller rotational speed in rps, D is the propeller diameter, T is the thrust, Q is the torque, V is the rov velocity, and J is the advance ratio.[17]

The hydrodynamic performance of the propeller is evaluated by varying the advance ratio, J. In our case we fixed the ship speed to $1.2m/s$ and varied the rotational speed from 1000 to 3200 rpm, which gives us an advance ratio ranging from 0.5 to 1.6.

3.6.4 Workbench Setup

Ansys Workbench is an integrated Simulation that includes a Wide range Of Systems in the toolbox Including analysis systems. component systems. custom systems, and design exploration [9].

Now from the toolbox, we will drag a fluent file to the workbench window, as shown in the figure 3.18. And then we save our project.

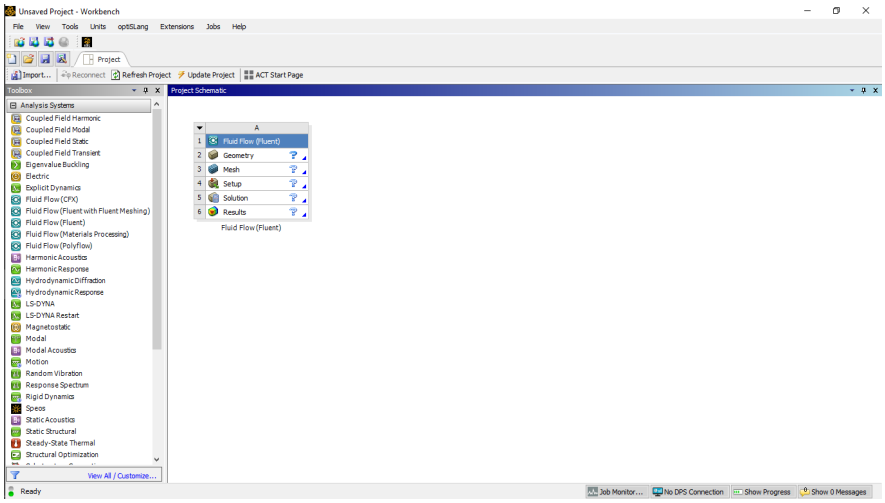

Figure 3.18: Opening Fluent from the toolbox in Ansys Workbench

3.6.5 Geometry

In the geometry tab, we will import our propeller geometry, and then right clic on it and open it with design modeller.

The geometry for the Fluid Flow (Fluent) study project can be edited either using DesignModeler or alternatively using SpaceCIaim. DesignModeler is a parametric modeler designed to draw 2D sketches and model 3D CAD parts. Ansys DesignModeIer has nine different toolbars as listed in Table 1.2 of [9].

The entire computational fluid region is divided into two domains. One is a stationary cylindrical domain and the other is a rotational cylindrical domain that surrounds the propeller.[17]

In our case, we initiated the process by importing the geometry that had been previously developed. This imported geometry was then opened within the DesignModeler software environment. The subsequent steps involved the creation of two primary enclosures to define the distinct fluid domains in our simulation.

The first enclosure was established to delineate the rotating fluid domain, while the second enclosure was introduced to define the stationary fluid domain. Employing boolean operations, we executed the following steps:

Subtracted the volume of the propeller from the smaller cylinder. This operation effectively retained only the region where the fluid would reside during the simulation.

Subtracted the smaller cylinder from the larger one, completing the division of the fluid domains.

As a result, two distinct domains emerged: "disc" and "medium," each representing the designated fluid regions for analysis. These domains are essential for accurately capturing the fluid dynamics within our simulation.

For visual clarity, Figure 3.19 illustrates the dimensions of the two enclosures that form the foundation of the "disc" and "medium" fluid domains. These geometric preparations lay the groundwork for our subsequent simulation setup and analysis phases.

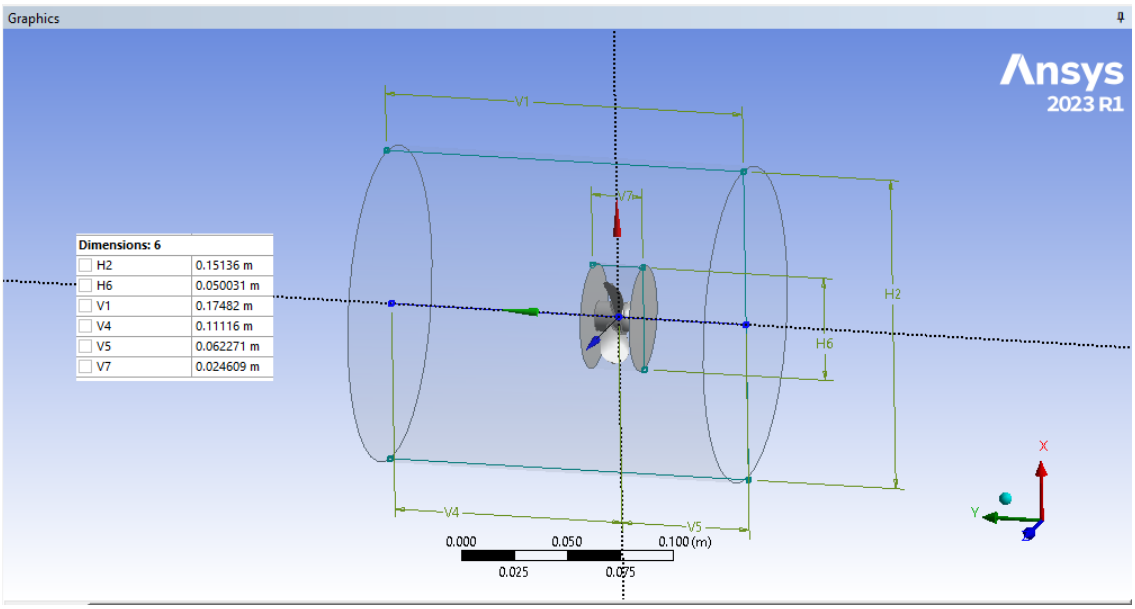

Figure 3.19: The final geometry of the propeller in DesignModeler

3.6.6 Meshing

In the meshing phase, we utilize the "Meshing" tab within the workbench window to create meshes for each distinct domain. Employing the "Mesh" option, we generate meshes that correspond to specific volumes. Three face sizing constraints are incorporated to ensure optimal mesh quality.

1. The first sizing constraint is applied to the inner surface of the "medium" volume, designated as "propeller surface" (earlier named "prop"). In this region, the element size is set to $0.5mm$.

2. The second sizing constraint targets the outer cylindrical surface of the aforementioned "medium" volume.

3. The third sizing constraint is focused on the internal cylindrical surface of the "disc" volume, which is essentially analogous to the previous constraint but on the opposite side of the second domain. Here, we assign an element size of $1mm$, and the same goes for the previous one.

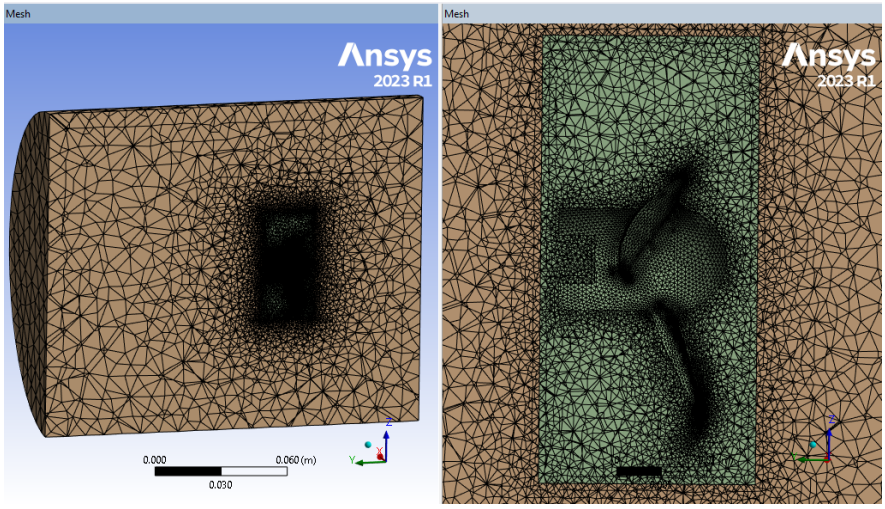

Figure 3.20: Section plane views of the resulting mesh of our geometry

Additionally, we establish an overarching maximum element size of $10mm$. The resulting mesh is presented in Figure 3.20, comprising a total of 1,371,178 cells. Specifically, the "medium" zone contains 1,090,473 tetrahedral cells, while the "disc" zone encompasses 280,705 tetrahedral cells.

It's worth noting that tetrahedral cells are employed throughout the fluid domains of this analysis. This choice is influenced by the intricate geometry of the propeller, which necessitates the use of tetrahedral cells to accurately capture complex details and interactions between the fluid and solid surfaces. Notably, the "medium" zone contains a higher number of elements despite being smaller in volume. This outcome can be attributed to the presence of the propeller within this zone, which introduces both fluid-solid interactions and intricate propeller features into the mesh.

This comprehensive meshing strategy is essential to accurately simulate the fluid dynamics and interactions within the propeller system. The subsequent sections will delve into the simulation setup and results analysis, providing a comprehensive assessment of propeller performance.

3.6.7 Simulation Setup

In the simulation setup, a steady-state approach was chosen, and the k-ω SST turbulence model was employed due to its well-established accuracy in propeller simulations [23]. The "medium" zone was designated as the rotating zone, with angular velocity varied for each simulation. The fluid used in both zones was seawater.

For the boundary conditions, an effort was made to replicate conditions the propeller would encounter during operation at a depth of 50 meters. To achieve this, a velocity-inlet boundary condition was employed with a velocity of 1.2 m/s, complemented by a pressure-outlet boundary condition. Both these boundary conditions featured a gauge pressure of 5 bars.

Concerning the external wall, a shear stress of -0.00612 Pa was specified in the direction of flow. This configuration aimed to replicate the shear force resulting from water viscosity.

In order to control the convergence of the calculations, the residual values were set to 1e-3. The simulation was run for 1000 iterations, and the results were analyzed using the post-processing tools available in Ansys Fluent.

3.6.8 Results Analysis

The figures 3.21 and 3.22 below display the outcomes of the simulations. Figure 3.21 illustrates the relationship between power consumption and generated thrust with respect to rotational speed, while figure 3.22 portrays the hydrodynamic coefficients in relation to rotational speed.

Analyzing the hydrodynamic coefficients, it is evident that our propeller exhibits favorable characteristics. The thrust coefficient showcases a relatively higher value compared to the torque coefficient. Both coefficients display a linear variation concerning the advance ratio, which indicates that controlling thrust through RPM adjustments will be straightforward. Despite reaching a peak of 0.36, the efficiency, although seemingly modest, is noteworthy for miniaturized plastic propellers. Manufacturers often emphasize power consumption as it conveys a more tangible value, as discussed further in the analysis of figure 3.21.

Upon comparing these results with those obtained from OpenProp, notable similarities exist in the thrust coefficient for corresponding advance ratios. However, the torque coefficient is slightly elevated, and the efficiency slightly diminished. This outcome was anticipated, given that OpenProp excels in generating optimal geometry for specified parameters, as evidenced in the thrust coefficient. Nevertheless, due to the reliance on numerous assumptions, OpenProp's estimation of efficiency tends to deviate from experimental values. Ansys Fluent, renowned for its reliability in performance evaluation per various scholarly sources, often yields lower efficiency estimations in higher advance ratios, suggesting the potential for even higher efficiency values in lower RPMs [17].

Shifting our focus to the power consumption and the relationship between generated

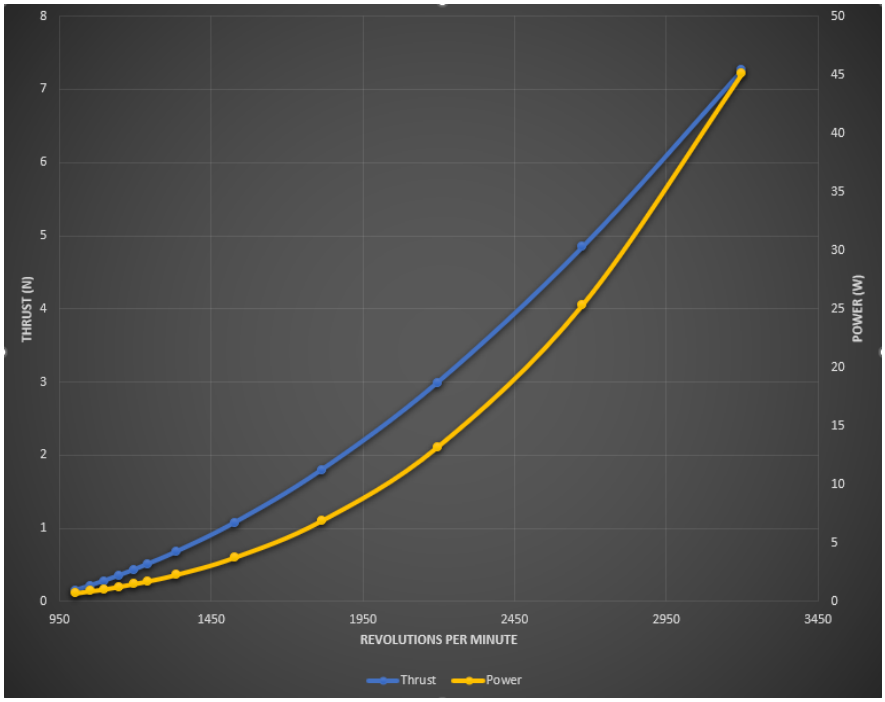

Figure 3.21: The power consumption and the generated thrust function of the rotational speed

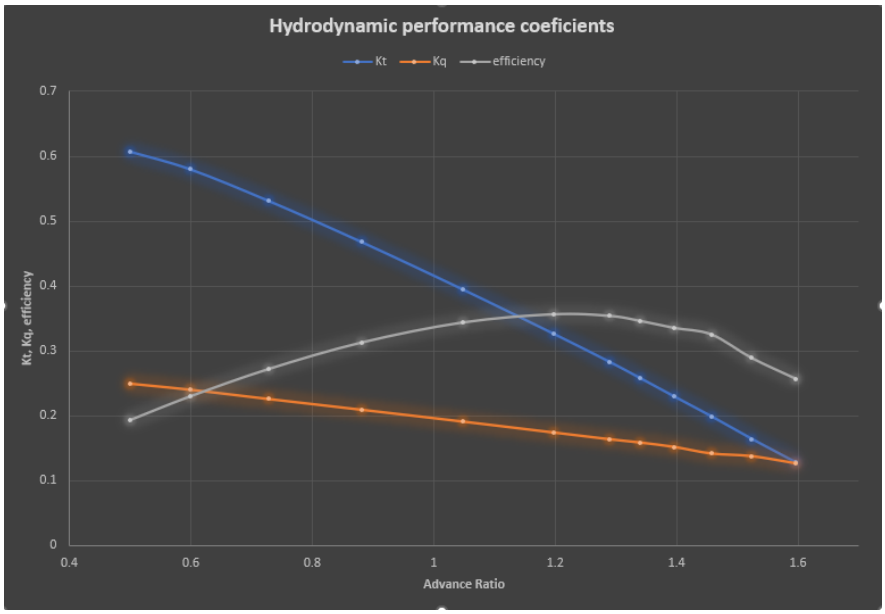

Figure 3.22: The hydrodynamic coefficients function of the rotational speed

thrust and rotational speed, two key observations arise. Firstly, the linearity of the thrust, previously highlighted, enhances the ROV's controllability. Secondly, in terms of power consumption, it is noticeable that RPMs below 2000 result in consumption below 10 watts, a favorable metric for our application. Correspondingly, the propeller generates a bit over 2N of thrust, and its minimum thrust of 0.15N is attained at 1000 RPM. The optimal efficiency point emerges at around 1350 RPM, producing a thrust of 0.7N and consuming 2.3 watts.

3.6.9 conclusion

In this section, we embarked on a thorough exploration of our designed propeller's performance using computational fluid dynamics (CFD) simulations through Ansys Fluent. This approach, as we have demonstrated, offers a cost-effective and efficient means of evaluating propeller performance, bypassing the traditional experimental testing that can be both resource-intensive and time-consuming.

Our bibliometric analysis revealed Ansys Fluent as a prevalent and reliable choice for conducting hydro numerical analyses on propellers. With a foundation rooted in the finite volume method, Fluent serves as a robust platform for solving complex fluid dynamics and heat transfer problems, crucial for our endeavor [9].

The assessment of hydrodynamic performance through thrust coefficient, moment coefficient, and efficiency measurements provides a comprehensive understanding of how the propeller interacts with the fluid medium. Through diligent simulation and calculation using fundamental equations, we garnered valuable insights into the propeller's behavior across various operating conditions. Our findings unveiled a thrust coefficient that demonstrates a promising linear relationship with the advance ratio, contributing to enhanced controllability. Furthermore, despite modest-seeming efficiency values, we underscored their significance, especially within the context of miniaturized plastic propellers.

Comparisons with OpenProp, while confirming certain similarities, also highlighted the nuanced differences that arise due to OpenProp's reliance on assumptions in efficiency estimations. Ansys Fluent, on the other hand, demonstrated its prowess in performance evaluation, often presenting more accurate efficiency estimations, albeit with potential variations in different RPM ranges [17].

Additionally, our meticulous setup involving geometry development, boundary conditions replication, and meshing strategies ensured that our simulations captured the intricate dynamics of the propeller within the fluid medium. The generated meshes, comprising tetrahedral cells, played a pivotal role in accurately simulating these complex interactions. Our results reinforced the propeller's viability for various RPM ranges and illuminated the power consumption dynamics and thrust generation, essential for ROV operation.

In conclusion, this sub-section represents a significant stride in our project journey. By integrating theoretical insights, software tools, and careful analysis, we've obtained valuable performance data for our propeller. This information not only validates our design choices but also lays a solid foundation for optimizing the propeller's efficiency and controllability as we continue to refine our ROV's capabilities.

3.7 Fabrication and assembly of the thruster

3.7.1 3D printing the propeller

For the prototype we will use the 3d plastic printing process to make the propeller, 3.23 enumerate the process steps.

We have chosen to use PETG filament for several reasons. PETG is well-known for its outstanding impact resistance, durability, and flexibility, which are crucial characteristics for our application as propellers are susceptible to debris impact. It offers higher tensile strength and chemical resistance, along with low moisture absorption, making it an excellent choice for underwater use. PETG is also easier to print compared to other materials, displaying minimal warping tendencies and accommodating a wide range of printing conditions. It provides glossy and transparent surface finishes that can be further enhanced through polishing or sanding, which is particularly important for propellers as surface smoothness directly affects efficiency. Although PETG is non-biodegradable, it is recyclable, adding to its appeal as one of our top choices for manufacturing our propellers. For more details, refer to [24] and [25].

3.7.2 Sealing the motor-propeller assembly

The motors in our ROV are meticulously safeguarded within a hermetically sealed enclosure (will be discussed in the fifth chapter), ensuring their imperviousness to water ingress. Nevertheless, the task of establishing a watertight connection between the propellers and the motors presents a formidable challenge, as the propellers necessitate submersion while upholding the motor's protective integrity. To surmount this challenge, we have implemented a specialized solution known as mechanical seals or garniture seals, as illustrated in Figure 3.24. These seals are affixed securely to the motor's sealed enclosure, facilitating the passage of the motor shaft while effectively thwarting the ingress of water. To further fortify the seal, we employ meticulous coating of marine-grade epoxy to reinforce the bond and enhance the overall water resistance of the assembly.

3.7.3 The final assembly design of the thruster

The final assembly design of the thruster is depicted in Figure 3.25. In this design, a brushless motor is securely fastened within a sealed compartment using bolts. Once the motor is in place, the compartment is sealed with epoxy. A shaft adapter connects the motor to the paddle fork and propeller. The paddle fork ensures that the propeller rotates in sync with the shaft, and a nut is employed to affix the propeller to the shaft adapter.

To maintain a watertight seal and prevent water from entering the compartment, we utilize the SKF R09-F rotary seal. This particular model was chosen because it accommodates

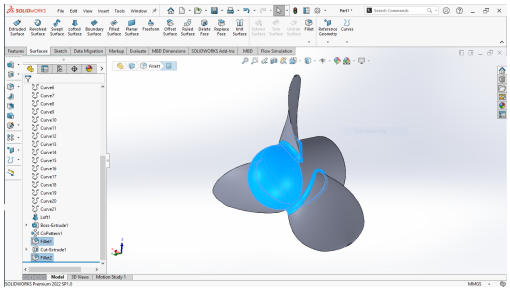

(a)Finalising the conception with fillets

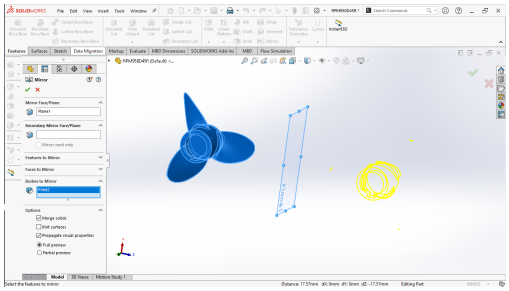

(b) Creating the second propeller with a mirror function

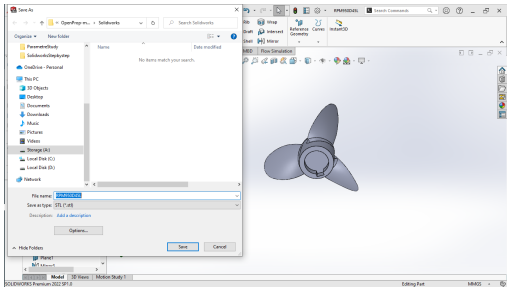

(c) Saving both propellers as STL files

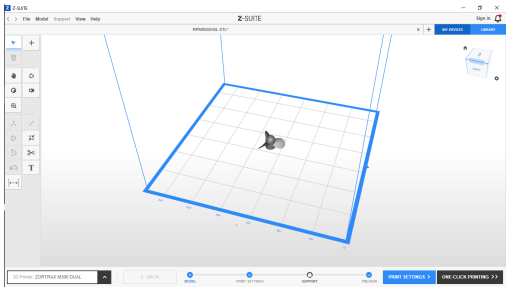

(d) Importing the files to Z-Suite

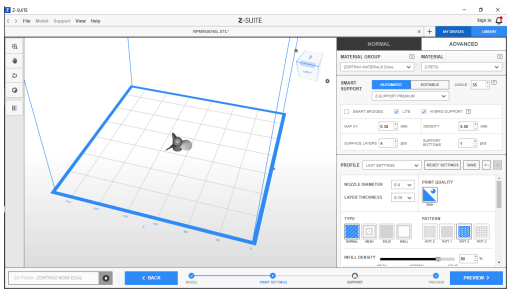

(e) Setting the printing parameters to the printer, and start the printing

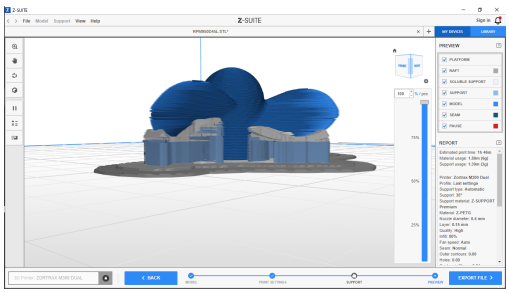

(f) Slicing and exporting the G-code

Figure 3.23: Propeller printing

a smaller shaft diameter of 5mm. It also boasts the ability to withstand high pressures of up to 100 bars and supports rotational speeds of up to 1500 RPM, which aligns perfectly with the requirements of our application [26].

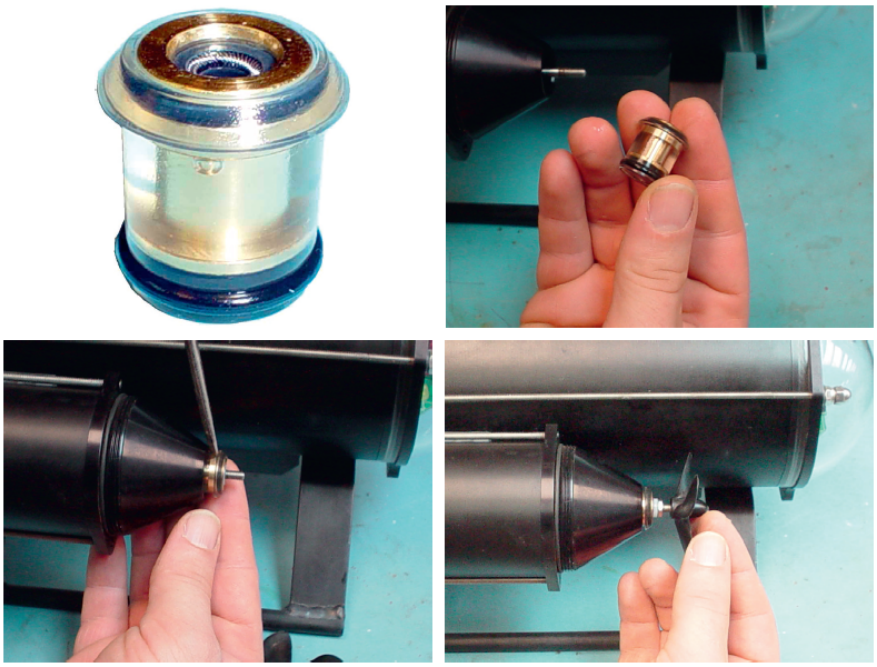

Figure 3.24: Fluid sealing of direct drive thruster coupling. From [1]

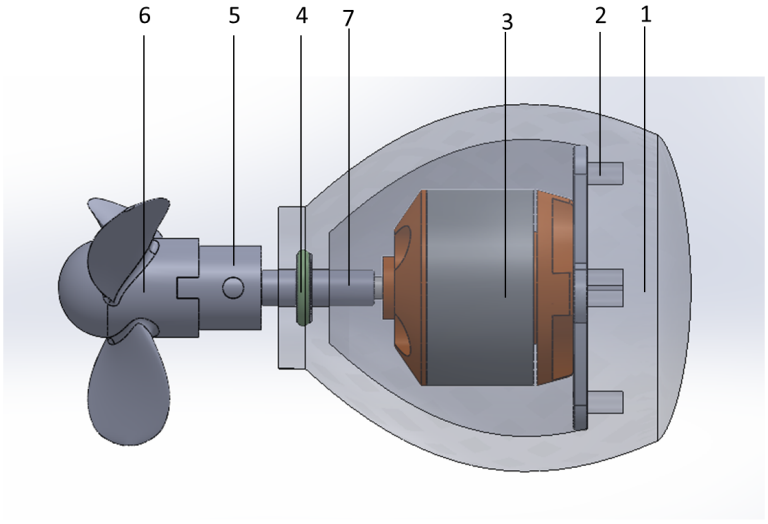

Figure 3.25: The final assembly design of the thruster

3.8 Sizing the Vertical Thruster

3.8.1 Constraints and Design Considerations

To appropriately size the vertical thruster, several points need to be addressed and constraints must be taken into consideration.

- The role of the vertical thruster in the thruster configuration should be understood. In the 3 thrusters configuration, the vertical thruster serves two purposes. First, it is activated independently to control the heave direction. Second, it is activated to incline the ROV in the pitch direction while using the rear propellers for propulsion in the surge direction. Placing the vertical thruster at the front ensures consistent vertical propulsion in both modes, meaning that when moving with one mode or another the motor turns in the same direction which make it easy to pass from one mode to the other and keep heaving to same direction, which enhances the user experience.

- The propeller should be positioned in the vertical longitudinal plane, with its center located at a certain distance $\mathcal{D}$ in front of the ROV's center of gravity. This positioning is crucial for maintaining stability and control.

- Estimating the righting moment of the ROV is essential to determine the appropriate $\mathcal{D}$. The righting moment ($M_0(\theta)$) is calculated using the formula:

$$M_0(\theta) = W \times BG \times \sin(\theta) \tag{3.9}$$

  where W is the weight of the ROV, BG is the distance between the center of buoyancy and center of gravity, and θ is the pitch angle. The maximum righting moment (M_{0max}) should not exceed 208 mN·m to ensure that the pitch angle remains between $-45°$ and $45°$. The moment generated by the vertical thruster is equal to $\mathcal{D}$ times the thrust of the vertical thruster (T_v), and it should not exceed M_{0max} for proper control. Thus, $T_v \times \mathcal{D} < 208, \text{mN·m}$. The dimension $\mathcal{D}$ should be in the range of 23-50 mm, corresponding to a maximum thrust of 4.2-9 N.

- The vertical dimension of the ROV is fixed at 60 mm, which imposes limits on the thruster's size. It cannot be as long as the rear thrusters, and its diameter should be under 50 mm.

3.8.2 The Proposed Solution

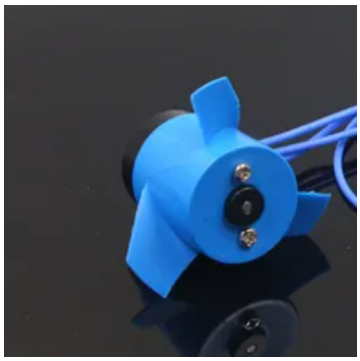

Figure 3.26: Under water ROV thruster with broshless motor

In order to meet all the aforementioned requirements, we have chosen to utilize a brushless motor thruster, as depicted in Figure 3.26. This thruster offers a compact design where the propeller is directly mounted on the motor, and the motor itself is waterproofed. It is capable of generating a maximum thrust of 11 N, which proves to be sufficient for our specific application. To control the thrust output, the motor speed can be adjusted, allowing us to set the maximum thrust within the desired range of 4.2-9 N based on the chosen $\mathcal{D}$. It is worth noting that this thruster operates at 12V, which aligns with the voltage requirement of the rear thrusters, thereby enabling the utilization of a single power supply for all thrusters.

In terms of dimensions, the thruster boasts a maximum diameter of 45 mm, which perfectly suits our application, while its length measures 49 mm, satisfying the specified requirement of being under 60 mm.

Additionally, it is important to highlight a crucial feature of this thruster: its capability to operate effectively in both forward and reverse directions. This attribute sets it apart from many other thrusters available on the market. The bidirectional functionality is essential for our ROV, as it allows for efficient heaving in both upward and downward directions.

3.9 Conclusion

In this chapter, we undertook a comprehensive exploration of the propeller design process. We closely examined various propeller types and identified the most suitable one for our Remotely Operated Vehicle (ROV) application. We discussed different ROV thruster configurations and carefully selected the optimal configuration. Additionally, we presented design considerations and constraints crucial to propeller design.

Moving forward, we utilized OpenProp for propeller design and conducted a parametric study to determine the most efficient configuration. The performance of the propeller was rigorously validated through simulations using Ansys Fluent. We delved into the simulation setup and thoroughly analyzed the results.

Finally, we detailed the fabrication and assembly process of the thruster, including the sizing of the vertical thruster. With the completion of the thruster design, we are now poised to progress to the next phase: designing the structural components of the ROV.

CHAPTER 4 : Electronic and Electrical Design of the ROV

4.1 Introduction

In the design of an ROV, the electronic and electrical systems play a crucial role in ensuring the successful operation and functionality of the underwater vehicle. This chapter focuses on the conception and integration of these systems, including the incorporation of an autopilot for enhanced control. The electronic and electrical design of the ROV encompasses various subsystems, such as power distribution, sensor integration, control systems and safety measures. These components work in harmony to enable precise maneuverability, data acquisition, and perfect .

Through this chapter, our goal is to provide comprehensive insights into the design considerations, challenges, and best practices for developing the electronic and electrical systems of an ROV, with a specific focus on the integration and utilization of an autopilot. By optimizing the electronic and electrical design, we aim to enhance the ROV's performance, autonomy, and overall mission capabilities in various underwater environments.

4.2 Electrical Component Overview

In this subsection, we provide an overview of the key electrical components utilized in the design of the ROV. The electrical components play a critical role in enabling the functionality and operation of various systems within the ROV. Understanding the purpose, characteristics, and interconnections of these components is crucial for designing an efficient and reliable electrical system.

Through this overview, we aim to provide insights into the purpose and functionality of each electrical component, as well as their integration within the larger electrical system of the ROV. By gaining a comprehensive understanding of these components, their interdependencies, and their interaction with other subsystems, we can optimize the electrical design of the ROV and ensure its reliable and efficient operation.

4.2.1 Autopilot

The autopilot system within our Remotely Operated Vehicle (ROV) serves as a crucial tool, aiding in control and stability, particularly in manual operation. It acts as a support system, enhancing stability and refining control inputs through sensors, algorithms, and control mechanisms. Continuously monitoring the ROV's orientation, position, and motion, it swiftly adjusts control inputs to counter disturbances like currents or turbulence [4]. Through sophisticated algorithms, it stabilizes the ROV amidst external factors, allowing users to focus on tasks with ease. Moreover, it offers intelligent control features like depth-hold and heading-

hold modes, enabling precise maneuvering. This combination of manual control and autopilot empowers users with accurate positioning and enhanced maneuverability, ultimately ensuring safer and more efficient underwater operations.

Construction of an autopilot :

In general, an autopilot system includes:

- A processor.
- Memory in electronic communication with the processor.
- GPS receivers in electronic communication with the processor.
- Three accelerometers in electronic communication with the processor.
- Three rate gyros in electronic communication with the processor.
- An absolute pressure sensor in electronic communication with the processor.
- A differential pressure sensor in electronic communication with the processor.
- A transceiver in electronic communication with the processor for receiving and transmitting signals.

The following figure illustrates the composition of the autopilot :

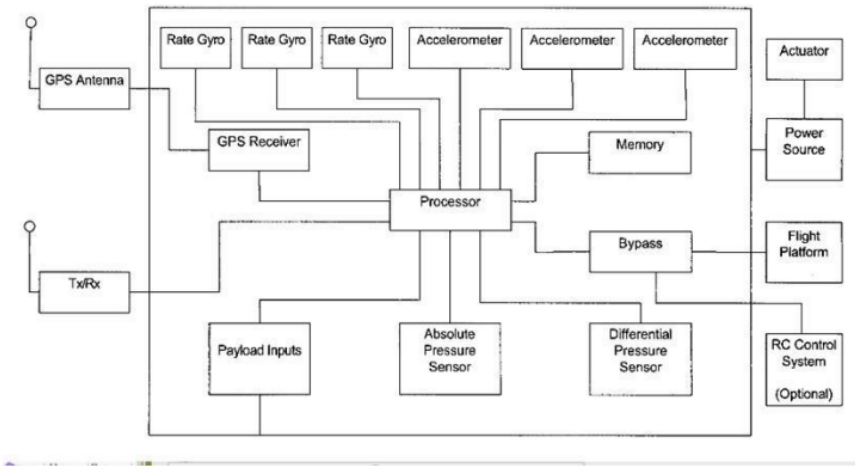

Figure 4.1: the composition of the autopilot

4.2.2 Companion Computer

The Companion Computer in the ROV setup streams video to the Topside Computer and relays MAVLink communications between the autopilot and the Topside Computer via Ethernet. It acts as a bridge, facilitating the exchange of data and commands between the vehicle and the control station.

In the figure (4.2), you can observe an illustration depicting an example of a companion computer that can be employed in the ROV setup:

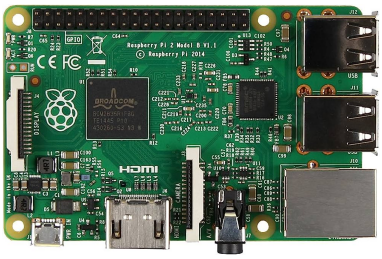

Figure 4.2: Example of a Companion Computer

4.2.3 Topside Computer

The Topside Computer serves as the central control unit where the live video feed and telemetry information from the ROV are received and displayed. It provides a user interface for operators to monitor and control the vehicle's operations. The Topside Computer accepts operator input from a joystick, allowing precise control over the connected vehicle.

4.2.4 Joystick

A joystick is used as an input device to control the ROV. Operators utilize stick control movements and button presses on the joystick to maneuver the vehicle underwater. The joystick provides intuitive and responsive control, enabling operators to navigate the ROV with precision.

4.2.5 Camera

The camera onboard the ROV allows the pilot to have a visual perspective from the vehicle's point of view. It captures and records video footage, enabling real-time monitoring and post-mission analysis. The camera can be mounted on a Camera Tilt Mount or other gimbal mechanism to adjust its position during operation, providing additional flexibility and improved visibility.

In our ROV system, we have opted to utilize the Low-Light HD USB Camera designed by blueRobotics, as depicted in Figure 4.3

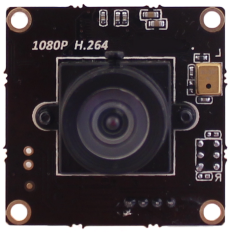

Figure 4.3: Low-Light HD USB Camera

4.2.6 Electronic Speed Controls (ESCs)

Electronic Speed Controls (ESCs) play a crucial role in controlling the speed and thrust of motors and thrusters in the ROV. These electronic components regulate the power supplied to the motors, allowing precise control over the vehicle's movement and maneuverability.

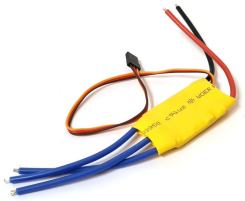

Figure 4.4: Electronic Speed Controls

4.2.7 Brushless DC Motors

Brushless DC motors play a vital role in the propulsion system of our ROV. These motors offer numerous advantages over traditional brushed motors, including higher efficiency, longer lifespan, and reduced maintenance requirements. The absence of brushes in brushless DC motors eliminates friction and wear, resulting in improved reliability and smoother operation.

The brushless DC motors utilized in our ROV provide precise and responsive control over thrust and maneuverability. Their compact design and high power-to-weight ratio make them well-suited for underwater applications. These motors are capable of generating the necessary propulsion force to navigate the ROV through water with enhanced speed and agility.

4.2.8 Power Sensing Module

The power sensing module provides analog current and voltage sensing capabilities to the autopilot onboard the ROV. It measures the battery level and monitors the power consumption of the vehicle. This information is vital for managing power resources and ensuring safe and efficient operation of the ROV.

Figure 4.5: Brushless DC motors

4.2.9 Power Supply

The power supply and distribution system in the ROV provide electrical power to all onboard electronics, including the high-current draw of the thrusters. A regulator within the system converts the main supplied power (from a battery or other source) into appropriate voltages for the more sensitive electronics. It ensures a stable and uninterrupted power supply to prevent system restarts and loss of control.

4.2.10 Tether

The tether is a length of cable that connects the Companion Computer to the Topside Computer. It enables low-latency, high-bandwidth communication between the control station and the underwater vehicle. The tether facilitates real-time data transmission, video streaming, and control commands, providing a reliable and efficient communication link that is well-suited for underwater environments.

4.2.11 Pressure Sensor

An external pressure sensor is utilized in the ROV to estimate the vehicle's depth. These sensors often include a simple temperature sensor as well.

4.2.12 Lights

Lights are essential for visual inspections and navigation, especially during nighttime operations, under cover, or at depths where sunlight does not reach. They provide crucial illumination for improved visibility and situational awareness.

4.2.13 Leak Sensors

Leak sensors are crucial components integrated into our ROV system to detect and provide timely alerts in the event of a potential leak. These sensors play a vital role in preventing any damage to the electronics housed within the enclosure. By promptly identifying and notifying

us about leaks, these sensors ensure the safety and protection of the sensitive components onboard.

4.2.14 Temperature Sensor

In addition to the integrated pressure sensor, our ROV incorporates an auxiliary temperature sensor. This sensor offers faster and more accurate temperature readings compared to relying solely on the integrated sensor. The accurate temperature measurements obtained from this sensor are particularly useful in research applications or scenarios where precise temperature information is crucial for estimating related phenomena.

4.2.15 Underwater Positioning and GPS (SBL and USBL)

The integration of an underwater positioning system and GPS (Short Baseline - SBL and Ultra-Short Baseline - USBL) further enhances the navigation capabilities of our ROV. This system serves multiple purposes, including precise location determination, real-time mapping of the ROV's current position, and location-tagging of collected data. By leveraging this positioning system, we can accurately navigate the ROV to specific locations and effectively monitor its movements during underwater missions.

4.2.16 Sonars

Sonars are invaluable tools in situations where visibility is limited. They provide range measurements to surfaces and can acoustically image targets, making them particularly useful in environments with low visibility. Sonars significantly aid in navigation, especially in structured environments where alternative positioning systems may not be available. By utilizing sonar technology, we can ensure safer and more efficient navigation of our ROV, even in challenging underwater conditions.

4.3 Final Hardware System Schematic

In this subsection, we present the final schematic of our hardware system for the ROV. This comprehensive schematic illustrates the integration and interconnection of all the key hardware components discussed throughout the chapter.

The final hardware system schematic showcases the complete architecture, including the electrical components, sensors, power distribution system and any additional peripherals or subsystems employed in our ROV design.

By visualizing the overall hardware system layout, this schematic provides a clear understanding of the system's organization, component placement, and the interplay between different subsystems. It serves as a valuable reference for system maintenance, troubleshooting, and future modifications or enhancements.

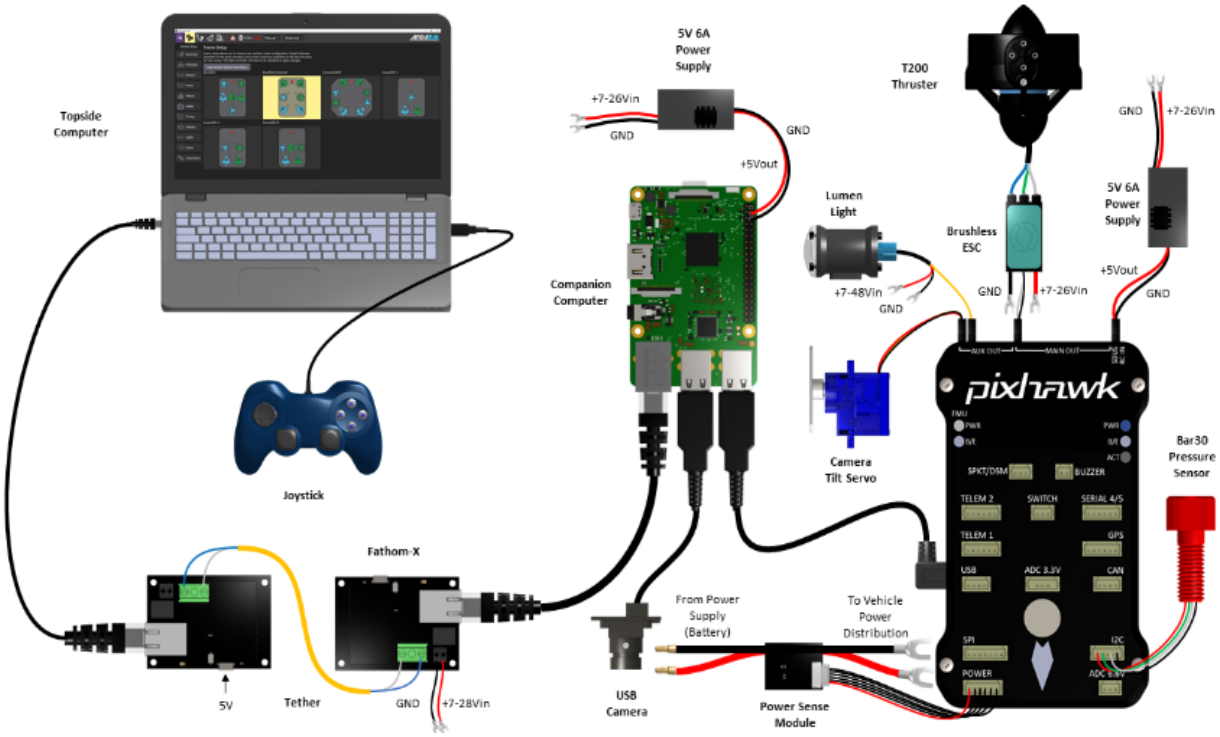

Figure 4.6: Final Hardware System Schematic, from [4]

4.4 ROV Programming and Setup

In this section, we delve into the programming and setup aspects of the ROV system. Successful deployment and operation of the ROV rely on efficient programming techniques and meticulous configuration. This subsection aims to provide comprehensive insights into the key steps involved in programming and setting up the ROV, enabling users to optimize its performance and functionality.

By focusing on programming and setup, we ensure that the ROV's software components and hardware configurations are appropriately aligned, resulting in seamless integration and smooth operation. This subsection encompasses various essential aspects, including software installation, firmware configuration, parameter tuning, and sensor calibration, among others.

Our objective is to equip users with the necessary knowledge and guidelines to effectively program and configure the ROV, enabling them to tailor its behavior, enhance its autonomy, and achieve optimal mission outcomes. Through careful programming and setup, users can harness the full potential of the ROV and accomplish complex underwater tasks with precision and efficiency.

ArduSub:

The ArduSub project offers a comprehensive open-source solution specifically tailored for remotely operated underwater vehicles (ROVs) and autonomous underwater vehicles (AUVs). It is an integral part of the ArduPilot project and originally derived from the ArduCopter

code. ArduSub provides extensive built-in capabilities such as feedback stability control, depth and heading hold, and autonomous navigation[4].

Designed with a focus on safety, rich features, flexibility, and user-friendliness, ArduSub caters to both experienced and novice users. It seamlessly integrates with Ground Control Station software, enabling the monitoring of vehicle telemetry and facilitating powerful mission planning activities. Additionally, it benefits from other components of the ArduPilot platform, including simulators, log analysis tools, and higher-level APIs for vehicle management and control.

ArduSub stands at the forefront of marine robotics and is suitable for anyone seeking to operate a vehicle beneath the water's surface. It supports various ROV configurations and allows for straightforward customization and integration of custom designs.

Programming and Configuration of ArduSub for the ROV :

To set up the configuration of ArduSub, we followed this steps :

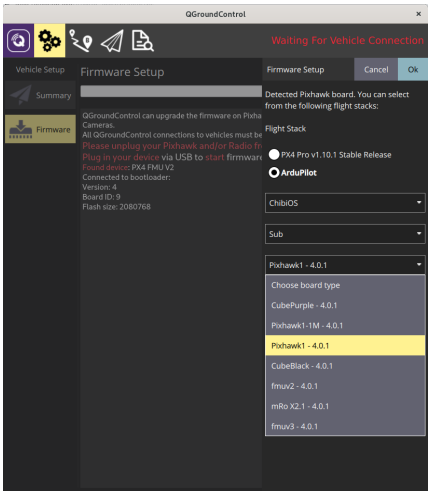

(a) Installing QGroundControl and choosing the right autopilot

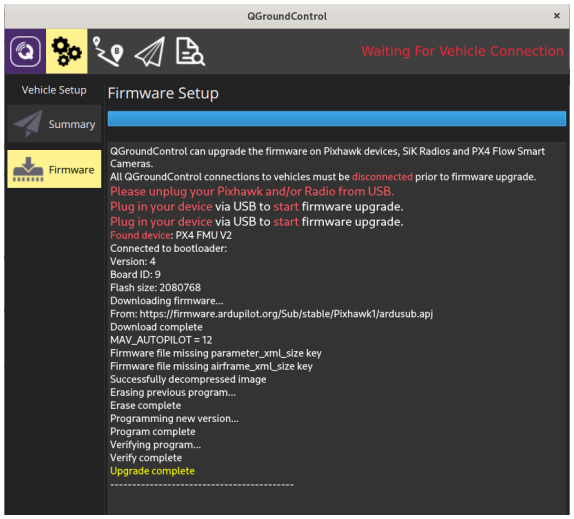

(b) Installation of the Firmware

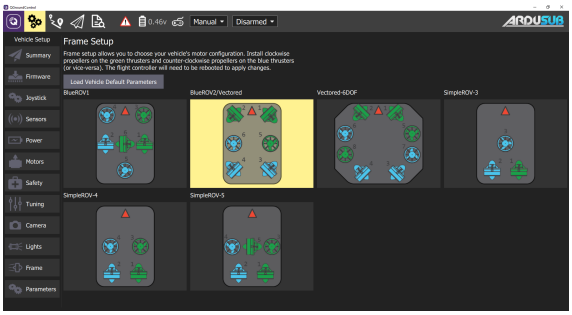

(c) Frame selection

(d) The default button setup for ArduSub

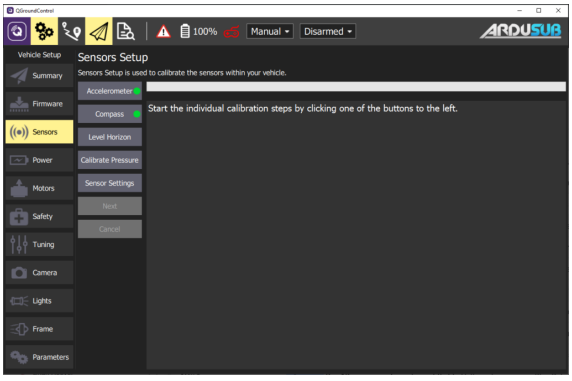

(e) Sensors Calibration

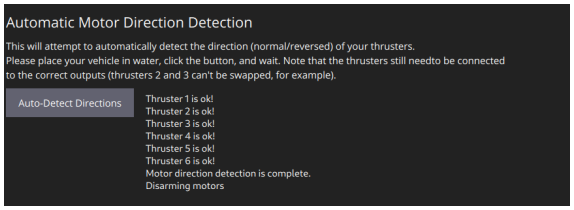

(f) Setting up the motors

Figure 4.7: Configuration steps for ArduSub (Part 1), from [4]

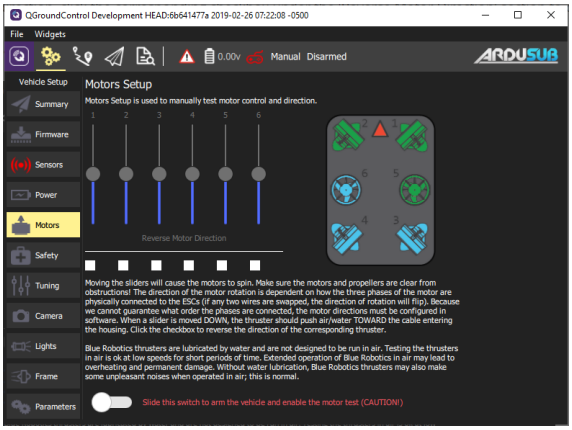

(g) Calibrating the Motors

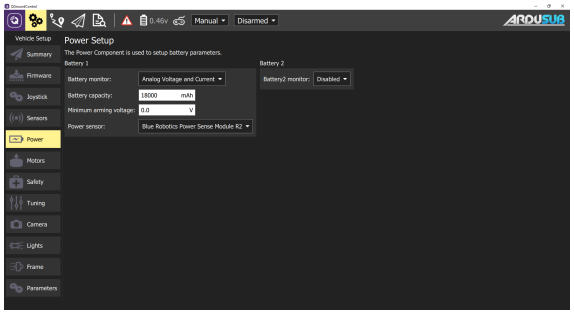

(h) Voltage and Current Measurement Setup

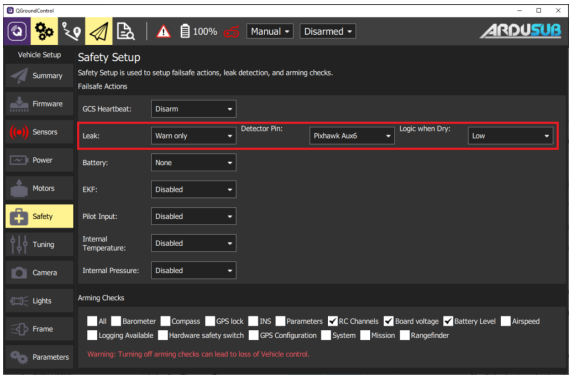

(i) SOS Leak Sensor Setup

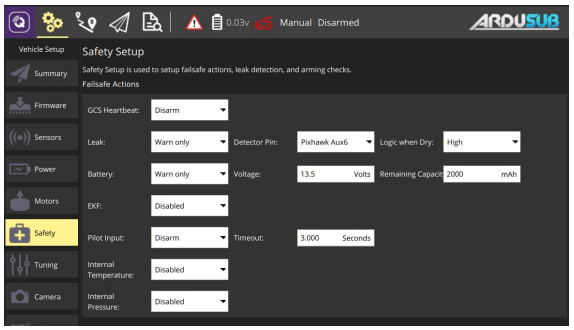

(j) Setting up Low Voltage Failsafe

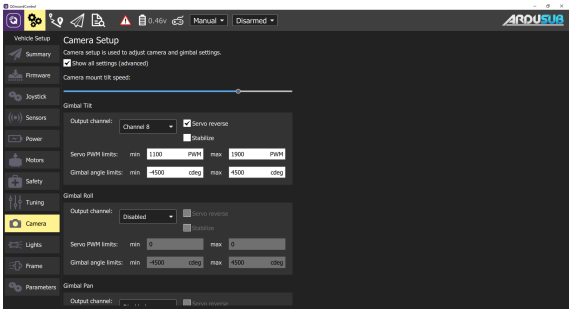

(k) Camera Tilt Setup

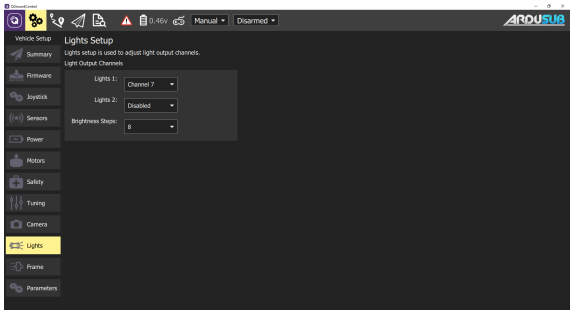

(l) Lights Setup

Figure 4.7: Configuration steps for ArduSub (Part 2), from [4]

Once these steps are completed and the autopilot is properly configured, the drone is now prepared for underwater diving.

4.5 Conclusion

In this comprehensive exploration of the electronic and electrical design of our ROV, we've meticulously crafted a system poised for precision and reliability in the depths. At its core, the

autopilot system stands as the sentinel, orchestrating stability and control. Supported by an array of sensors, it deftly navigates through challenging underwater terrains, compensating for external forces. The companion and topside computers serve as vital intermediaries, facilitating seamless communication with the surface. The joystick, intuitive in its control, empowers operators to maneuver with finesse. Meanwhile, the propulsion system, governed by electronic speed controls and brushless DC motors, endows the ROV with agility and efficiency in motion. Our robust power management system ensures judicious energy use and system resilience, guaranteeing uninterrupted operations.

On the software front, the ArduSub framework provides a solid foundation, offering extensive capabilities for stability control, depth and heading hold, and autonomous navigation. Its adaptability caters to a wide user base, from novices to seasoned operators. The configuration steps, meticulously outlined, guide users through a seamless setup process, ensuring optimal performance. This meticulous attention to both hardware and software facets culminates in a formidable platform, ready to explore and operate with precision in the enigmatic depths. Our final hardware schematic serves as a visual testament to the integrated design, outlining the harmonious interplay of components.

In conclusion, the electronic and electrical design of an ROV is a complex and critical aspect of its development. By considering the design considerations, challenges, and best practices discussed in this chapter, we can create a robust and efficient electrical system that empowers the ROV to navigate underwater environments with precision, collect valuable data, and accomplish its mission objectives effectively.

CHAPTER 5 : 3D Conception of the ROV

5.1 Waterproofing of Electrical Components

5.1.1 Introduction

Background and Significance

In the realm of underwater exploration and research, the reliable operation of equipment is of paramount importance. When it comes to Remotely Operated Vehicles (ROVs), ensuring the integrity of electrical components against water ingress becomes a critical consideration. The corrosive and damaging effects of water on sensitive electronics necessitate the implementation of robust waterproofing strategies.

The significance of effective waterproofing extends beyond the preservation of equipment; it directly influences the success of marine missions, data collection accuracy, and the safety of equipment operators. The consequences of inadequate waterproofing can range from equipment malfunctions to complete mission failures, making it a vital aspect of ROV design and construction.

Approach Overview

To address the challenge of waterproofing the electrical components within our ROV, a systematic and proven approach has been adopted. The cornerstone of our approach involves encapsulating these sensitive components within a meticulously designed sealed box. This box serves as a protective barrier against the intrusion of water while maintaining the functionality of the ROV's electronics.

A key element of our waterproofing strategy is the use of O-ring joints. O-rings, known for their resilience and effectiveness in sealing applications, play a pivotal role in maintaining the integrity of the sealed box. By strategically placing O-rings at critical junctures, we ensure a reliable and watertight seal, even when subjected to varying pressures and underwater conditions.

The subsequent sections of this report delve into the details of our waterproofing methodology, the design considerations for the sealed box, the critical role that O-rings play in achieving an effective seal, and the steps taken to install them accurately. Through the implementation of this approach, we aim to demonstrate the successful prevention of water ingress and the overall success of our observatory-class ROV project.

5.1.2 O-Ring Selection, Characteristics, and Dimensions

Introduction

O-rings have been selected as a fundamental component for the sealing mechanism within the sealed box of our observatory-class ROV. This choice is backed by several key advantages that align with our project's objectives and requirements. O-rings exhibit exceptional sealing

performance across a wide range of pressure, temperature, and tolerance conditions, ensuring the integrity of the sealed box even under varying operational scenarios. Additionally, the inherent durability of O-ring materials corresponds to the normal aging period, leading to a reliable service life. Notably, O-ring failure is often gradual and easily detectable, facilitating timely maintenance and replacement[27]. Moreover, the utilization of O-rings proves to be cost-effective, further contributing to the practicality and sustainability of our design. These reasons collectively underscore the rationale behind our decision to incorporate O-rings as a critical sealing solution in our observatory-class ROV's sealed box.

O-Ring Selection Criteria

The selection of an appropriate O-ring for our ROV's sealed box involves a careful evaluation of various criteria to ensure optimal sealing performance and long-term reliability. The following key criteria have been considered:

- **Material Compatibility:** Our material selection hinges on crucial factors including chemical resistance, temperature resilience, material hardness, and compression set.
- **Dimensions:** The O-ring diameter we choose must seamlessly integrate with the dimensions of our box while adeptly accommodating the necessary pressure containment.

Material selection

As previously mentioned, the chosen O-ring material must fulfill our specific criteria. Consequently, we have opted for an **FKM** O-ring due to its exceptional qualities that align with our requirements. Notably, FKM boasts impressive resistance to seawater and a wide range of chemicals, making it an ideal choice. Its resilience to temperatures ranging from -30°C to 204°C[28]. Moreover, the hardness rating of 70 Ra significantly contributes to a minimized compression set, which in turn reduces the necessary compression force for effective sealing. This advantageous feature remains evident even under lower temperatures, ensuring operational efficiency. In addition, FKM showcases remarkable tensile strength of 15 MPa (150 Bar), making it well-equipped to endure the challenges of our intended application [5]. Given the demanding marine environment, the prudent selection of FKM stands as a pivotal decision, poised to deliver steadfast and reliable sealing performance within our operational context.

O-ring Dimensions

The diameter of the O-ring doesn't directly affect its pressure-resisting capacity; however, it does impact the acceptable clearance gap (figure 5.1) . Opting for a larger diameter leads to a correspondingly larger permissible clearance gap, while a smaller diameter would result in a more constricted, demanding clearance gap. Such tight constraints could escalate the complexity and cost of sealing box manufacturing, necessitating higher precision. Fortunately, we can refer to Table 5.1 for insights. This table, derived from a manufacturer, offers recommended clearance gaps suitable for pressures up to 100 bar.[5]

Table 5.1: Permitted Extrusion Gap for Use of O-Rings up to 100 bar, from [5]

O-ring Cross Section (mm)	Maximum Diametral Clearance (mm)
1.6	0.12
1.78	0.13
2.4	0.14
2.62	0.13
3.0	0.15
3.53	0.15
5.33	0.18

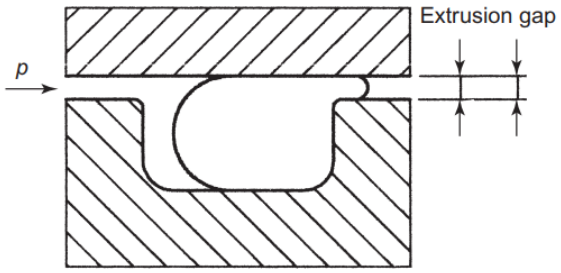

Figure 5.1: Clearance Gap, from [5]

Based on the insights from this table, we have decided to adopt an O-ring diameter of **3.53 mm**, as it strikes a balance by offering a reasonable and achievable clearance gap.

Characteristics of the Selected O-Ring

You will find below a summary of the key characteristics of the selected O-ring presented in a table:

Table 5.2: Characteristics of the Selected O-Ring

Characteristic	Value
Diameter	3.53 mm
Hardness	70 Ra
Temperature Range	-30°C to 204°C
Compression Set	14.5%
Compression Load	1.9 Kg/cm

This concise tabular representation outlines the defining attributes of the chosen O-ring, providing a clear reference for its compatibility with our specific sealing requirements.

5.1.3 Sealing box

Within this section, we embark on a comprehensive exploration of our sealing strategy, delving into intricate details that underscore the heart of our project's success. We immerse ourselves

in a nuanced discussion that encompasses material selection, the identification of the most fitting sealing methods tailored to our precise needs, and the meticulous dimensioning of the groove. Our main goal remains unchanged: to ensure a completely sealed enclosure, protecting our equipment from water with careful planning and clear thinking.

Box Material Selection

Meticulous deliberation has been dedicated to the critical task of choosing the materials for the construction of the protective sealed enclosure enveloping the electrical components of our observatory-class ROV. This material selection process carries profound implications for the box's overall robustness, its ability to repel water infiltration, and its compatibility with the demanding aquatic milieu.

Upon a comprehensive survey of available materials, our collaborative judgment has solidified in favor of **High-density polyethylene** (PEHD) as the prime candidate for fabricating the sealed box encompassing our ROV's delicate components . Polyethylene's merits, including its commendable corrosion resistance, low density, and a favorable melting point of 135°C, align harmoniously with the challenges posed by the marine environment. It boasts a tensile strength of 275.2 bars and a tensile elongation of 41.28 bars, affirming its capacity to withstand the anticipated 6 bars of pressure. These attributes converge seamlessly with the requisites of our project, instilling confidence in the material's potential to underpin the dependable, cost-effective, and successful operation of our ROV.

Type of Sealing Selections

Within the realm of static O-ring sealing, a diverse array of strategies exists, among them flange/face sealing and Dovetail Face Seal. Each approach possesses distinct advantages and limitations. After thorough deliberation, we have judiciously chosen the **flange/face sealing** configuration (as depicted in Figure 5.2). This selection aligns harmoniously with our observatory-class ROV's sealed box, primarily owing to its substantial and uniform sealing surface. This surface substantiates the achievement of reliable seals, resilient even when subjected to fluctuating pressures and varying environmental conditions. Furthermore, this configuration ensures uniform pressure distribution, effectively minimizing stress concentrations and nurturing sustained operational longevity. The streamlined assembly process and ease of maintenance inherent to flange/face seals synergistically augment our endeavors. Their adaptability to an assortment of sealing materials caters aptly to our unique operational requisites. With a well-defined geometry designed to counteract extrusion risks, these seals are well-equipped to withstand the system's maximum 6 bar pressure. Ultimately, the robust reliability, versatility, and enduring performance of flange/face seals seamlessly align with our exacting marine environment and sealing prerequisites.

Groove Dimensions

Armed with a comprehensive understanding of our O-ring, which corresponds to the Q8201 model with a diameter of 3.53 mm and a verified compression ratio of 25% for PKM, we are

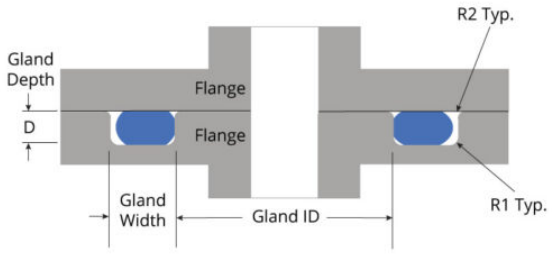

Figure 5.2: Flange/face sealing, from [5]

now poised to delve into the intricate realm of groove dimensioning. This pivotal stage is characterized by the interplay of three critical parameters: groove depth "H," groove width "W," and groove corner radius "r" (as depicted in Figure 5.3). Referencing manufacturer-supplied

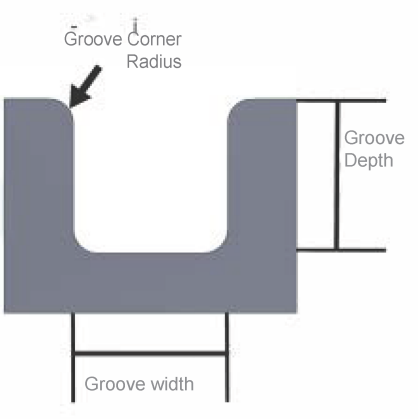

Figure 5.3: Groove Parameterization, from [5]

data, a comprehensive table provides recommended groove dimensions for our specific O-ring model, as displayed below:

Table 5.3: A table of recommended groove dimensions, from [5]

Ring Size	Cross-Section		Dynamic Recommended Gland Depth "C"		Static Recommended Gland Depth "C"		Dynamic Axial Groove Width "D"		Static Axial Groove Width "D"	
	(in)	(mm)	(in)	(mm)	(in)	(mm)	(in) +0.005/-0.000	(mm) +0.13/-0.00	(in) +0.005/-0.000	(mm) +0.13/-0.00
Q8201 – Q8284	0.139 ±0.004	3.53 ±0.10	0.122	3.10	0.112	2.85	0.188	4.78	0.155	3.94

According to this invaluable reference:

- Groove width for our model is 3.94.
- Groove depth for our model is 2.85.

For the groove corner radius, a calculative approach is employed:

- Corner radius $= 0.25 * D_{o-ring} = 0.8825$.

These refined dimensions form the basis for the precise and effective execution of our groove design, further reinforcing our sealing solution's robustness and reliability.

5.2 The 3D Model

With our comprehensive understanding of the various components and their functionalities, we're now ready to translate these concepts into reality. The initial step in this process involves the meticulous creation of a 3D model that encompasses all the intricacies of the ROV, both internally and externally. This section is dedicated to 3D modeling of each individual part and final assembly of the ROV, ensuring a detailed and accurate representation of the entire ROV.

5.2.1 The sealed box for the main electronic parts

The sealed box contains all the main electronic parts, the battery and power distribution module, the ESCs, the flight controller, and the raspberry pi zero. They are distributed in a way to minimise the volume and respect the desired overall dimensions for the ROV. The figure 5.4 bellow shows this sealed box and the components inside it.

As you can see the two parts of the box are pressed one against the other by 28 bolts and nuts. We used 316 stainless steel M4 bolts and nuts, this materiel is known as marine-grade stainless steel, it has a superior corrosion resistance in saltwater environments.

The assembly process in enumerated below:

1. Preparation: We started by making sure that both PEHD parts were clean, free from debris, and had smooth, flat mating surfaces. We checked the O-ring to ensure it was in good condition, without any visible damage.

2. Lubrication: We applied lubricant, a suitable silicone or grease, to the O-ring. This helped facilitate a better seal and prevented damage during assembly.

3. O-ring Placement: We carefully placed the lubricated O-ring in the groove or channel on one of the PEHD parts, making sure it was evenly seated and did not twist or kink.

4. Alignment: We aligned the two PEHD parts, ensuring that the bolt holes were perfectly matched. We also ensured that the O-ring remained in its groove.

5. Bolt Insertion: We inserted the bolts through the pre-drilled holes in both PEHD parts, starting with a few bolts to hold the parts together.

6. Hand-Tightening: We hand-tightened the initial bolts evenly to compress the O-ring slightly. This helped distribute the pressure evenly and ensured a uniform seal.

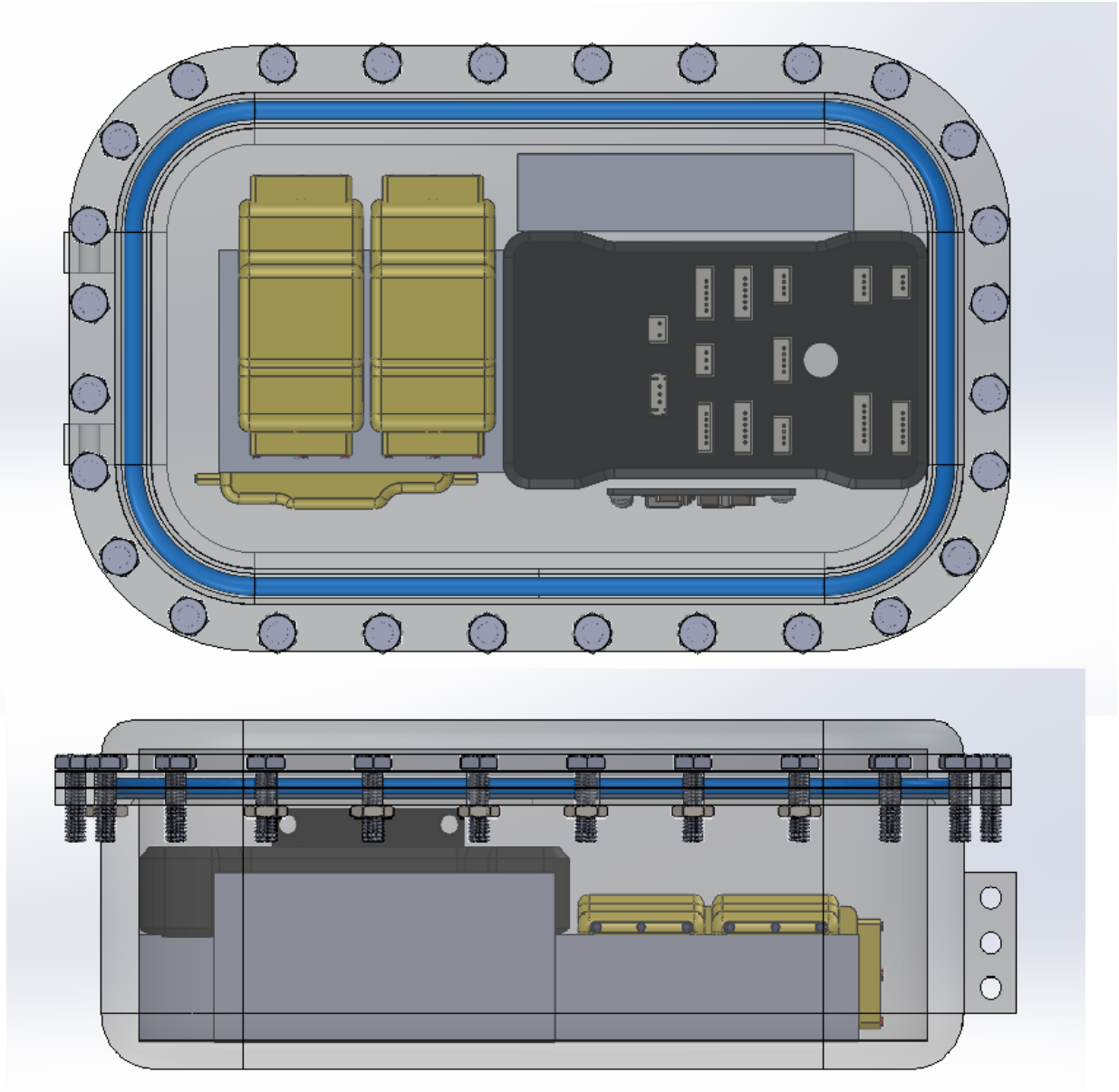

Figure 5.4: The Sealed Box containing the electronic components

7. Alternate Tightening: We continued adding bolts, alternating between sides to ensure even compression. We tightened each bolt a little at a time to avoid creating gaps in the seal.

8. O-ring Check: We periodically checked the position of the O-ring to ensure it remained properly seated in its groove and wasn't pinched or displaced during the tightening process.

9. Optional Torque: For added precision, we used a torque wrench (optional) and followed the manufacturer's specifications to tighten the bolts to the specified torque evenly across all bolts.

10. Leak Inspection: After securing all bolts, we performed a visual inspection to ensure

the O-ring was properly seated, and there were no gaps or visible damage. We checked for any signs of water intrusion.

11. Optional Sealant: If desired, we applied a gasket adhesive or sealant around the edges of the PEHD parts to provide an extra layer of security. We allowed the sealant to cure per the manufacturer's instructions.

12. Waterproof Test: Before using the box underwater with our equipment, we conducted a waterproof test by submerging it in a controlled environment (e.g., a tub of water) for an extended period to ensure there were no leaks.

13. Regular Maintenance: We planned to periodically inspect and maintain the O-ring and bolts to ensure they remained in good condition. We knew that replacing the O-ring as needed, especially if it showed signs of wear or damage, was essential.

5.2.2 The camera compartment

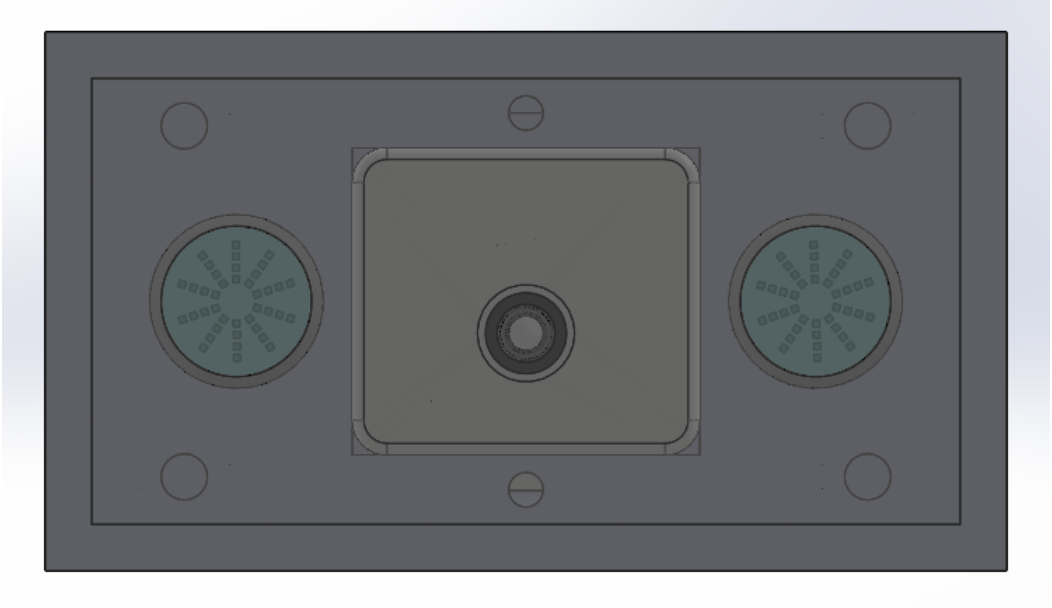

Figure 5.5: The Camera compartment

The camera compartment houses a central camera module flanked by two 1000 lumen LED light modules on each side. This configuration enhances underwater visibility. The compartment is constructed using PETG material and sealed with a 5mm Plexiglas (acrylic sheet) plate on the camera side. Plexiglas is chosen for its exceptional transparency, impact resistance, and lightweight properties. Its transparency ensures clear image capture, while its durability protects camera equipment. Plexiglas is also corrosion-resistant in saltwater and maintains optical clarity for high-quality imaging. Its ease of fabrication allows for custom housing designs. Proper sealing and maintenance are essential for underwater camera

enclosures.

The assembly of the PEHD box and plexiglass is done following the steps below:

1. Clean and Prepare: We ensure both the Plexiglas and PEHD surfaces are clean and free from dust, dirt, and oils. We use a mild solvent or alcohol to clean them thoroughly.

2. Fit the Plexiglas: We place the Plexiglas sheet in the designated opening of the PEHD box to ensure a precise fit.

3. Apply Silicone Sealant: Using a marine-grade silicone sealant/adhesive, we apply a continuous and even bead of sealant along the edges of the Plexiglas sheet where it contacts the PEHD box. We make sure to completely seal the entire perimeter.

4. Assemble the Parts: We carefully place the Plexiglas sheet onto the PEHD box, ensuring it lines up correctly with the opening. We press it down gently to spread the sealant and create a good bond.

5. Secure with Clamps or Fasteners: We use clamps or fasteners to hold the Plexiglas and PEHD box together firmly while the silicone sealant cures. We follow the manufacturer's instructions for the curing time, which typically ranges from several hours to a day.

6. Check for Leaks: After the sealant has cured, we carefully inspect the seal for any gaps or areas where the sealant may not have adhered correctly. If necessary, we apply additional sealant to any problem areas and allow it to cure.

7. Test the Waterproof Seal: Before using the underwater housing with our camera, we perform a waterproof test by submerging it in a controlled environment (e.g., a tub of water) for an extended period to ensure there are no leaks.

8. Regular Maintenance: We periodically inspect and maintain the sealant to ensure it remains watertight. Over time, the sealant may degrade or develop cracks, so resealing may be necessary.

5.2.3 Preventing Water Condensation

One common issue encountered with sealed boxes, especially camera enclosures, is water condensation. When sealing is performed in environments with high water vapor content in the air, the trapped air within the sealed box contains a similar amount of water vapor. This moisture can condense when the ROV operates in colder temperatures, potentially causing damage to electronic components and creating fog inside the Plexiglas, obstructing the camera's vision.

To mitigate this problem, we adopt a two-fold approach:

1. Controlled Assembly Environment: We conduct the assembly and sealing of our boxes in a controlled environment with dry air. This ensures that the air inside the sealed box contains minimal moisture from the outset.

2. Silica Gel Desiccant Packs: As an additional layer of protection, we place Silica Gel desiccant packs inside our boxes. Silica Gel is highly effective at absorbing moisture, thereby further preventing condensation.

By implementing these measures, we eliminate the risk of this potentially catastrophic issue.

5.2.4 The assembly of the different components of the ROV

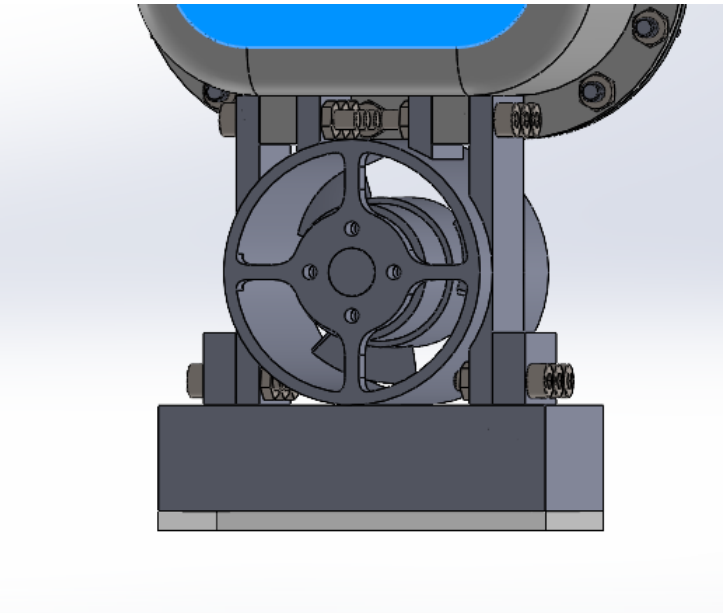

Figure 5.6: A picture showing the connections between the vertical thruster's hub, the sealed box and the camera compartiment

After sealing each component separately, it's time to assemble them together. We've opted for a straightforward assembly using M4 hex socket head bolts and nuts, all made from marine-grade stainless steel, ensuring durability and corrosion resistance.

The vertical thruster is attached to its duct using four bolts. The duct, with two extensions, serves as connections to both the camera compartment and the sealed box. Consequently, the sealed box is securely connected to the duct with six bolts, and the camera compartment is also affixed to the duct using six bolts. These components are constructed from PETG material.

You can see the connections mentioned above illustrated in Figure 5.6.

A similar system is employed to attach the two horizontal thrusters to the sealed box. Each thruster features two 5mm-thick arm extensions that sandwich an 8mm-thick arm

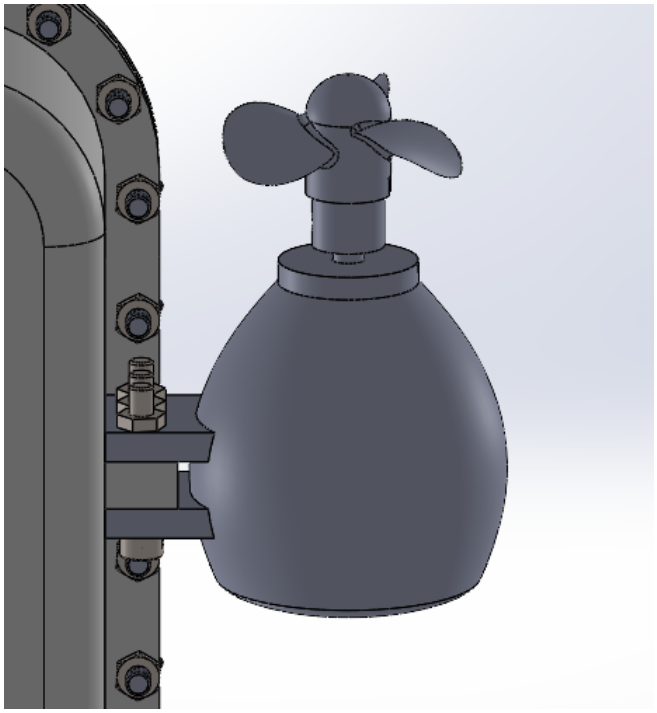

Figure 5.7: A picture showing the connection between the horizontal thruster, and the sealed box

extension from the sealed box. This assembly is securely fastened in place using three bolts and nuts.

The final result can be observed in Figure 5.7.

5.2.5 Addressing Electric Connections

One of the challenges we encountered in the ROV's design was establishing electrical connections to various critical components inside the sealed box, including the thrusters, tether connector, battery charging port, and camera. Our objective was to achieve these connections without compromising the integrity of the sealing mechanisms.

To resolve this issue, we adopted a specialized solution known as the WetLink penetrator, which is manufactured by BlueRobotics. This innovative device enables the safe passage of electrical wires between sealed and non-sealed compartments, ensuring that the seal remains watertight.

The WetLink penetrator, as illustrated in Figure 5.8, consists of several components, including a primary bolt and its corresponding nut, an O-ring positioned within the bolt, and a smaller bolt used to secure the seal inside the head of the main bolt.

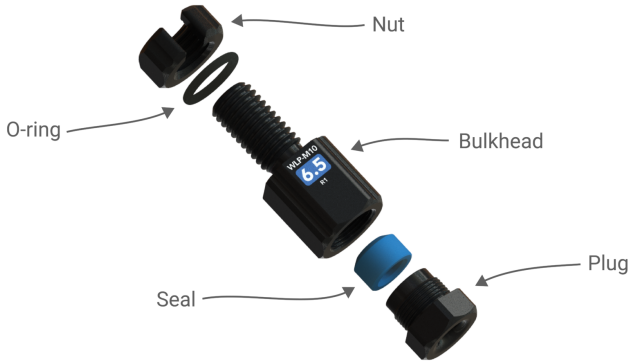

Figure 5.8: Components of the WetLink penetrator [6]

Figure 5.9 demonstrates the strategic placement of WetLink penetrators within our ROV to facilitate the required electrical connections while preserving the sealing of both the sealed box and the camera compartment.

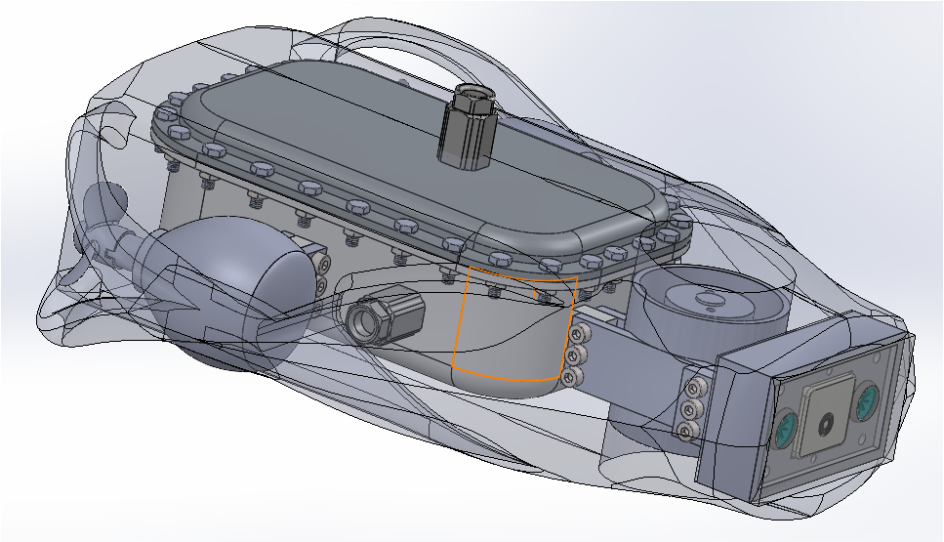

Figure 5.9: Placement of WetLink penetrators in our ROV

5.2.6 Designing the exteror shell

The design of the exterior shell for the ROV places a strong emphasis on aesthetics, ensuring it not only performs efficiently but also presents a visually pleasing appearance. This streamlined shell is divided into two sections, upper and lower (as shown in figure, which can be securely fastened together using marine-grade stainless steel bolts and nuts, simplifying assembly and maintenance. The choice of PEHD material, with a 3mm thickness, strikes an ideal balance between strength and weight, enhancing hydrodynamic efficiency while providing impact resistance. This thoughtfully designed shell contributes to the ROV's optimal performance and esthetic appeal in underwater operations.

(a) Lower Shell Section **(b)** Upper Shell Section

Figure 5.10: Figure depicting the Upper and Lower sections comprising the exterior shell of the ROV.

5.2.7 Calibrating the Weight Distribution of the ROV

Achieving stability in water is crucial for the ROV's performance. As discussed in Chapter 2, ensuring that the center of gravity lies vertically beneath the center of buoyancy is vital. To accomplish this, a meticulous weight analysis of the ROV, including all its components, is necessary. We initiate this process by estimating the total weight of the ROV and its overall volume to assess its balance. As presented in Table 5.4, the ROV's components and their respective weights are detailed, resulting in a total weight of 2620g.

The ROV's total volume, when considering its exterior shell, amounts to $3.2dm^3$. To attain neutral buoyancy, the ROV's weight should approximate 3200g. Consequently, we have a margin of 580g for additional weight. This extra mass will consist of small lead blocks strategically positioned at the ROV's base within the shell. These blocks serve a dual purpose: lowering the center of gravity and aligning it precisely beneath the geometric center. This adjustment enhances the ROV's equilibrium, bolstering its resistance to rolling and overall stability underwater.

In this design, the X axis is the transversal axis, Y is the vertical axis and -Z is the longitudinal axis.

Component	Qty	Unit Weight (g)	Weight (g)	X	Y	Z
Pixhawk	1	38	38	-2.22	-0.64	33.94
Raspberry PI ZERO	1	9	9	30.1	-12.2	26.82
ESC	3	25	75	-5.77	-8.55	-37.25
Matek Power Hub	1	6	6	-28.15	-3.66	29.42
Battery 3s 5000mAh	1	360	360	-2.5	-17.7	5.06
Bolt M4	28	2	56	0	18.12	-1.4
Socket Bolt M4	18	3.6	64.8	0	-7.34	-70.07
Nut	46	0.6	27.6	2.01	7.03	-36.37
Moteur A2212	2	72	144	0	-3.22	14.17
Vertical Thruster	1	100	100	0	-5.12	-123.94
Camera Module	1	20	20	-15.31	1.35	-161.11
LED Module	2	20	40	0	-1.97	-170.89
Sealed Box PETG Lower	1	288.5	288.5	0	-11.56	-3.02
Sealed Box PETG Cover	1	139	139	0	25.11	-1.44
Hub Vertical Thruster PETG	1	70	70	0	-9.88	-119.85
Horizontal Thruster	2	173	346	0	-3.22	14.42
Camera Box PETG	1	49.3	49.3	0	-3.02	-162.08
Plexiglass	1	18.2	18.2	0	-1.97	-180.44
PETG Ext Shell	1	727	727	0	-2.23	-33.45
WetLink	4	10.5	42	0	11.48	-27.97
		Total	**2620.4**	-0.6	-4	-25.4

Table 5.4: Components Weights and Quantities

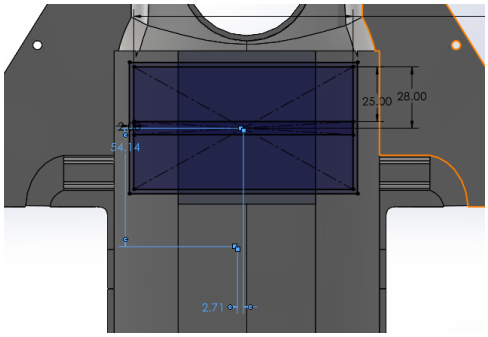

(a) Sketch of the LeadBlocks holder

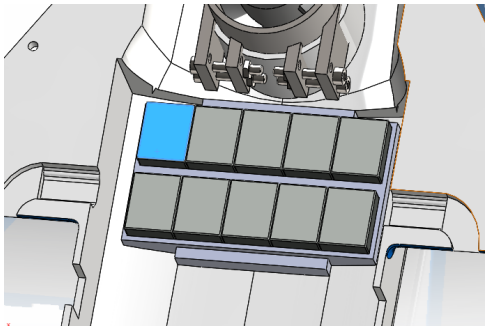

(b) Lead Blocks after being placed on the lower shell

Figure 5.11: Figure depicting the placement of the lead Blocks on the Lower shell

The geometric center of the ROV is at coordinates X = 0, Y = -2.31, and Z = -31.24. To achieve proper stability, we must shift the center of gravity from its initial position at X = -0.6 and Z = -25.4 to align with the geometric center, specifically X = 2.71 mm and Z = -31.24 mm, while ensuring the Y-coordinate remains as low as possible.

The 580g converts to 10 blocks of dimensions $35 \times 20 \times 7.1mm^3$ that will be positioned at the upper surface of the lower part of the shell of the ROV, in a pattern of 2×5 as shown in the figure 5.11.

$$\frac{X_0 \times 580 - 0.6 \times 2620}{580 + 2620} = 0$$

$$\frac{Z_0 \times 580 - 25.4 \times 2620}{580 + 2620} = -31.24$$

The solutions to these equations are $X_0 \approx 2.71$ mm and $Z_0 \approx -54.14$ mm, which are the values with which our pattern will be offset from the center.

These blocks will be securely positioned using plastic guides protruding from the shell and affixed firmly to the shell with epoxy resine.

5.2.8 Preserving Mass Distribution and Equilibrium with Expanding Foam

One of the primary goals in our ROV design is to preserve its mass distribution and equilibrium in underwater environments. To achieve this, it is crucial to prevent any water ingress into the spaces between the exterior shell and the sealed compartments. Expanding foam emerges as an optimal solution to address this objective effectively.

Expanding foam boasts several advantageous qualities that align with our mission. Firstly, its low density ensures minimal impact on the ROV's overall weight, crucial for maintaining buoyancy and equilibrium. Furthermore, expanding foam's innate water-resistant properties ensure that it does not absorb water over time, which could otherwise alter the ROV's mass distribution and impact its stability.

Ease of application is another compelling attribute. This foam can be precisely injected into gaps and voids, expanding to fill and conform to the space, creating a robust, water-

tight seal. This straightforward application process enhances the efficiency of our assembly, aligning with our design goals.

In summary, the use of expanding foam serves as a pivotal strategy to safeguard the mass distribution and equilibrium of our ROV by preventing water ingress into the spaces between the exterior shell and the sealed compartments. This ensures that our ROV operates with optimal stability and performance in underwater environments.

5.3 Final Assembly of the ROV

Now that we've completed all the necessary components for the ROV, it's time to take charge of the final assembly. The following steps shows how to assmble parts and ensure a seamless and functional integration of all parts:

- Begin by placing the added weight inside the shell, making sure they are positioned in the bottom section. This crucial step ensures that the center of gravity is not only below but also perfectly aligned with the geometric center.
- Using the provided nuts, securely fasten the interior components we discussed earlier to the exterior shell.
- Thread all necessary cables and make the electrical connections. Before finalizing the attachment, conduct thorough testing to confirm proper functionality.
- Now, cover all the interior components with the top section of the shell.
- Finally, fasten the top section to the bottom section using the provided nuts. This will complete the assembly process.

Figure 5.12 shows a final render of the ROV assembly and an exploded view of this later.

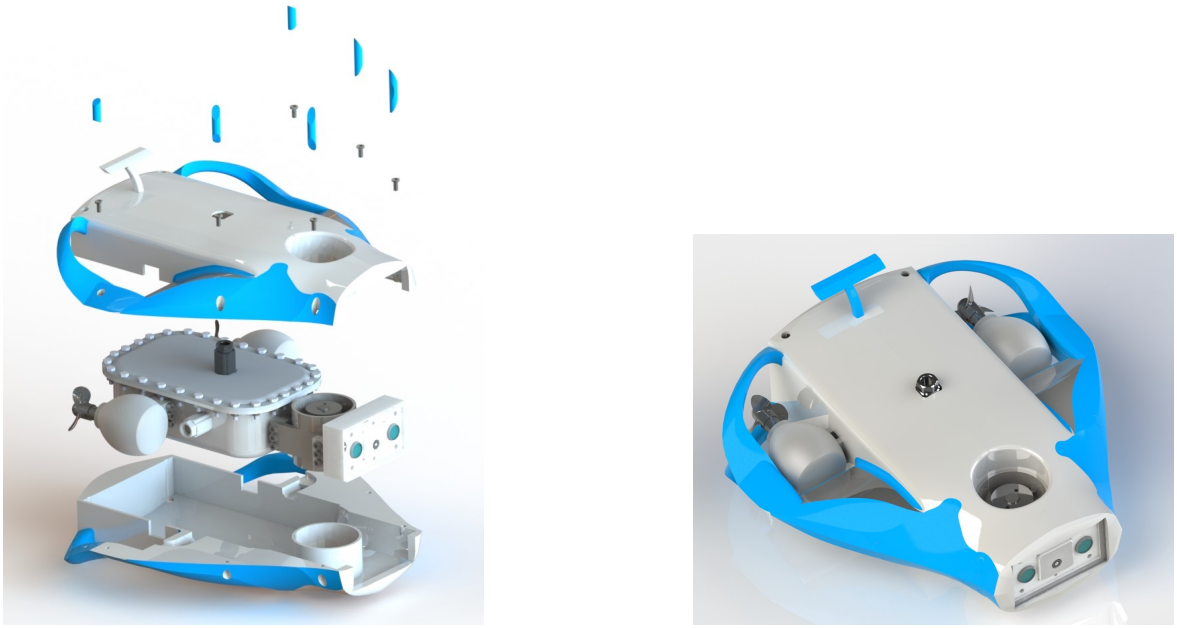

(a) ROV's exploded view

(b) ROV's Render

Figure 5.12: Figure showing the final design of the ROV

5.4 Conclusion

In conclusion, the design and construction of the ROV represented a complex engineering endeavor, showcasing meticulous planning and innovative solutions. The waterproofing of electrical components was achieved through the careful selection of appropriate O-rings and the design of a sealing box. Each compartment in the 3D model served a specific function; the sealed box protected the main electronic parts from water intrusion, while the camera compartment was fortified against water condensation, significantly enhancing the ROV's imaging capabilities underwater.

A crucial step in the process was the calibration of the ROV's weight distribution, underscoring the importance of equilibrium in underwater operations. Small Lead blocks were strategically added to the bottom of the ROV to achieve this balance, ensuring stability and functionality. The meticulous application of expanding foam further guaranteed no cavities that could compromise the ROV's integrity.

Moreover, aesthetics were a fundamental aspect of our design philosophy. The combination of an appealing exterior with a hydrodynamic shape resulted in an ROV that not only looked impressive but also enhanced its performance. Perfect symmetry concerning both the horizontal and transverse planes was maintained, eliminating side drag forces and improving controllability.

In the final stages, all components were assembled, preserving the ROV's integrity and functionalities while ensuring robust protection against water.

Conclusions and Outlook

The objective of this study was to develop a commercial observatory underwater Remotely Operated Vehicle (ROV) for the Algerian market, or at the very least, create a minimum viable product to present to investors with tangible results. This encompassed meticulous steps such as market analysis, feature selection based on extensive market study, design of a proficient propulsion system, development of a user-friendly control program, and the detailed design and calibration of all ROV components.

Our journey commenced with an in-depth market analysis, illuminating the current market landscape, popular ROV models, and customer preferences. Shifting our focus to the Algerian market, we discerned the specific needs of local customers, establishing a precise set of specifications tailored to meet these demands effectively.

Venturing into the technical domain, our exploration initiated with the kinematic modeling of the ROV, employing a cinematic model to bridge the global reference frame representing the user and the local reference frame embodying the ROV. This led to the derivation of essential kinematic equations linking the state and velocity vectors. Transitioning to hydrodynamics, we emphasized the significance of achieving neutral buoyancy, elucidating the critical role of transverse stability hinging on the relative positions of the center of gravity and center of buoyancy. Delving into drag forces, encompassing skin friction, form drag, and tether drag, we calculated these forces meticulously to estimate the thrust required for the ROV's desired speed.

Upon determining the necessary thrust, we embarked on the design of the propulsion system. Opting for a fixed thruster configuration, we meticulously designed vertical thrusters using OpenProp code. Rigorous testing through ANSYS Fluent refined our propeller designs, resulting in a propulsion system capable of surpassing the fixed threshold of 3N thrust while maintaining exceptional energy efficiency.

Chapter four delved into the ROV's control system, a meticulously crafted mechanism anchored by an advanced autopilot system. Integrated sensors ensured the ROV's stability underwater, while seamless communication with the surface was facilitated through companion and topside computers. Our focus here was on delivering an unparalleled piloting experience, making the ROV accessible to a wide range of users.

In the fifth chapter, the meticulous assembly of all ROV components was executed, ensuring the integrity of water-sealed compartments and preserving the ROV's balance. While the ROV's total weight slightly exceeded the initial 2.5kg limit, resting at 3kg, it remained highly portable. Attention to aesthetics was paramount; our ROV boasts an appealing symmetrical facade and streamlined shape, minimizing drag.

Despite our achievements, the road ahead offers boundless opportunities for product refinement. Future perspectives include optimizing the ROV's weight and volume, enhancing the camera's capabilities, integrating personalized features through advanced image processing, introducing swaying capabilities, and developing more compact and efficient thrusters

by employing waterproof motors. Improving sealing capabilities for deeper water exploration and refining the ROV's aesthetics through advanced polishing techniques and exterior design enhancements are also on the horizon.

While envisioning these advancements, we remain cognizant of the delicate balance between increased costs and augmented value, ensuring the final product remains economically viable. Our current creation, though a foundational step, is destined for continual improvement, reflecting our commitment to innovation in the field of underwater technology.

References

[1] R. D. Christ and R. L. Wernli Sr, *The ROV manual: a user guide for remotely operated vehicles*. Butterworth-Heinemann, 2013.

[2] J. Carlton, *Marine propellers and propulsion*. Butterworth-Heinemann, 2018.

[3] B. Epps, "Openprop v2. 4 theory document," *MIT Department of Mechanical Engineering Technical Report, Cambridge, MA. Available at: http://openprop. mit. edu. Accessed December*, vol. 15, p. 2010, 2010.

[4] "ArduSub." `https://www.ardusub.com/quick-start/vehicle-frame.html`. Accessed: October 30, 2023.

[5] R. K. Flitney, *Seals and sealing handbook*. Elsevier, 2011.

[6] "WetLink Penetrator Data Sheet." Online. Accessed on: 15/09/2023.

[7] E. M. Research, "Global underwater drone market outlook," 2023. Accessed: 19/03/2023.

[8] A. Khadhraoui, *Modélisation et simulation interactive pour la navigation d'un robot sous-marin de type ROV Observer*. PhD thesis, Université Paris Saclay, 2015.

[9] J. E. Matsson, *An introduction to ANSYS fluent 2022*. Sdc Publications, 2022.

[10] L. G. García-Valdovinos, T. Salgado-Jiménez, M. Bandala-Sánchez, L. Nava-Balanzar, R. Hernández-Alvarado, and J. A. Cruz-Ledesma, "Modelling, design and robust control of a remotely operated underwater vehicle," *International Journal of Advanced Robotic Systems*, vol. 11, no. 1, p. 1, 2014.

[11] D.-G. Caprace, P. Chatelain, and G. Winckelmans, "Lifting line with various mollifications: theory and application to an elliptical wing," *AIAA Journal*, vol. 57, no. 1, pp. 17–28, 2019.

[12] Y.-c. Pan, H.-x. Zhang, and Q.-d. Zhou, "Numerical prediction of submarine hydrodynamic coefficients using cfd simulation," *Journal of Hydrodynamics*, vol. 24, no. 6, pp. 840–847, 2012.

[13] M. Motallebi-Nejad, M. Bakhtiari, H. Ghassemi, and M. Fadavie, "Numerical analysis of ducted propeller and pumpjet propulsion system using periodic computational domain," *Journal of Marine Science and Technology*, vol. 22, pp. 559–573, 2017.

[14] G. L. Chahine, "Numerical simulation of bubble flow interactions," *Journal of Hydrodynamics*, vol. 21, no. 3, pp. 316–332, 2009.

[15] R. Zhang and H.-x. Chen, "Numerical analysis of cavitation within slanted axial-flow pump," *Journal of Hydrodynamics*, vol. 25, no. 5, pp. 663–672, 2013.

[16] F. Stern, Z. Wang, J. Yang, H. Sadat-Hosseini, M. Mousaviraad, S. Bhushan, M. Diez, Y. Sung-Hwan, P.-C. Wu, S. M. Yeon, *et al.*, "Recent progress in cfd for naval architecture and ocean engineering," *Journal of Hydrodynamics*, vol. 27, no. 1, pp. 1–23, 2015.

[17] V. R. Krishna, S. P. Sanaka, N. Pardhasaradhi, and B. R. Rao, "Hydro-elastic computational analysis of a marine propeller using two-way fluid structure interaction," *Journal of Ocean Engineering and Science*, vol. 7, no. 3, pp. 280–291, 2022.

[18] H. Schmucker, F. Flemming, and S. Coulson, "Two-way coupled fluid structure interaction simulation of a propeller turbine," *International Journal of Fluid Machinery and Systems*, vol. 3, no. 4, pp. 342–351, 2010.

[19] L. Yan, P.-f. Zhao, W. Qiang, and Z.-h. Chen, "Urans computation of cavitating flows around skewed propellers," *Journal of Hydrodynamics, Ser. B*, vol. 24, no. 3, pp. 339–346, 2012.

[20] J. Sahili and K. Zaidan, "Rov propellers optimization using cad design and cfd modeling and experimental validation," in *2018 6th RSI International Conference on Robotics and Mechatronics (IcRoM)*, pp. 418–421, IEEE, 2018.

[21] J. Zhang, Q. Wu, G. Wang, and T. Liu, "Numerical analysis on propulsive efficiency and pre-deformated optimization of a composite marine propeller," *Science China Technological Sciences*, vol. 63, pp. 2562–2574, 2020.

[22] M. Bennaya, J. F. Gong, M. M. Hegaze, and W. P. Zhang, "Numerical simulation of marine propeller hydrodynamic performance in uniform inflow with different turbulence models," *Applied Mechanics and Materials*, vol. 389, pp. 1019–1025, 2013.

[23] D. T. Bui, "Numerical simulation of the performance of bow thruster taking into account turbulence model influence using rans method,"

[24] K. Szykiedans, W. Credo, and D. Osiński, "Selected mechanical properties of petg 3-d prints," *Procedia Engineering*, vol. 177, pp. 455–461, 2017. XXI Polish-Slovak Scientific Conference Machine Modeling and Simulations MMS 2016.September 6-8, 2016, Hucisko, Poland.

[25] Prusa Polymers, "TECHNICAL DATA SHEET: Prusament PETG," 2020.

[26] "SKF R09-F Rotary Seal Data Sheet." Online. Accessed on: 12/09/2023.

[27] P. Boissinot, P. Langlois, and A. Pádua, *Matériaux et joints d'étanchéité pour les hautes pressions*. Intégrations (Saint-Étienne), Publications de l'Université de Saint-Etienne, 2004.

[28] P. O. Parker and O. Ring Handbook, "5700, 2007," *PH Corporation (Ed.). Cleveland, OH.*

[29] R. D. Christ and R. L. Wernli Sr, *The ROV manual: a user guide for observation class remotely operated vehicles.* Elsevier, 2011.

[30] W. Wang and C. M. Clark, "Modeling and simulation of the videoray pro iii underwater vehicle," in *OCEANS 2006-Asia Pacific*, pp. 1–7, IEEE, 2006.

Annexes A : Business Model Canvas

Business Model Canvas

Partenaires Clés

- Fournisseurs de composants électroniques et mécaniques
- Entreprises de logistique et de livraison
- Partenaires de distribution et de vente au détail
- Instituts de recherche océanographique pour la validation

Ressources Clés

- Recherche et développement pour améliorer le produit
- Production et assemblage des ROV
- Tests et contrôle qualité
- Service après-vente et maintenance

Ressources Clés

- Équipe de développement et de R&D
- Personnel de production et d'assemblage
- Ingénieurs spécialisés en électronique et en mécanique marine
- Fournisseurs de composants électroniques et mécaniques

Proposition de Valeur

- Technologie de pointe pour l'exploration sous-marine
- Réduction des coûts liés à la plongée humaine
- Capable d'atteindre des profondeurs élevées
- Facilité d'utilisation et d'entretien

Relation avec les Clients

- Support client en ligne
- Service clientèle pour les requêtes et les retours
- Formation à l'utilisation du ROV
- Mises à jour régulières du produit

Canaux

- Ventes en ligne (site web)
- Partenariats avec des fournisseurs marins
- Participation à des salons et expositions
- Réseaux de distribution spécialisés

Segments de Clientèle

- Pêcheurs professionnels
- Industries marines (exploration, maintenance, etc.)
- Instituts de recherche océanographique
- Entreprises de travaux sous-marins
- Entreprises de surveillance de l'environnement marin

Structure de Coûts

- Coûts de recherche et développement
- Coûts de production (matières premières, main d'œuvre, etc.)
- Coûts de marketing et de publicité
- Coûts liés à la location de locaux/bureaux
- Coûts opérationnels (salaires, frais généraux, etc.)

Sources de Revenus

- Vente de ROV et de ses accessoires
- Contrats de maintenance et de service
- Location de ROV pour des projets spécifiques

Annexes B : Technical Drawings of ROV Components

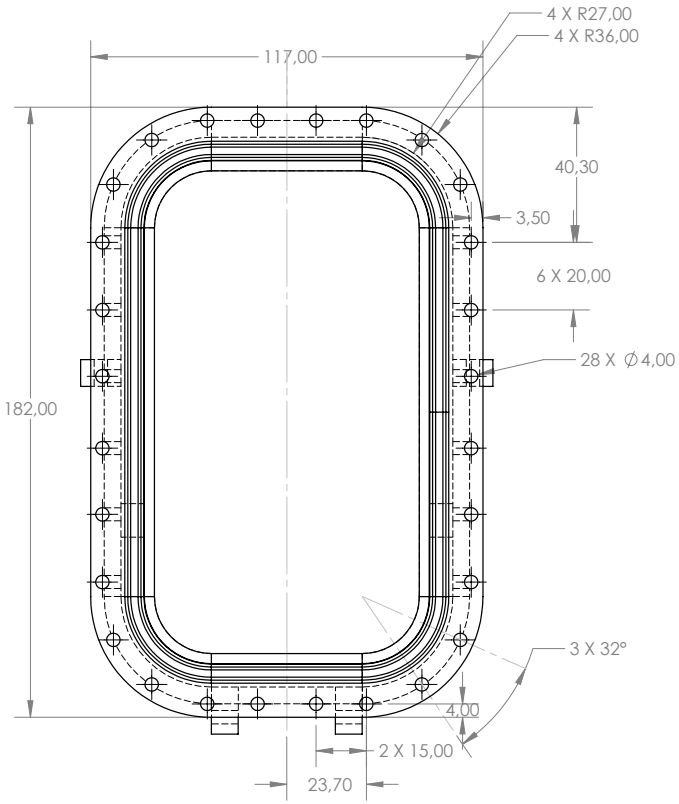

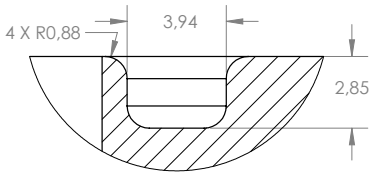

DETAIL H
SCALE 5 : 1

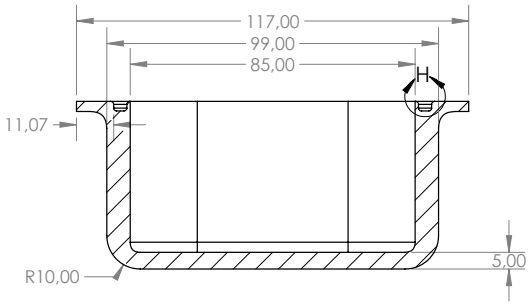

SECTION G-G
SCALE 2 : 3

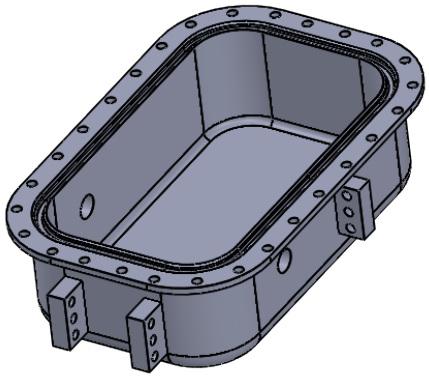

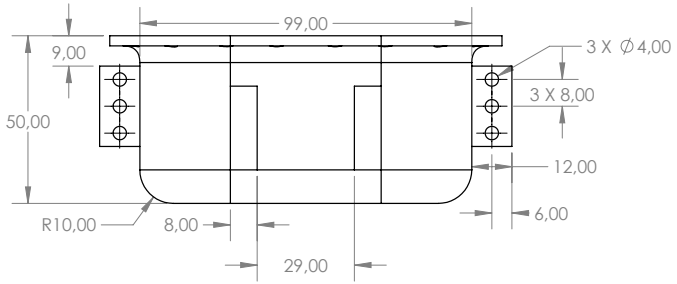

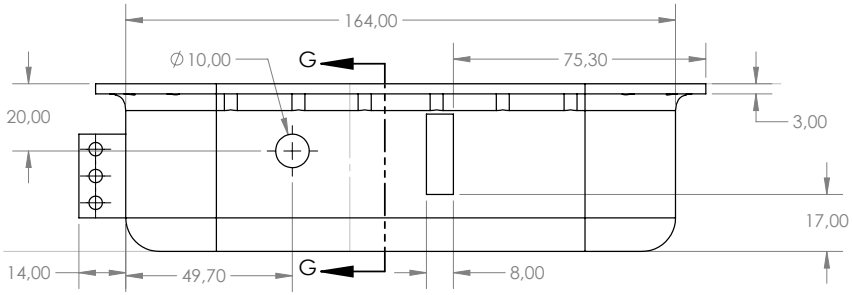

National Polytechnic School

Scale	Size		Sealed Box	Department Mechanical Engineering
2:3	A4			
Checked by	Sedjal Hamid		Designed by	Mehaba Hani
	BENKOUSSAS Bouzid			Bouarrou Sami
				Date : 20/09/2023

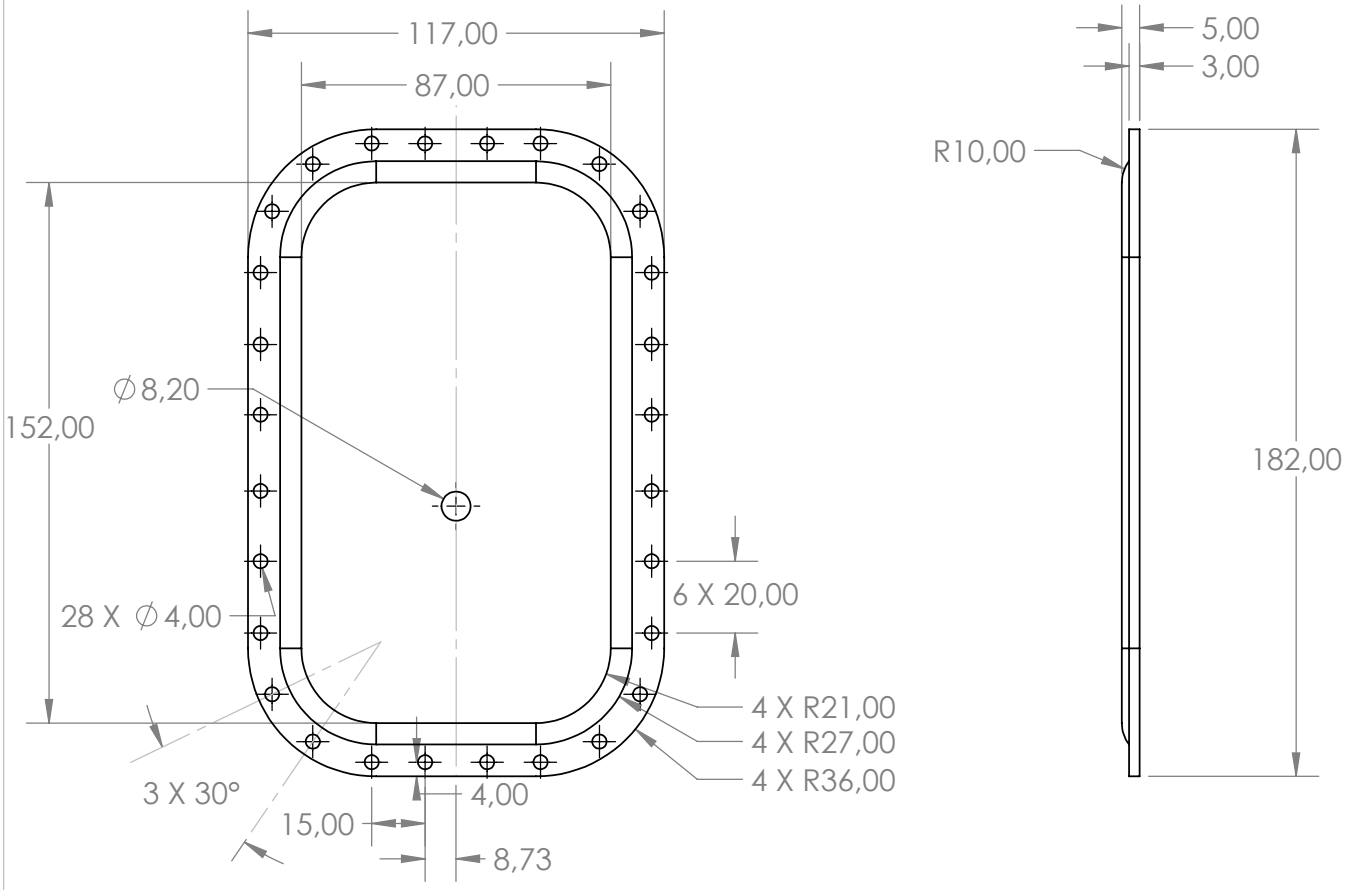

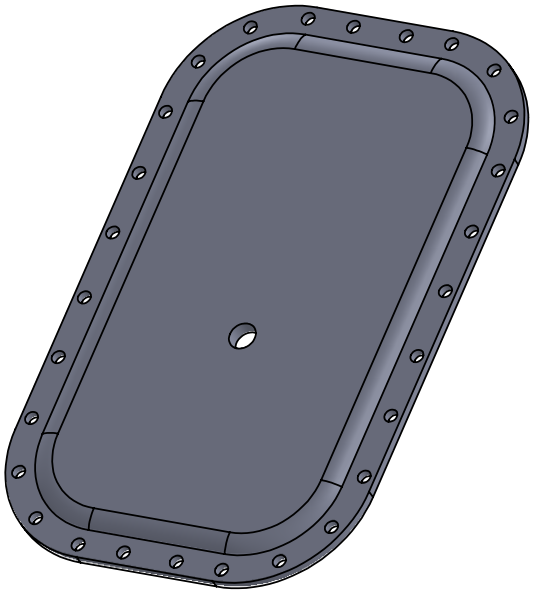

National Polytechnic School

Scale	Size		Sealed Box Cover		Department Mechanical Engineering
1:2	A4				
Checked by	Sedjal Hamid		Designed by	Mehaba Hani	Date : 20/09/2023
	BENKOUSSAS Bouzid			Bouarrou Sami	

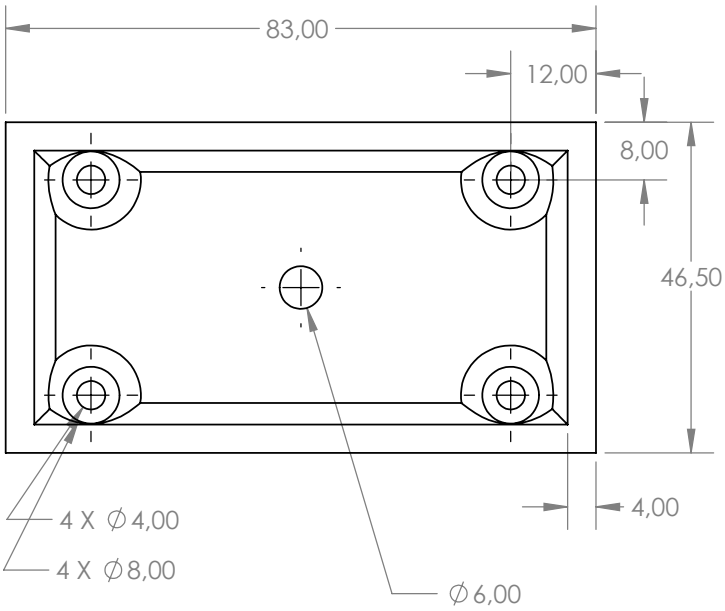

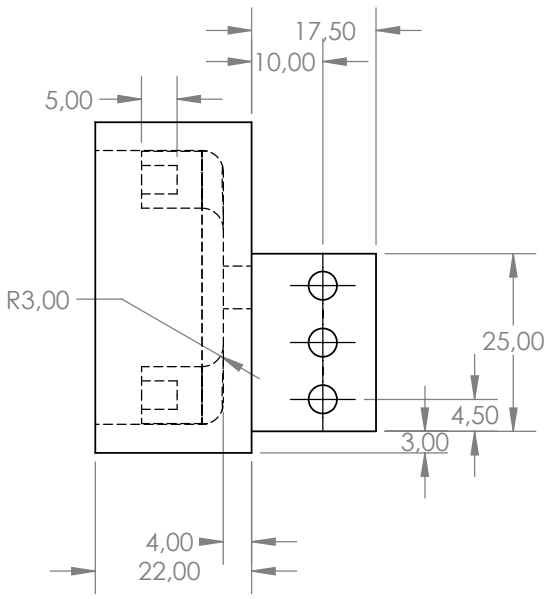

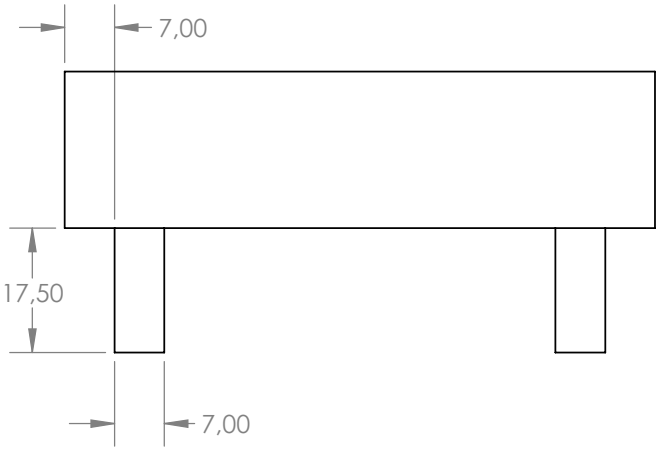

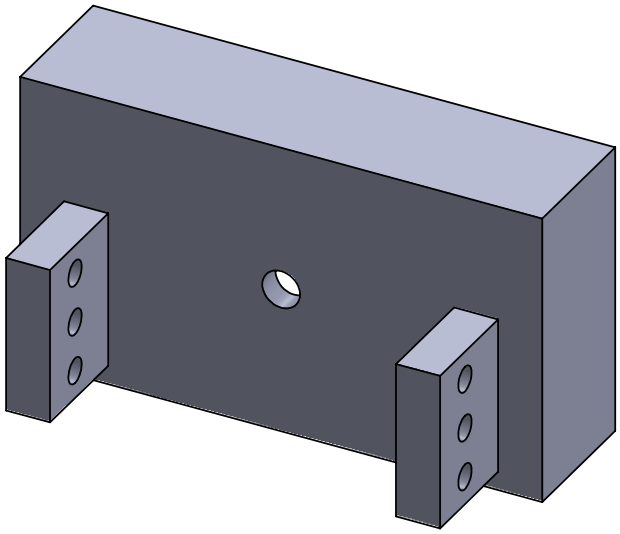

National Polytechnic School

Scale	Size		Camera Cover		Department Mechanical Engineering
1:1	A4				
Checked by	Sedjal Hamid		Designed by	Mehaba Hani	Date : 20/09/2023
	BENKOUSSAS Bouzid			Bouarrou Sami	

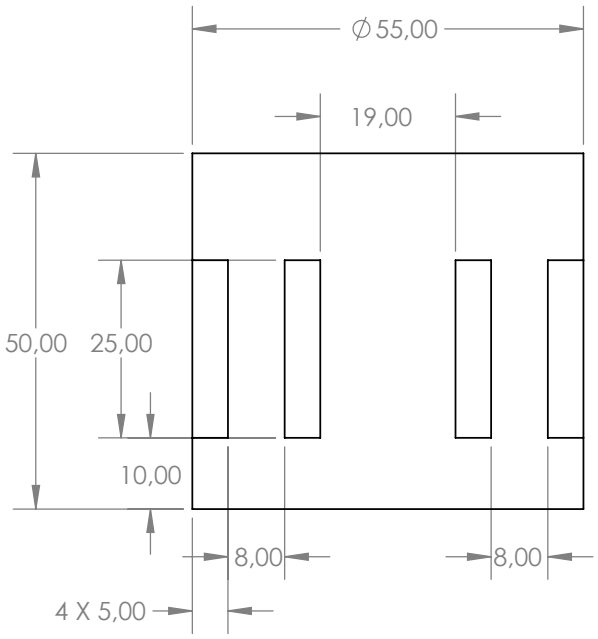

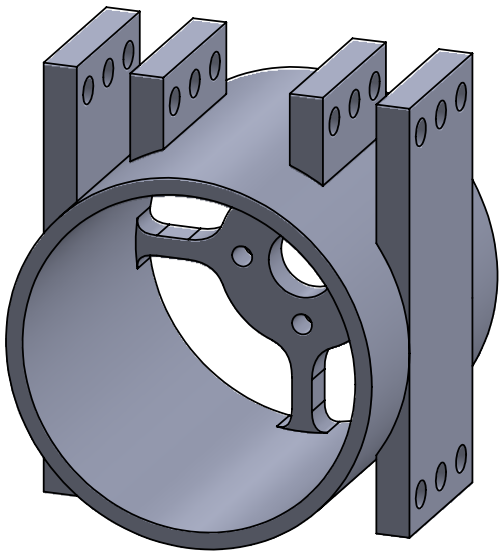

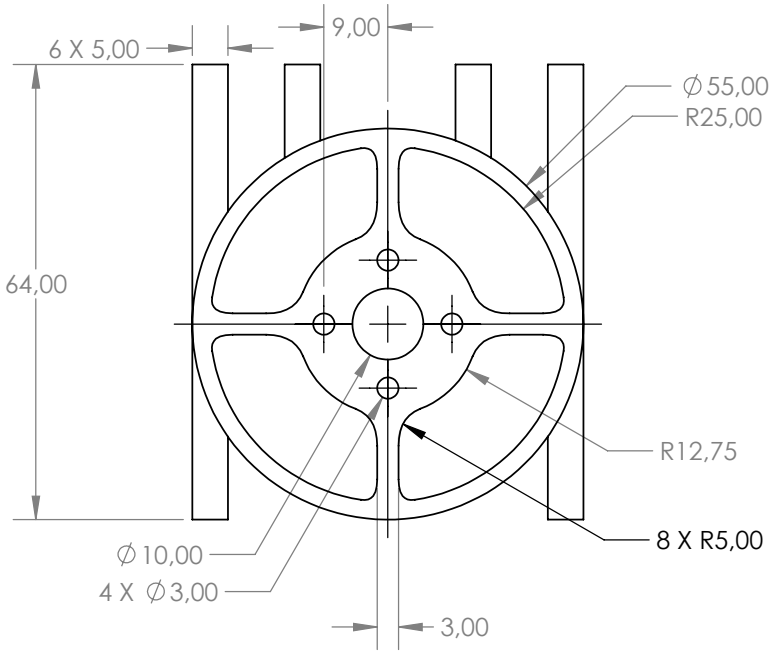

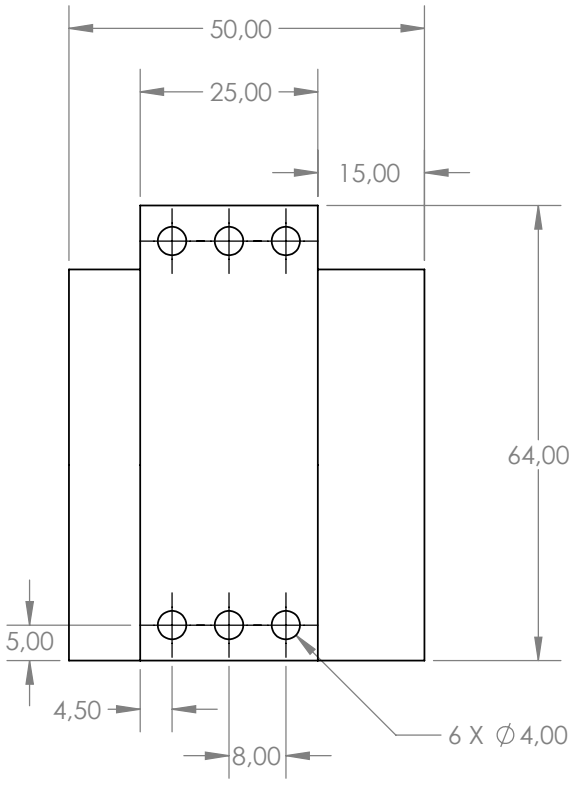

National Polytechnic School

Scale	Size		Vertical Thruster Shell		Department Mechanical Engineering
1:1	A4				
Checked by	Sedjal Hamid		Designed by	Mehaba Hani	Date : 20/09/2023
	BENKOUSSAS Bouzid			Bouarrou Sami	